https://doi.org/10.15388/vu.thesis.853
https://orcid.org/0000-0001-6599-6556

VILNIUS UNIVERSITY
CENTER FOR PHYSICAL SCIENCES AND TECHNOLOGY

Vytautas Bubilaitis

Spectral Characteristic of Molecular Aggregates at Various Intensities of Optical Fields

DOCTORAL DISSERTATION

Natural Sciences,
Physics (N 002)

VILNIUS 2025

The dissertation was prepared between 2019 and 2024 in Vilnius University, Institute of Chemical Physics.

Academic supervisor – Prof. Dr. Darius Abramavičius (Vilnius University, Natural Sciences, Physics, N 002).

This doctoral dissertation will be defended in a public meeting of the Dissertation Defence Panel:

Chairman – Prof. Habil. Dr. Egidijus Anisimovas (Vilnius University, Natural Sciences, Physics, N 002).
Members:
Assoc. Prof. Dr. Jevgenij Chmeliov (Vilnius University, Natural Sciences, Physics, N 002),
dr. Vytautas Dūdėnas (Vilnius University, Natural Sciences, Physics, N 002),
Prof. Habil. Dr. Vidmantas Gulbinas (Center for Physical Sciences and Technology, Natural Sciences, Physics, N 002),
Assoc. Prof. Dr. Thorsten Hansen (University of Copenhagen, Natural Sciences, Physics, N 002).

The dissertation shall be defended at a public meeting of the Dissertation Defence Panel at 14:00 on December 12, 2025 in room A101 of the Center for Physical Sciences and Technology.
Address: Saulėtekio ave. 3, Vilnius, Lithuania
Tel. +370 5 264 9211; e-mail: office@ftmc.lt

The text of this dissertation can be accessed at the libraries of Vilnius University and Center for Physical Sciences and Technology, as well as on the website of Vilnius University:
www.vu.lt/lt/naujienos/ivykiu-kalendorius

https://doi.org/10.15388/vu.thesis.853
https://orcid.org/0000-0001-6599-6556

VILNIAUS UNIVERSITETAS
FIZINIŲ IR TECHNOLOGIJOS MOKSLŲ CENTRAS

Vytautas Bubilaitis

Spektrinės molekulinių agregatų charakteristikos įvairaus intensyvumo optiniuose laukuose

DAKTARO DISERTACIJA

Gamtos mokslai,
Fizika (N 002)

VILNIUS 2025

Disertacija rengta 2019–2024 metais Vilniaus universitete Cheminės fizikos institute

Mokslinis vadovas – prof. dr. Darius Abramavičius (Vilniaus universitetas, gamtos mokslai, fizika, N 002).

Gynimo taryba:
Pirmininkas – prof. habil. dr. Egidijus Anisimovas (Vilniaus universitetas, gamtos mokslai, fizika, N 002).
Nariai:
doc. dr. Jevgenij Chmeliov (Vilniaus universitetas, gamtos mokslai, fizika, N 002),
dr. Vytautas Dūdėnas (Vilniaus universitetas, gamtos mokslai, fizika, N 002),
prof. habil. dr. Vidmantas Gulbinas (Fizinių ir technologijos mokslų centras, gamtos mokslai, fizika, N 002),
doc. dr. Thorsten Hansen (Kopenhagos universitetas, gamtos mokslai, fizika, N 002).

Disertacija ginama viešame Gynimo tarybos posėdyje 2025 m. Gruodžio mėn. 12 d. 14 val. Nacionaliniame fizinių ir technologijos mokslų centro A101 auditorijoje. Adresas: Saulėtekio al. 3, Vilnius, Lietuva, tel. +370 5 264 9211; el. paštas office@ftmc.lt

Disertaciją galima peržiūrėti Vilniaus universiteto ir Fizinių ir technologijos mokslų centro bibliotekose ir VU interneto svetainėje adresu: *https://www.vu.lt/naujienos/ivykiu-kalendorius*

Contents

INTRODUCTION

Molecular aggregates are versatile systems showing unique electronic excitations and excited state dynamics. Functionally, they are employed by Nature in photosynthetic light harvesting and energy funneling[1,2]. In specific conditions the aggregates are formed from synthetic dye molecules thus making a unique playground for design and studies of various quantum phenomena depending on the nature and the number of coupled chromophores[3–7], which are molecules that are sensitive to optical fields. To understand, predict and control their optical properties in various spectroscopy experiments, theory and simulations must be developed and coordinated.

The core minimal system, which mimics the properties of molecular aggregates is the chromophoric dimer[8–10]. Due to resonance interaction between the chromophores, the system shows absorption bands shifted from the ones of independent chromophores. An additional excited state absorption (ESA) appears even if contributing molecules are considered as two-level systems. Properties of such model system can be simulated with high confidence at the level of single excitations when considering complex bath structure leading to non-Markovian exciton relaxation. Exciton is an eigenstate of Hamiltonian, a delocalized excitation. However, it is nontrivial to simulate spectra of chromophore aggregates when the number of contributing chromophores is much larger, and the level of excitation is high. The main limitation is due to the exponential growth of computational time due to the aggregate size and the number of excitations when considering an arbitrary excitation intensity.

Two-dimensional electronic spectroscopy (2DES) is a routine tool that has been designed to visualize excitation dynamics and correlations in chromophoric aggregates[11–14]. The chronologically ordered three excitation pulses (characterized by wave vectors K_1, K_2, K_3) induce a nonlinear response at least third order in the incoming field. The induced nonlinear polarization at a signal wave vector $\pm K_1 \mp K_2 + K_3$ is then detected by a heterodyne detection (by applying an additional pulse for detection timing). The resulting polarization is a function of the time delays between the neighboring pulses and detection time (t_1, t_2, t_3), there are 3 times because there is also a fourth

pulse, the signal detection. Two Fourier transforms, with respect to the two t_1 and t_3 delays between pulses, projects the signal onto two frequencies (ω_1, ω_3) in two dimensions. This reveals exciton evolution, which becomes a function of the t_2 time (delay time), which follows exciton populations and intraband coherences.

For low optical field intensities when the number of excitations is low, signal can be analyzed in perturbative regime [12,15]. The low number of excitations allows us to count quanta taking part in specific processes and determine the order of interaction and separate them order by order. In this work when we talk about order, we mean the order of interaction between system and optical field, i. e. power.

However, at higher field intensity various processes become indistinguishable, the perturbative regime essentially does not converge, and excitation-induced effects of different orders appear at various types of signals, for example, some signal of 2DES, like $+K_1 - K_2 + K_3$. Including effects which are usually associated with much lower order measurements (even as low as the first order signals). This can lead to misinterpretation of spectral features and thus requires a special non-perturbative treatment.

Looking at the third order in the field in the standard pump-probe setup [16], the intensity of the detected signal scales linearly with the pump pulse intensity. The intensity of the excitation field used in measurement is usually controlled to achieve a better signal-to-noise ratio and is not used as a parameter that may additionally reshape the signal. If the signal contains purely third order contributions, there should be no intensity dependency (apart from the intensity scaling). But as the excitation density becomes higher, additional processes, related to exciton-exciton interaction at higher orders to the field become involved. Hence, certain physical processes change with different density of excitations in material, which is partly determined by the intensity of the excitation electric field, via higher nonlinear processes.

Exciton-exciton annihilation (EEA) is one of such processes that strongly depends on the density of excitations [17–21,9,22]. That process is the consequence of internal conversion when the highly excited chromophore, resonant to double-quantum resonance, quenches one excitation and relaxes into its lowest excited state, thus leaving only one-quantum excitation. Time dependence of exciton decay kinetics in large molecular clusters and aggregates can give information on exciton diffusion [23]. Overlapping higher order processes are generated at least at the fifth order when two additional interactions happen with any ex-

citation pulses. However, recently a 2D signal at $\pm 2K_1 \mp 2K_2 + K_3$ which comes at distinct spectral window has been shown to specifically excite the double-exciton energy band and detect features related to EEA[24]. But the fine structure of these spectral features still requires further study.

Exciton interaction with vibrational degrees of freedom (phonons) is the source of exciton localization (due to static disorder) and exciton relaxation (dynamic fluctuations)[19]. Already mentioned EEA appears due to vibronic coupling at nonlinear excitation regime[25,20,26,22]. These effects play against the exciton formation. In molecular systems the phonons are mostly local vibrations (or static diagonal disorder), which affect chromophore excitation energies without spatial correlations. As a result, they modulate chromophore transition energies and tune the chromophores away from stable resonances. This means equation complexity cannot trivially be reduced by changing to a delocalized exciton basis, when all local and non-local effects must be considered.

Vibrational degrees of freedom are treated indirectly, using Redfield relaxation theory. In Redfield relaxation theory, the vibrational degrees of freedom are assumed to consist of an infinite number of harmonic oscillators that are coupled to the system. The coupling between system and bath is assumed to be small and second order perturbation theory is applied according to it. Assuming that the bath is Markovian e. i. neglecting memory effects, the bath is treated as in a mean field like theory, oscillators are "frozen" at thermal equilibrium which is defined by the temperature of the bath. With this, the Redfield relaxation theory description is acquired.

Equations for non-perturbative calculations of spectra of a set of coupled electronic oscillators by using a Nonlinear Exciton Equations (NEE) formalism have been derived[9]. Non-perturbative methods generate endless hierarchies of equations that, in general, cannot be solved[27]. NEE generate the endless hierarchy of coupled equations. For practical use specific assumptions are needed to give a solid basis to ending the hierarchy at some well-defined level. By adding or dropping EEA terms we can reason about the number of excitations, which effectively can exist in the system. Following that, if we have terms that are related to a very high number of excitations, we factorize them and treat them as products of lower order terms. Depending on a specific system of interest and a specific spectroscopic measurement, such factorization is not arbitrary. This can lead to unexpected results from equations, e.g., diverging solutions, giving nonphysical effects or losing some properties that are impor-

tant. However, as a positive feature, due to the high number of excitations, the factorized equations may lead to correct multi-quanta cumulative average spectral features which cannot be easily captured using perturbative regimes. Hence, the systematic analysis of various factorization schemes is necessary. However, as a positive feature, due to the high number of excitations, the factorized equations may lead to correct multi-quanta cumulative average spectral features which cannot be easily captured using perturbative regimes.

One strategy to reduce the required computational resources for solving NEE is to restrict the number of excitations. This corresponds to restricting the types of nonlinear processes to the ones that are the most prominent at e.g., the low excitation level. The next option is related to restricting the theory to only bright optical excitations, which can be extracted by considering specific system symmetries. This usually requires a change from molecular/site basis to exciton basis, where system-specific symmetries may result in only a few optically accessible resonances in the whole band of allowed states. Rewriting the model into exciton basis and truncating the base, transforms the model to an effectively reduced problem in the spirit of the renormalization group in condensed matter physics[28,29], as truncating in exciton basis correspond some parameter renormalization in molecular basis.This results in describing the aggregate in terms of a small number of effective quasiparticles. This approach effectively reduces the size of the problem and even infinite size aggregates can be "solved" analytically[30].

In this thesis the highly nonlinear effects in nonlinear absorption, pump-probe and 3rd-5th order 2DES spectra of chromophoric aggregates[31–33] are considered.

We describe how the inclusion of EEA terms into NEE affects the 2D spectra at various levels of wave-mixing[31]. We limit this analysis to dimer and trimer systems for 2DES spectra. To extract highly nonlinear 2D signals the phase cycling method[34] was applied. Significant changes can be seen in 2D spectra when EEA is active, which could be associated with dynamic exciton symmetry breaking.

We compare several factorization types[33] for a linear chromophore aggregate from low to high excitation field intensities by calculating the simplest possible absorption spectrum. We show that at high excitation intensity additional induced absorption may be seen, while its characteristics are very sensitive to system nonlinearities and, hence, the type of factorization. This can be used in a specific application for a specific molecular system.

We study the behavior of NEE solutions with EEA terms for J aggregate when restricting the calculations to subsets of excitons[32]. For this, we calculate pump-probe spectra at various optical field intensities. We show the spectra converge when only several excitons are used in calculations.

Layout of the dissertation

This dissertation follows the 3 published main studies. These 3 studies each take the same model and expand it in a different direction.

We start with presenting an overview of general theory about Frenkel excitons, the treatment of environmental degrees of freedom, Nonlinear exciton equations and Phenomenological treatment of Exciton-exciton annihilation. Later, we present each study in separate chapters. Each chapter starts with model parameters followed by the results and discussion. Finally, the conclusions are presented together for all chapters.

List of articles

Articles included in doctoral dissertation

[A1] **V. Bubilaitis**, D. Abramavičius, Compact modeling of highly excited linear aggregates using generalized quantum particles, Chemical Physical, **588**, 112445, 2025, https://doi.org/10.1016/j.chemphys.2024.112445

[A2] **V. Bubilaitis**, D. Abramavičius, Signatures of exciton-exciton annihilation in 2DES spectra including up to six-wave mixing processes, The Journal of Chemical Physical, **161(10)**, 104106, 2024, https://doi.org/10.1063/5.0223724

[A3] **V. Bubilaitis**, D. Abramavičius, Nonlinear exciton equation factorization for non-perturbative absorption modeling, Lithuanian Journal of Physics, **65(1)**, 1-18, 2025, https://doi.org/10.3952/physics.2025.65.1.3

Articles related to doctoral dissertation

[B1] **V. Bubilaitis**, J. Hauerb and D. Abramavicius, Simulations of pump probe spectra of a molecular complex at high excitation intensity, Chemical Physical, **527**, 110458, 2019, https://doi.org/10.1016/j.chemphys.2019.110458

Articles not included in doctoral dissertation

[C1] **V. Bubilaitis**, O. Rancova and D. Abramavičius, Vibration-mediated energy transport in bacterial reaction center: Simulation study, The Journal of Chemical Physical, **154**, 214115, 2021, https://doi.org/10.1063/5.0048815

[C2] L. Baliulyte, E.Urniezius, **V. Bubilaitis**, M. Macernis, L. Cupellini, D. Abramavicius, Origins of curvature in meso-tetra(4-sulfonatophenyl) porphine aggregation: molecular dynamics and electronic spectroscopy, Molecular Systems Design & Engineering, **10**, 635-648, 2025, https://doi.org/10.1039/D5ME00010F

List of conference presentations

[D1] **V. Bubilaitis**, D. Abramavičius, Žadinimo-zondavimo spektrų modeliavimas esant dideliam žadinimo intensyvumui, Lietuvos nacionalinė fizikos konferencija 43, Lithuania, Kaunas, Oct. 3-5, **2019**. (Poster)

[D2] **V. Bubilaitis**, D. Abramavičius, Žadinimo-zondavimo spektrų modeliavimas prie didelių žadinimo intensyvumų J agregatuose, Lietuvos nacionalinė fizikos konferencija 44, Lithuania, Vilnius, Oct. 6-8, **2021**. (Poster)

[D3] **V. Bubilaitis**, D. Abramavičius, Modeling of Pump-probe spectra at high excitation intensities for J aggregates, Computational Methods in Photosynthesis Comphot2021, Virtual Environment, Nov. 8-11, **2021**. (Poster)

[D4] **V. Bubilaitis**, D. Abramavičius, Nonlinear exciton equations at fifth order to the optical field: Intensity dependent nonlinear spectra dynamics in J-type aggregate, Nordic Femtochemistry 2022, Finland, Jyväskylä, Jun. 8-10, **2022**. (Poster)

[D5] **V. Bubilaitis**, D. Abramavičius, Nonlinear exciton equations at fifth order to the optical field: Intensity dependent nonlinear spectra dynamics in J-type aggregate, ECAMP22, Lithuania, Vilnius, Jun. 27-Jul. 1, **2022**. (Poster)

[D6] **V. Bubilaitis**, D. Abramavičius, Nonlinear exciton equations at fifth order to the optical field: Intensity dependent nonlinear spectra dynam-

ics in J-type aggregate, Hanseatic Workshop on "Exciton Dynamics and Spectroscopy", Lithuania, Vilnius, Aug. 24-26, **2022**. (Poster)

[D7] **V. Bubilaitis**, D. Abramavičius, Nonlinear exciton equations at fifth order to the optical field: Intensity dependent nonlinear spectra dynamics in J-type aggregate, EuroCC workshop and training on using HPC, Lithuania, Vilnius, Dec. 16, **2022**. (Oral)

[D8] **V. Bubilaitis**, D. Abramavičius, Nonlinear exciton equations factorization for nonperturbative absorption modeling, 2ND EUROCC VILNIUS WORKSHOP ON USING HPC, Lithuania, Vilnius, Jun. 14, **2024**. (Oral)

[D9] **V. Bubilaitis**, D. Abramavičius, Exciton-exciton annihilation dynamics in six-wave mixing 2DES spectra, Nordic Baltic Femtochemistry Conference 2024, Estonia, Tartu, Jul. 10-12, **2024**. (Poster)

Author's contribution

The author developed and expanded NEE equations in addition to writing numerical computation packages for computing NEE equations calculation of various 1D and 2D spectra. Also, all the computations and the analysis of results were performed by the author.

Goals of the dissertation

1. Investigate NEE applicability for computations involving large molecular aggregates.
2. Study the limitations of different approximations that can be applied for practical NEE computations.
3. Investigate the use of NEE for computations of higher order nonlinear spectra.

Statements to be defended

1. Factorization of NEE and rewriting the system into exciton basis and truncating the base improves the efficiency of calculations of nonlinear spectra for J aggregates made of many molecules.

2. NEE allow description of generalized particles for both paulions and bosons with a single parameter that allows smooth transition from one description to another.

3. The addition of EEA terms homogenizes the results of different NEE models.

4. EEA together with system nonlinearities breaks exciton symmetry rules due to the local nature of the molecular processes, leading to the emergence of additional features in spectra, as related to “dark” excitons.

5. Phase cycling is efficient in separating different wave mixing components when calculating highly nonlinear resonant multidimensional spectra.

List of abbreviations

NEE	Nonlinear exciton equations
MSRT	Markovian secular Redfield relaxation theory
EEA	Exciton-exciton annihilation
2DES	Two dimensional electronic spectroscopy
ESA	Excited state absorption

1 THEORY

1.1 J aggregates

In this work our model systems will be J aggregates. Idealized linear aggregate is a system composed of a chain of identical molecules. The molecules are coupled between the nearest neighbors with same value for all couplings. Also each molecules in the aggregate has same transition dipolar moment. The transition dipole moment of molecules in chain are aligned with respect to the chain axis. If the transition dipoles are aligned perpendicular to the chain axis then such aggregate is called H aggregate. If the transition dipoles are aligned parallel to the chain axis then such aggregate is called J aggregate. The result of these properties is that of all eigenstates of J aggregate excitations, only the lowest energy one has nonzero transition dipole moments. This property we will exploit in later parts of this work for increasing efficiency of spectra calculations.

1.2 Frenkel exciton model for molecular aggregate

We start with a very generic model of a simple collection of electrons and nuclei. With the Born-Oppenheimer assumption the electrons and nuclei can be treated separately as their masses differ by 3 orders of magnitude. The coordinates of nucleus are then treated as parameters for electron motion.

The Hamiltonian for interacting charged particles in atomic units can then be written as:

$$\hat{H}_S = \sum_{\alpha} \hat{K}_\alpha + \frac{1}{2} \sum_{\alpha\beta}^{\alpha\neq\beta} \frac{1}{|\boldsymbol{r}_\beta - \boldsymbol{r}_\alpha|} - \sum_{n\alpha} \frac{q_n}{|\boldsymbol{R}_n - \boldsymbol{r}_\alpha|} + \frac{1}{2} \sum_{nm}^{n\neq m} \frac{q_n q_m}{|\boldsymbol{R}_\beta - \boldsymbol{R}_\alpha|}, \tag{1.2.1}$$

here $\hat{K}_\alpha$ is the kinetic energy of α electron, $\boldsymbol{r}_\alpha$ denotes electron coordinates, $\boldsymbol{R}_n$- nucleus with charge q_n. The 4 terms in equation: the sum of electron kinetic energy, the electron-electron interaction energy, the electron-nucleus

interaction energy and nucleus-nucleus interaction energy. Only the electrostatic interaction is considered.

Going up in scale we can group electrons and nucleus to corresponding molecules. Thus, arrive at bigger picture Hamiltonian with Hamiltonian of each molecule and interaction between molecules:

$$H_S = \sum_{m}^{N} H_m + \frac{1}{2} \sum_{mm'}^{m \neq m'} V_{mm'}, \tag{1.2.2}$$

Where H_m is the chromophoric Hamiltonian of m-th molecule:

$$\begin{aligned} H_m = & \sum_{\alpha \in r_m} K_\alpha + \frac{1}{2} \sum_{\alpha\beta}^{\alpha \neq \beta} \frac{1}{\left| \boldsymbol{r}_\beta^{(m)} - \boldsymbol{r}_\alpha^{(m)} \right|} \\ & - \sum_{n\alpha} \frac{q_n}{\left| \boldsymbol{R}_n^{(m)} - \boldsymbol{r}_\alpha^{(m)} \right|} + \frac{1}{2} \sum_{nk}^{n \neq k} \frac{q_n q_k}{\left| \boldsymbol{R}_\beta^{(m)} - \boldsymbol{R}_\alpha^{(m)} \right|}, \end{aligned} \tag{1.2.3}$$

here $\boldsymbol{R}_n^{(m)}$ and $\boldsymbol{r}_\alpha^{(m)}$ are the coordinate of nuclei and electrons belonging the m-th molecule. The $V_{mm'}$ are the interaction terms between m and m' molecules:

$$\begin{aligned} V_{mm'} = & \frac{1}{2} \sum_{\alpha\beta}^{\alpha \neq \beta} \frac{1}{\left| \boldsymbol{r}_\beta^{(m)} - \boldsymbol{r}_\alpha^{(m')} \right|} + \frac{1}{2} \sum_{nk}^{n \neq k} \frac{q_n q_k}{\left| \boldsymbol{R}_\beta^{(m)} - \boldsymbol{R}_\alpha^{(m)} \right|} \\ & - \sum_{n\alpha} \left(\frac{q_n}{\left| \boldsymbol{R}_n^{(m')} - \boldsymbol{r}_\alpha^{(m)} \right|} + \frac{q_n}{\left| \boldsymbol{R}_n^{(m)} - \boldsymbol{r}_\alpha^{(m')} \right|} \right). \end{aligned} \tag{1.2.4}$$

The molecular system is composed of multiple chromophoric molecules. Chromophores are molecules that are sensitive to light via optically-induced electronic transitions. Here the molecule is treated as a 2(paulion) or 3(boson) level system with specific transition energy J and anharmonicity K when the molecule is excited more than one time. Interaction with light is described by transition dipole moment $\boldsymbol{\mu}_m$. Coupling between different molecules is mostly electrostatic resonant interaction which can be expressed as Coulomb dipole-dipole interaction with assumption that the size of molecules is smaller than distances between molecules.

Molecular system can then be described by the Frenkel exciton Hamiltonian:

$$\begin{aligned}\hat{H} &= \sum_{m,n} J_{mn}\hat{b}_m^\dagger \hat{b}_n + \frac{1}{2}\sum_m K_m \hat{b}_m^{\dagger 2}\hat{b}_m^2 \\ &+ \sum_m \mu_m^-(t)\hat{b}_m^\dagger + \sum_m \mu_m^+(t)\hat{b}_m. \end{aligned} \tag{1.2.5}$$

Indices m, n label different oscillators (chromophores) positioned on different sites and forming a specific lattice. The diagonal elements of the matrix J_{mn} are electronic transition energies ($m = n$), the remaining elements ($m \neq n$) are the resonant couplings, K_m is the $m-$th oscillator anharmonicity, while $\hat{b}_m^\dagger$ ($\hat{b}_m$) is the excitation creation (annihilation) operator for oscillator m. In general K should be a 4-th order tensors, $K_{mnkl}\hat{b}_m^\dagger \hat{b}_n^\dagger \hat{b}_k \hat{b}_l$, representing different types of anharmonic corrections, such as correction of the resonant couplings due to excitation occupation, K_{mnnl} and electrochromic shifts due to excitation occupation, K_{mnnm}. However here we keep only diagonal elements.

Optical field consists of excitation pulses labeled by l and the system-field interaction is defined by a dot product of the optical electric field and the chromophore transition dipole moment $\boldsymbol{\mu}_m$:

$$\mu_m^\pm(t) = \sum_l \boldsymbol{\mu}_m \cdot \boldsymbol{E}_l(t - t_{0l}) \exp(\pm \mathrm{i}\omega_l(t - t_{0l}) \mp \mathrm{i}\boldsymbol{K}_l \boldsymbol{r}), \tag{1.2.6}$$

which defines the exciton creation or annihilation amplitude; we have also made the rotating wave approximation (RWA), where each exciton creation/annihilation process is associated with the specific optical frequency. $\boldsymbol{E}_l(t)$ is the pulse envelope function, centered at zero. t_{0l} is the pulse's central time and ω_l - carrier frequency.

1.3 Generalized commutation relations

Multi-particle statistics are defined by a specific commutation relation. For paulions[35,36]:

$$[\hat{b}_n, \hat{b}_m^\dagger] = \delta_{mn}(1 - 2\hat{b}_m^\dagger \hat{b}_n). \tag{1.3.1}$$

This commutation relation forbids multiple excitations of a single chromophore. The model thus defines two-level electronic oscillators. In the case of bosons, we have:

$$[\hat{b}_n, \hat{b}_m^\dagger] = \delta_{mn}, \tag{1.3.2}$$

which allows multiple excitations of chromophores. To keep the same level of complexity in mathematical formulation, it is convenient to use the generalized commutation relations, such as:

$$[\hat{b}_n, \hat{b}_m^\dagger] = \delta_{mn}(1 - 2\eta\hat{b}_m^\dagger\hat{b}_n), \tag{1.3.3}$$

with $\eta = 0$ being bosons and $\eta = 1$ - the paulions.

Here we added a parameter that allows to go from one description to other, in theory. But the excitation properties between two edge values (paulions and bosons) are not tested. Therefore in following sections in addition to doing calculations for paulions and bosons we also test the "middle" case setting parameter $\eta = 0.5$. This is a choice with goal of testing if the results are physical and converge. Also we demonstrate how this case compares with paulions and bosons.

The validity of this approach can be argued as follows. While we treat molecule as single whole unit, they are multielectron systems. Neither paulionic nor bosonic model is explicitly correct for the electronic excitations of such molecular system. Molecular chromophores can be excited to higher excited states while the transition dipoles do not follow harmonic oscillator scheme. This is why having a tunable parameter for "paulionicity" may allow to better represent molecular system.

1.4 Coherent exciton dynamics - Nonlinear Exciton Equations

Quantum mechanics has several formulations[37,38]. Nonlinear Exciton Equations (NEE) are based on the Heisenberg picture. In the Heisenberg picture the whole time dependence is contained inside operators ($\hat{A}_H(t)$) and the state ($|\psi(0)\rangle$) is static, time independent and corresponds to the initial conditions. To contrast the Schrodinger picture is a picture in which the operators ($\hat{A}_S$) are mostly static (they can contain explicit time dependence) and all the remaining time dependence is contained inside the state ($|\psi(t)\rangle$). The expectation value in the Heisenberg picture is:

$$\langle A(t)\rangle = \langle\psi(0)|\hat{A}_H(t)|\psi(0)\rangle \tag{1.4.1}$$

Equations of motion in the Heisenberg picture are acquired from the commutation expression assuming the Hamiltonian does not have explicit time dependence:

$$\mathrm{i}\frac{d\hat{A}}{dt} = [\hat{A}, \hat{H}]. \tag{1.4.2}$$

Here $\hat{A}$ is an arbitrary operator in the Heisenberg picture.

The goal is to calculate how molecular systems respond to external optical electric field. The related observable is polarization; the corresponding operator can be defined as:

$$\hat{\boldsymbol{P}} = \sum_n \boldsymbol{\mu}_n \hat{b}_n + \sum_n \boldsymbol{\mu}_n^\dagger \hat{b}_n^\dagger, \tag{1.4.3}$$

with expectation value:

$$\langle \boldsymbol{P}(t) \rangle = \sum_n \boldsymbol{\mu}_n \langle \hat{b}_n \rangle + \sum_n \boldsymbol{\mu}_n^\dagger \langle \hat{b}_n^\dagger \rangle. \tag{1.4.4}$$

Starting from the lowest order operators, $\hat{b}_n$, a system of differential equations known as NEE[39,40] is generated. Note that we set $\hbar = 1$, which allows frequency and energy variables to be used interchangeably. Introducing composite operators, $\hat{\sigma}_{uv} \equiv \hat{b}_u^\dagger \hat{b}_v$, $\hat{y}_{uv} \equiv \hat{b}_u \hat{b}_v$, $\hat{z}_{kuv} \equiv \hat{b}_k^\dagger \hat{b}_u \hat{b}_v$ and $\hat{g}_u = (1 - 2\eta\hat{\sigma}_{uu})$, we find the first few equations of NEE:

$$\mathrm{i}\frac{d\hat{b}_u}{dt} = \sum_n J_{un}\hat{g}_u\hat{b}_n + (1-\eta)K_u\hat{b}_u^\dagger\hat{g}_u\hat{y}_{uu} + \mu_u^-(t)\hat{g}_u, \tag{1.4.5}$$

$$\begin{aligned}\mathrm{i}\frac{d\hat{\sigma}_{uv}}{dt} =& \sum_n J_{vn}\hat{b}_u^\dagger\hat{g}_v\hat{b}_n - \sum_m J_{mu}\hat{b}_m^\dagger\hat{g}_u\hat{b}_v \\ &+ (1-\eta)K_v\hat{b}_u^\dagger\hat{\sigma}_{vv}\hat{b}_v - (1-\eta)K_u\hat{b}_u^\dagger\hat{\sigma}_{uu}\hat{b}_v \\ &+ \mu_v^-(t)\hat{b}_u^\dagger\hat{g}_v - \mu_u^+(t)\hat{g}_u\hat{b}_v,\end{aligned} \tag{1.4.6}$$

$$\begin{aligned}\mathrm{i}\frac{d\hat{y}_{uv}}{dt} =& \sum_n J_{vn}\hat{g}_v\hat{y}_{un} + \sum_n J_{un}\hat{g}_u\hat{y}_{vn} \\ &- 2\eta\delta_{uv}\sum_n J_{vn}\hat{g}_v\hat{y}_{vn} \\ &+ (1-\eta)\left(K_v\hat{\sigma}_{vv} + K_u\hat{\sigma}_{uu}\right)\hat{y}_{uv} \\ &+ (1-\eta)\delta_{uv}K_v\left(1 - \eta\left(3-2\eta\right)\hat{\sigma}_{vv}\right)\hat{y}_{vv} \\ &+ \mu_v^-(t)\hat{g}_v\hat{b}_u + \mu_u^-(t)\hat{g}_u\hat{b}_v - 2\eta\delta_{uv}\mu_v^-(t)\hat{g}_v\hat{b}_v,\end{aligned} \tag{1.4.7}$$

$$
\begin{aligned}
\mathrm{i}\frac{d\hat{z}_{kuv}}{dt} =& \sum_n J_{vn}\hat{b}_k^\dagger \hat{g}_v \hat{y}_{un} + \sum_n J_{un}\hat{b}_k^\dagger \hat{g}_u \hat{y}_{vn} \\
&- 2\eta\delta_{uv}\sum_n J_{vn}\hat{b}_k^\dagger \hat{g}_v \hat{y}_{vn} - \sum_m J_{mk}\hat{b}_m^\dagger \hat{g}_k \hat{y}_{uv} \\
&+ (1-\eta)\hat{b}_k^\dagger \left(K_v\hat{\sigma}_{vv} + K_u\hat{\sigma}_{uu} - K_k\hat{\sigma}_{kk}\right)\hat{y}_{uv} \\
&+ (1-\eta)\delta_{uv}K_v\hat{b}_k^\dagger \left(1-\eta\left(3-2\eta\right)\hat{\sigma}_{vv}\right)\hat{y}_{vv} \\
&+ \mu_v^-(t)\hat{b}_k^\dagger \hat{g}_v \hat{b}_u + \mu_u^-(t)\hat{b}_k^\dagger \hat{g}_u \hat{b}_v \\
&- 2\eta\delta_{uv}\mu_v^-(t)\hat{b}_k^\dagger \hat{g}_v \hat{b}_v - \mu_k^+(t)\hat{g}_k\hat{y}_{uv}.
\end{aligned} \tag{1.4.8}
$$

This endless hierarchy needs to be closed to be at least numerically solvable. First expectation values need to be calculated; in this work we mark expectation values dropping hats:

$$
b_u(t) \equiv \langle\hat{b}_u\rangle,\ \sigma_{uv}(t) \equiv \langle\hat{\sigma}_{uv}\rangle,\ y_{uv}(t) \equiv \langle\hat{y}_{uv}\rangle, z_{kuv}(t) \equiv \langle\hat{z}_{kuv}\rangle. \tag{1.4.9}
$$

Higher order terms are factorized into product of lower order terms, in the following equations changes such as $\langle\hat{b}_u^\dagger\hat{b}_v^\dagger\hat{b}_v\hat{b}_v\rangle \to \langle\hat{b}_u^\dagger\rangle\langle\hat{b}_v^\dagger\hat{b}_v\rangle\langle\hat{b}_v\rangle \to b_u^*\sigma_{vv}b_v$ were made, presuming that $\hat{b}_v^\dagger\hat{b}_v$ is population operator and it quickly loses coherence with other $\hat{b}_u^\dagger\hat{b}_n$ terms, while preserving operator order. More about the reasoning and validity of such simplification is described in the following chapters. In addition Certain terms were dropped with following assumptions: triple excitations are neglected, so terms like $\langle\hat{b}_u^\dagger\hat{b}_v^\dagger\hat{b}_v\hat{b}_n\hat{b}_n\rangle$, $\langle\hat{b}_u^\dagger\hat{b}_n\hat{b}_n\rangle\mu_v^-(t)$, $\langle b_k^\dagger b_v^\dagger b_v b_u\rangle\mu_v^-(t)$, and their conjugates. With all these assumptions, we arrive at such equations:

$$
\begin{aligned}
\mathrm{i}\frac{db_u}{dt} =& \sum_n J_{un}b_n - 2\eta\sum_n J_{un}z_{uun} \\
&+ (1-\eta)K_u z_{uuu} + \mu_u^-(t) - 2\eta\mu_u^-(t)\sigma_{uu},
\end{aligned} \tag{1.4.10}
$$

$$
\begin{aligned}
\mathrm{i}\frac{d\sigma_{uv}}{dt} =& \sum_n J_{vn}\sigma_{un} - \sum_m J_{mu}\sigma_{mv} \\
&- 2\eta \sum_n J_{vn} b_u^* \sigma_{vv} b_n \\
&+ 2\eta \sum_m J_{mu} b_m^* \sigma_{uu} b_v \\
&+ (1-\eta) K_v b_u^* \sigma_{vv} b_v \\
&- (1-\eta) K_u b_u^* \sigma_{uu} \sigma_v \\
&+ \mu_v^-(t) b_u^\dagger - 2\eta \mu_v^-(t) z_{uvv}^\dagger \\
&- \mu_u^+(t) b_v + 2\eta \mu_u^+(t) z_{uuv},
\end{aligned} \tag{1.4.11}
$$

$$
\begin{aligned}
\mathrm{i}\frac{dy_{uv}}{dt} =& \sum_n J_{vn} y_{un} + \sum_n J_{un} y_{vn} \\
&- 2\eta \delta_{uv} \sum_n J_{vn} y_{vn} \\
&+ (1-\eta)\delta_{uv} K_v y_{vv} \\
&+ \mu_v^-(t) b_u + \mu_u^-(t) b_v - 2\eta \delta_{uv} \mu_v^-(t) b_v,
\end{aligned} \tag{1.4.12}
$$

$$
\begin{aligned}
\mathrm{i}\frac{dz_{kuv}}{dt} =& \sum_n J_{vn} z_{kun} + \sum_n J_{un} z_{kvn} \\
&- 2\eta \delta_{uv} \sum_n J_{vn} z_{kvn} \\
&+ (1-\eta)\delta_{uv} K_v z_{kvv} - \sum_m J_{mk} z_{muv} \\
&+ \mu_v^-(t)\sigma_{ku} + \mu_u^-(t)\sigma_{kv} \\
&- 2\eta \delta_{uv} \mu_v^-(t) \sigma_{kv} - \mu_k^+(t) y_{uv}.
\end{aligned} \tag{1.4.13}
$$

Within these equations now we can observe the role of η parameter. We see that it scales anharmonicity $(1-\eta)K_u$ and affects the population saturation though transition dipole moment rescaling $(1-2\eta\sigma_{uu})\,\mu_u^-(t)$. In the test case of $\eta = 0.5$ we still have saturation of population effects (paulionic effect), but allow higher excitation with some excitation energy anharmonicity (bosonic

effect). So both effect are retained.

1.5 Relaxation in NEE

1.5.1 Linear relaxation description

The above formulation does not include dephasing and relaxation effects. To calculate realistic spectra, we need to include these effects in our equations. For this we extend the model by adding the surrounding (phonon) degrees of freedom[41]. Equations with many operators should reflect multiple excitation correlations where a broad range of relaxation processes take place. Specific requirements in the relaxation process must be fulfilled. The most important thing is the conservation of total probability in the single exciton band as the exciton lifetime is usually much longer compared to the intraband exciton relaxation.

The environment is added as an infinite set of harmonic oscillators linearly coupled to the chromophores. The oscillators then experience transition energy fluctuations, via an added system-environment Hamiltonian term:

$$\hat{H}_{SB} = \frac{1}{2}\sum_{m}\sum_{\alpha}\left[c_{m\alpha}\hat{b}_m^{\dagger}\hat{b}_m\right]\hat{Q}_{\alpha} + h.c.; \tag{1.5.1}$$

here Q_α is the coordinate of $\alpha-$the bath oscillator, $c_{m\alpha}$ is the interaction strength. We further accept the standard local-bath assumption where the bath oscillators are grouped around the chromophores and statistical properties of all sites are the same, while statistically independent. In the Heisenberg picture with respect to the bath the Hamiltonian elements become fluctuating, which can be denoted by $\tilde{J}_n(t)$ for energy fluctuations and associated with amplitudes c.

Markovian secular Redfield relaxation theory (MSRT)[42,15,43,44] at the second order with respect to the system-bath coupling is used to describe the relaxation. We start from the general expression of the combined system and bath density operator W. For the reduced dynamics $\hat{\rho} = \mathrm{Tr}_B\left(\hat{W}\right)$ in Born and Markov approximation (the bath is at thermal equilibrium, $\hat{\rho}_{eq}$, and the fluctuation correlations decay fast), we can write:

$$\frac{\mathrm{d}\hat{\rho}(t)}{\mathrm{d}t} = -\mathrm{i}\left[\hat{H}_0, \hat{\rho}(t)\right] - R^{(\rho)}\hat{\rho} \tag{1.5.2}$$

where $R^{(\rho)}$ is the relaxation superoperator given by[43]

$$\begin{aligned} R^{(\rho)}\hat{\rho} = \int_0^\infty \mathrm{d}\tau \sum_n \{ & \hat{\sigma}_{nn}\mathcal{G}(\tau)\hat{\sigma}_{nn}\mathcal{G}(-\tau)\hat{\rho}C_n(\tau) \\ & + \hat{\rho}\mathcal{G}(\tau)\hat{\sigma}_{nn}\mathcal{G}(-\tau)\hat{\sigma}_{nn}C_n^*(\tau) \\ & - \hat{\sigma}_{nn}\hat{\rho}\mathcal{G}(\tau)\hat{\sigma}_{nn}\mathcal{G}(-\tau)C_n^*(\tau) \\ & - \mathcal{G}(\tau)\hat{\sigma}_{nn}\mathcal{G}(-\tau)\hat{\rho}\hat{\sigma}_{nn}C_n(\tau)\}\,, \end{aligned} \tag{1.5.3}$$

where $\mathcal{G}(t) = \exp\left(-\mathrm{i}\hat{H}_0 t\right)$ is the propagator associated with $\hat{H}_0$ system Hamiltonian, $\hat{\sigma}_{nn} = \hat{b}_n^\dagger \hat{b}_n$, $C_n(\tau) = \langle H_{SB,n}(\tau)H_{SB,n}(0)\rangle$ is the Hamiltonian fluctuation correlation function of site n, where $\hat{H}_{SB} = \sum_n \hat{\sigma}_{nn}H_{SB,n}(\tau)$. In the above Eq. 1.5.3 we use a standard assumption of molecular aggregates that fluctuations of different sites are uncorrelated (all other types of correlation functions vanish). With these assumptions, the correlation function can be calculated[12]:

$$C_n(\tau) = \sum_\alpha \frac{c_{n\alpha}^2}{2}\left(\coth\frac{\beta\omega_\alpha}{2}\cos\omega_\alpha t - \mathrm{i}\sin\omega_\alpha t\right), \tag{1.5.4}$$

here ω_α is the frequency of a bath oscillator, $\beta = \frac{1}{k_b t}$ is parameter of bath temperature.

We take $\hat{H}_0 = \sum_{m,n} J_{mn}\hat{b}_m^\dagger \hat{b}_n$ (linear part of $\hat{H}$, without electric field terms), then $\mathcal{G}(t)$ are easy to solve and allow to acquire simple expressions.

Expressing this relaxation superoperator in eigenstate basis allows having simple expressions for propagators and allows establishing the secular relaxation terms.

It is convenient to denote the Fourier-Laplace transform of the correlation function:

$$M(\omega) = \int_0^\infty \exp(i\omega t)C(t)\,dt. \tag{1.5.5}$$

The real part of this function is responsible for energy relaxation, while the imaginary part is for the bath-induced spectral line shift. We drop assume all $C_n(t) = C(t)$ same for all sites. It is conveniently expressed by the temperature-independent fluctuation spectral density $C''(\omega)$[45,46]:

$$M(\omega) = \frac{1}{2}(1+\coth(\beta\omega/2))C''(\omega) - \mathrm{i}\int \frac{\mathrm{d}\omega'}{2\pi}\frac{1+\coth(\beta\omega'/2)}{\omega'-\omega}C''(\omega'). \quad (1.5.6)$$

Next, we take inspiration from 1.5.3, and extend the idea for NEE equations. In Fig. 1.5.1a) we show all diagrams reflecting the secular system-bath interaction configurations in eigenstate basis corresponding to Eq. 1.5.3. Starting from the density matrix element ab or aa on the bottom of a diagram we have interactions with the phonon field on the left or on the right, denoted by curvy lines, and arrive at the final configuration. Two diagrams in the middle contribute to energy relaxation (or transfer, if taken in real space), and two others contribute to population or coherence decay.

The NEE variables are equivalent to specific blocks of the system density matrix at low excitation intensity. For example, b variables denote projectors $|0\rangle\langle e|$, $|e\rangle\langle f|$, etc. where $|e\rangle$ denote singly excited states, $|f\rangle$ - double, hence they reflect the corresponding blocks of the system density matrix. Similarly, $\hat{\sigma} = \hat{b}^\dagger\hat{b}$ is the single exciton $|e\rangle\langle e'|$ density matrix in the electronic excited band. We can thus use the general relaxation superoperator expressions specific to these blocks for the NEE variables.

However, to calculate the complete set of propagators entering Eq. 1.5.3, we need to consider multi-exciton blocks of the Hamiltonian. The single exciton block is relatively simple. In the site basis this block is defined by the matrix J and the single exciton eigenstates are given by

$$\sum_n J_{mn}\theta_{n,a} = J_a\theta_{m,a}, \quad (1.5.7)$$

where J_a is the a-th exciton energy and $\theta_{m,a}$ is the exciton wavevector. However, computing eigenstates of the double, triple, and more exciton blocks is not a simple task when the number of sites is large. As the NEE variables encode the infinite set of blocks with ever increasing number of excitations, to avoid computation of multi-exciton eigen states, we make an additional approximation that the system anharmonicities (Pauli blocking in our particular case) are excluded when computing the relaxation superoperators (the Pauli exclusion is included in the equations of motion). Notice that this does not interfere with EEA since the EEA is interband process, while the energy relaxation here is considered within one band. In this way the coherent (no bath) multi-particle

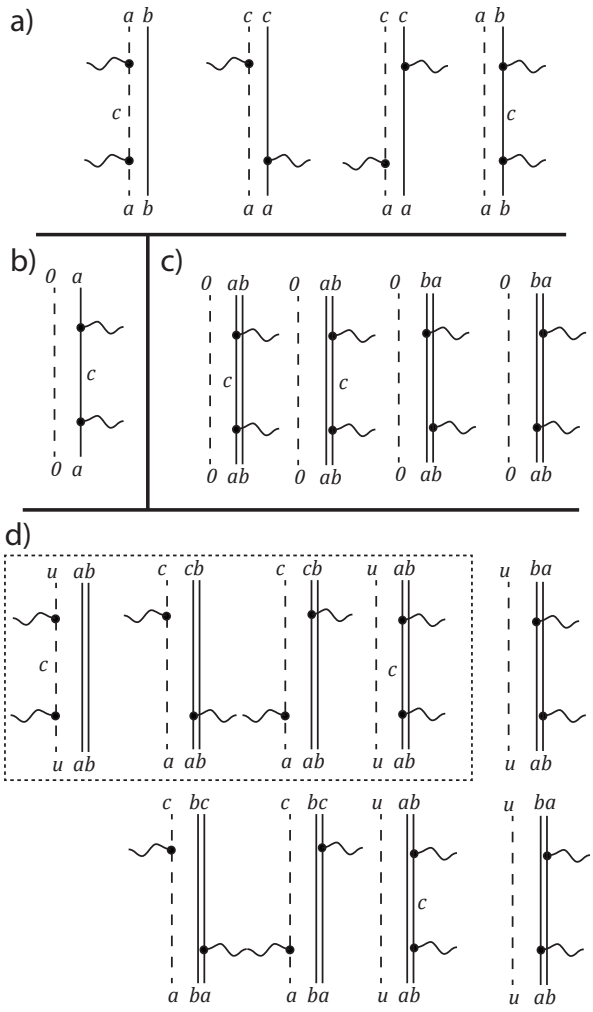

Figure 1.5.1: Feynman diagrams reflecting the system-bath interaction configurations for (a) general reduced density matrix, (b) b variable, (c) y variable, (d) z variable. Wavy lines represent interactions with the bath (phonons). The letters at the bottom and the top of each diagram represent states before and after interactions, respectively. Final state indices are specifically chosen for secular interactions. Notice that changes of states originate due to off diagonal interaction with phonons, while the diagonal interaction would not cause a change of state. As the phonon bandwidth is much smaller than the optical bandwidth, all states (apart from ground state 0) are inside the single exciton band.

propagators with respect to $\hat{H}_0$ (Eqs. 1.4.10-1.4.13) become equal to products of single particle propagators and the relaxation and multi-exciton blocks reduce to the single-exciton blocks $|0\rangle\langle e|$ and $|e\rangle\langle e'|$. Hence, denoting

$$b(t) = \mathcal{G}_1^{(b)}(t)b(0) \tag{1.5.8}$$

we write

$$\mathcal{G}_{1,2}^{(bb)} = \mathcal{G}_1^{(b)}\mathcal{G}_2^{(b)} \tag{1.5.9}$$

$$\mathcal{G}_{1,2}^{(b^\dagger b)} = \mathcal{G}_1^{(b)*}\mathcal{G}_2^{(b)} \tag{1.5.10}$$

$$\mathcal{G}_{1,2,3}^{(b^\dagger bb)} = \mathcal{G}_1^{(b)*}\mathcal{G}_2^{(b)}\mathcal{G}_3^{(b)} \tag{1.5.11}$$

and so on. The subscripts of the propagators denote the exciton index (as of independent quasi-particle) in the composite multi-particle state. In diagrammatic representation now some lines of two or more particles in Fig. 1.5.1a) split in two due to propagator factorization, i. e. the double-exciton state is represented by two exciton particles. Consequently, in the one-exciton eigenstate basis we find the following secular relaxation terms for the b variable (Fig. 1.5.1b) coming from a single diagram

$$R_{a,a}^{exc(b)} \quad = \quad \sum_c \Lambda_{acca} M(\omega_{ca}). \tag{1.5.12}$$

the Λ_{abcd} is the exciton overlap tensor $\Lambda_{abcd} = \sum_u \theta_{u,a}\theta_{u,b}\theta_{u,c}\theta_{u,d}$. Diagrams for y variable are shown in Fig. 1.5.1c). Based on the diagrams we can count the non vanishing terms and write the expression for the secular relaxation terms:

$$R_{ab,ab}^{exc(y)} = R_{a,a}^{exc(b)} + R_{b,b}^{exc(b)} + 2\Lambda_{aabb} M(0),\ a \neq b. \tag{1.5.13}$$

$$R_{ab,ba}^{exc(y)} = \Lambda_{abba}\left(M(\omega_{ab}) + M(\omega_{ba})\right),\ a \neq b. \tag{1.5.14}$$

$$R_{aa,aa}^{exc(y)} = 2R_{aa}^{exc(b)} + 2\Lambda_{aaaa} M(0). \tag{1.5.15}$$

It may seem surprising that $R_{ab,ab}^{exc(y)}$ and $R_{ab,ba}^{exc(y)}$ are different, however this is the consequence of factorization of the exciton propagator. So, the sum $R_{ab,ab}^{exc(y)} + R_{ab,ba}^{exc(y)}$ enters the final equation of motion, which means that $y_{ab} = y_{ba}$ is kept.

The variable $\sigma \equiv \langle \hat{b}^\dagger \hat{b} \rangle$ corresponds to the full one-exciton block of the density matrix so its relaxation operator contains the standard terms of the popu-

lation transport and of the coherence decay terms. For $a \neq b$ we have:

$$R^{exc(\sigma)}_{aa,bb} = -k_{ab}, \tag{1.5.16}$$

where $k_{ab} = 2\Lambda_{abba}\Re M(\omega_{ba})$ is the rate of population transfer from b to a,

$$R^{exc(\sigma)}_{ab,ab} = R^{exc(b)*}_{a,a} + R^{exc(b)}_{b,b} \tag{1.5.17}$$

and for diagonal population terms we have $R^{(\sigma)}_{aa,aa} \equiv k_{aa} = \sum_c^{c\neq a} k_{ca}$.

Variable $z \equiv \langle \hat{b}^\dagger \hat{b} \hat{b} \rangle$ is factorized as shown in Fig. 1.5.1d) so, we get contributions to relaxation from nine diagrams. These diagrams can be grouped to represent the terms that are the same as in y and σ variables. For example, the dotted lines encircle the same diagrams as in Fig.1.5.1a) where one exciton is not affected by the interactions. We group the result into the following set of terms:

$$R^{exc(z)}_{uua,vva} = R^{exc(z)}_{uua,vav} = R^{exc(z)}_{uau,vav} = R^{exc(z)}_{uau,vva} = -k_{uv},\ u \neq v \tag{1.5.18}$$

$$R^{exc(z)}_{uua,uua} = R^{exc(z)}_{uau,uau} = k_{uu} + R^{exc(b)}_{a,a},\ u \neq a \tag{1.5.19}$$

$$R^{exc(z)}_{uua,uau} = R^{exc(z)}_{uau,uua} = X_{uuaa}(M(\omega_{au}) + M(\omega_{ua})),\ u \neq a \tag{1.5.20}$$

$$R^{exc(z)}_{uuu,uuu} = k_{uu} + R^{(b)}_{u,u}, \tag{1.5.21}$$

finally for $u \neq a$, $u \neq b$

$$\begin{aligned} R^{exc(z)}_{uab,uab} =& R^{exc(b)*}_{u,u} + R^{exc(b)}_{a,a} + R^{exc(b)}_{b,b} \\ &+ 2(\Lambda_{aabb} - \Lambda_{uuaa} - \Lambda_{uubb})M(0), \end{aligned} \tag{1.5.22}$$

$$R^{exc(z)}_{uab,uba} = \Lambda_{abba}\left(M(\omega_{ab}) + M(\omega_{ba})\right). \tag{1.5.23}$$

By grouping terms:

$$\begin{aligned} R_{2,uab} =& R^{exc(b)*}_{u,u} + R^{exc(b)}_{a,a} + R^{exc(b)}_{b,b} \\ &+ 2(\Lambda_{aabb} - \Lambda_{uuaa} - \Lambda_{uubb})M(0) \\ &+ (1-\delta_{a,b})\Lambda_{abba}(M(\omega_{ab}) + M(\omega_{ba})), \end{aligned} \tag{1.5.24}$$

$$R_{1,a} = R^{exc(b)*}_{a,a} + R^{exc(b)}_{a,a} - 3k_{aa} - 2\Lambda_{aaaa}M(0). \tag{1.5.25}$$

A cleaner representation **in exciton basis** can be acquired:

$$\begin{aligned} i\frac{dz_{uab}}{dt} =& ... - iR_{2,uab}z_{uab} - i\delta_{ua}k_{ub}z_{bbb} \\ &+ i\delta_{ua}R_{1,u}z_{uub} + i\delta_{ub}R_{1,u}z_{uau} \\ &+ i\delta_{ua}\sum_{l} 2k_{ul}z_{llb} - i\delta_{ua}\delta_{ub}R_{1,u}z_{uuu} \\ &+ i\delta_{ub}\sum_{l} 2k_{ul}z_{lal} - i\delta_{ub}k_{ua}z_{aaa}. \end{aligned} \tag{1.5.26}$$

This description can be simplified by forcing the triple quantum coherence description with $R^{exc(z)}_{abcabc} = (R^{(b)}_a)^* + R^{(b)}_b + R^{(b)}_c$. The "full" model is numerically unstable for larger systems of fully paulionic type of particles, while the simplified model works for an arbitrary system (section 2.2).

For NEE in site basis, relaxation terms are transformed into the site basis as follows:

$$R^{(b)}_{n,m} = \sum_a \theta_{n,a}\theta_{m,a}R^{exc(b)}_{a,a}, \tag{1.5.27}$$

$$R^{(y)}_{nm,n'm'} = \sum_{a,b,c,d} \theta_{n,a}\theta_{m,b}\theta_{n',c}\theta_{m',d}R^{exc(y)}_{ab,cd}, \tag{1.5.28}$$

$$R^{(\sigma)}_{nm,n'm'} = \sum_{a,b,c,d} \theta_{n,a}\theta_{m,b}\theta_{n',c}\theta_{m',d}R^{exc(\sigma)}_{ab,cd}, \tag{1.5.29}$$

$$R^{(z)}_{nml,n'm'l'} = \sum_{a,b,c,d,f,g} \theta_{n,a}\theta_{m,b}\theta_{l,c}\theta_{n',d}\theta_{m',f}\theta_{l',g}R^{exc(z)}_{abc,dfg}. \tag{1.5.30}$$

And these term are added to NEE **in site basis**:

$$\frac{\mathrm{d}b_u}{\mathrm{d}t} = \ldots - R^{(b)}_{u,u'} b_{u'}, \tag{1.5.31}$$

$$\frac{\mathrm{d}\sigma_{uv}}{\mathrm{d}t} = \ldots - R^{(\sigma)}_{uv,u'v'} \sigma_{u'v'}, \tag{1.5.32}$$

$$\frac{\mathrm{d}y_{uv}}{\mathrm{d}t} = \ldots - R^{(y)}_{uv,u'v'} y_{u'v'}, \tag{1.5.33}$$

$$\frac{\mathrm{d}z_{kuv}}{\mathrm{d}t} = \ldots - R^{(z)}_{kuv,k'u'v'} z_{k'u'v'}. \tag{1.5.34}$$

1.5.2 Exciton-exciton annihilation

EEA is a process that causes nonlinear excitation population decay[20]. In this work phenomenological interband relaxation process for EEA is used as outlined in ref.[9]. At high excitation intensity multiparticle excitations should be expected, however, then EEA will quench the excitations. The process reflects the molecular internal conversion process when the molecule is doubly excited into highly excited molecular states. When the internal conversion process is fast compared to intermolecular exciton hopping rate we can use our formalism and the EEA process can be represented as an incoherent distance dependent transition $\alpha(|\boldsymbol{r}_m - \boldsymbol{r}_n|)\hat{b}^\dagger_m \hat{b}_m \hat{b}^\dagger_n \hat{b}_n \rightarrow \hat{b}^\dagger_n \hat{b}_n$, where we have $m \neq n$, $\alpha(|\boldsymbol{r}_m - \boldsymbol{r}_n|) \equiv \alpha(r_{mn})$ is the amplitude of the process depending on the distance between sites m and n. For the weak intermolecular coupling. the function $\alpha(r_{mn})$ can be taken as the Förster excitation transfer rate[21,26]. If the sites are tightly packed in the real space so that the nearest-neighbor distance can be defined, the rate of the process on site m can be associated with the nearest neighbors, $\alpha(r_{mn}) = \kappa_0 \delta^{(n-n)}_{mn}$. Here $\delta^{(n-n)}_{mn}$ is equal to 1, when m and n are nearest neighbours and 0 otherwise, κ_0 is the annihilation parameter.

It should be noted that this decay channel contributes to the "lifetime" broadening of all related coherences, according to well-known relation: the lifetime-related decay rate for coherence mn is $\tau^{-1}_{mn} = (k_{mm} + k_{nn})/2$[43], where $k_{mm} = \kappa_0 \sum_{\mathrm{n-n}} \sigma_{nn}$, the sum is over the nearest neighbors.

With this EEA behavior in NEE can be achieved with terms in form as[9]:

$$\frac{\mathrm{d}A_{nk\ldots}}{\mathrm{d}t} = \ldots - \frac{\kappa_0}{2} \sum_m \sigma_{mm}(G_{mn} + G_{mk} + \ldots) A_{nk\ldots}. \tag{1.5.35}$$

Here on the left side $nk\ldots$ denotes an arbitrary set of indices and then on the

right side for each of them we have a term like G_{mn}, where $G_{mn} = (\delta_{mn}^{(n-n)} + \delta_{mn})$, which has in addition self-site annihilation. This scheme is in accord with previous models, e. g. $dn/dt \sim -n^2$, which have been used in pump-probe spectra analysis and supported by experiments (see e.g., ref. [18,25]).

This description of EEA applies to the site basis and thus can be efficiently used in site basis equations of motion.

$$\frac{\mathrm{d}b_u}{\mathrm{d}t} = \ldots - \frac{\kappa_0}{2} \sum_m \sigma_{mm} G_{mu} b_u, \tag{1.5.36}$$

It should be noted that $\sigma_{nn} b_u$ is about the same order as z_{nnu} to the optical field. Thus, in a pump-probe experiment where first order terms cancel out, if κ is comparable to J then there can be a significant effect on pump-probe spectra from EEA terms even at low excitation intensities compared to when EEA is not included. This should not be surprising as the excited state absorption is related to the properties of two excitons, i. e. the EEA contributes to broadening of the excited state absorption lineshape. For the σ variables the EEA enters at the fourth order:

$$\frac{\mathrm{d}\sigma_{uv}}{\mathrm{d}t} = \ldots - \frac{\kappa_0}{2} \sum_m \sigma_{mm} (G_{mu} + G_{mv}) \sigma_{uv}, \tag{1.5.37}$$

$$\frac{\mathrm{d}y_{uv}}{\mathrm{d}t} = \ldots - \frac{\kappa_0}{2} \sum_m \sigma_{mm} (G_{mu} + G_{mv}) y_{uv}, \tag{1.5.38}$$

$$\frac{\mathrm{d}z_{kuv}}{\mathrm{d}t} = \ldots - \frac{\kappa_0}{2} \sum_m \sigma_{mm} (G_{mk} + G_{mu} + G_{mv}) z_{kuv}. \tag{1.5.39}$$

Notice that the product σz implies the fifth order relaxation process, while $\sigma\sigma$ is the fourth order process.

1.6 Closing NEE for numerical calculations

NEE equation factorization is employed to close the hierarchy at a specific selected level. This reduces the complexity of calculations and computational costs but may remove or add new behavior to spectroscopic results. For example, a simple factorization:

$$\langle \hat{b}_k^\dagger \hat{b}_n^\dagger \hat{b}_k \hat{b}_n \hat{b}_n \rangle = \sigma_{kk} z_{nnn} \tag{1.6.1}$$

neglects operator order, which becomes significant when $k = n$. However, when $k \neq n$ we find isolated population of $k-$th chromophore and the remaining are characteristics of $n-$the chromophore. In contrast a different factorization seems more appropriate for other indices:

$$\langle \hat{b}_n^\dagger \hat{b}_n^\dagger \hat{b}_m \hat{b}_m \hat{b}_l \rangle = y_{nn}^* y_{mm} b_l. \tag{1.6.2}$$

Here the operator order is preserved, but another crucial difference is that the latter description considers all variables as optical coherence terms. It can be expected that the terms related to populations (factorized in the former way) would persist longer compared to later factorization into coherences. In both these cases another effect is neglected, when $k = n = m = l$, where variable $\langle \hat{b}_n^\dagger \hat{b}_n^\dagger \hat{b}_n \hat{b}_n \hat{b}_n \rangle$ is essentially the optical coherence between 2-nd and 3-rd molecular excitations. Notice that the variable $\hat{b}_n \hat{b}_n \hat{b}_n$ is the triple excitation coherence and by factorizing the variable we may lose associated resonances that could be controlled by paulionicity or bosonicity.

Factorization of high order variables additionally allows to avoid deriving relaxation rates for higher order terms. For the lower order terms Redfield relaxation rates are easily expressed in exciton basis. In the site basis the terms are cumbersome and quickly become computationally excessive when calculating the higher order terms.

Next we will present several possible schemes for closing NEE at various levels of complexity.

1.6.1 Complete factorization

The complete factorization of all variables into the smallest possible $b(t)$ variables allow to have very compact form of the equations,

$$\begin{aligned} \mathrm{i}\frac{db_u}{dt} =& (1 - 2\eta b_u^* b_u) \left(\sum_n J_{un} b_n + (1-\eta) K_u b_u^* b_u^2 + \mu_u^-(t) \right) \\ &+ \mathrm{i} \sum_n R_{u,n}^{(b)} b_n - \mathrm{i}\frac{\kappa_0}{2} \sum_n b_n^* b_n G_{nu} b_u. \end{aligned} \tag{1.6.3}$$

This equation describes coupled nonlinear oscillators. It is remarkable that the chromophoric anharmonicities are still included as well as excitation amplitude nonlinearity via $(1 - 2\eta b_u^* b_u)$ term. However, the double-excitation energy of oscillators is included approximately. Notice that a similar approach has been used to describe highly nonlinear excitations of carbon nanotubes[47].

1.6.2 Restricted coherent state factorization

If the system remains coherent, the wavefunction description is completely valid and daggered and non-daggered operators evolve independently. This can be utilized to describe resonances up to double excitations by using only two equations[9]:

$$\begin{aligned}
\mathrm{i}\frac{db_u}{dt} =& \sum_n J_{un}\left(b_n - 2\eta b_u^* y_{un}\right) + \mu_u^-(t)\left(1 - 2\eta b_u^* b_u\right) \\
&+ (1-\eta)K_u\left(b_u^* y_{uu} - 2\eta y_{uu}^* y_{uu} b_u\right) \\
&- \mathrm{i}\sum_n R_{un}^{(b)} b_n - \mathrm{i}\frac{\kappa_0}{2}\sum_n b_n^* G_{nu} y_{nu},
\end{aligned} \tag{1.6.4}$$

$$\begin{aligned}
\mathrm{i}\frac{dy_{uv}}{dt} =& \sum_n J_{vn}\left(1 - 2\eta b_v^* b_v\right) y_{un} + \sum_n J_{un}\left(1 - 2\eta b_u^* b_u\right) y_{vn} \\
&- 2\eta\delta_{uv}\sum_n J_{vn}\left(1 - 2\eta b_v^* b_v\right) y_{vn} \\
&+ \mu_v^-(t)\left(b_u - 2\eta b_v^* y_{vu}\right) + \mu_u^-(t)\left(b_v - 2\eta b_u^* y_{uv}\right) \\
&- 2\delta_{uv}\eta\mu_v^-(t)\left(b_v - 2\eta b_v^* y_{vv}\right) \\
&+ (1-\eta)\left(K_v b_v^* b_v + K_u b_u^* b_u\right)\hat{y}_{uv} \\
&+ (1-\eta)\delta_{uv}K_v\left(1 - \eta(3-2\eta)b_v^* b_v\right) y_{vv} \\
&- \mathrm{i}\sum_{n,m} R_{uv,nm}^{(y)} y_{nm} \\
&- \mathrm{i}\frac{\kappa_0}{2}\sum_n b_n^* b_n G_{nu} y_{uv} - \mathrm{i}\frac{\kappa_0}{2}\sum_n b_n^* b_n G_{nv} y_{uv}.
\end{aligned} \tag{1.6.5}$$

Here $\langle \hat{b}_v \hat{b}_u \hat{b}_n \rangle = b_v y_{un}$ is additionally factorized by neglecting triple coherences; the annihilation terms were replaced by changing $\sigma_{nm} = b_n^* b_m$. Notice that factorization of conjugated and not conjugated operators holds in the pure state limit, when the system is described by a wavefunction; the bra and ket wavefunctions then propagate independently, so conjugated and not conjugated variables become independent. We call this limit completely coherent. It can be considered only at low temperatures or at short times when the system is in a complete coherent state.

In molecular systems exciton decoherence usually plays an important role, the system turns into the mixed state; the coherent model becomes insufficient. σ and z variables include the exciton population variables when bra and ket

states become correlated, and thus including these variables in the models is highly desirable, when applying the equations to realistic molecular systems.

1.6.3 Direct factorization

Another alternative is retaining σ and y, using $\hat{g}_v = (1 - 2\eta\hat{\sigma}_{vv})$ as a hint for factorization. So, as a first step all populations are identified and isolated. Retaining σ means keeping population-induced effects, which last longer than coherences. This type of factorization should be more suitable for experiments that deal with delay times longer than coherence times. The following set of three equations are obtained:

$$\begin{aligned}
\mathrm{i}\frac{db_u}{dt} =& \sum_n J_{un}\left(1 - 2\eta\sigma_{uu}\right) b_n + (1-\eta)K_u\sigma_{uu}b_u \\
&- 2\eta(1-\eta)K_u b_u^*\sigma_{uu}y_{uu} + \mu_u^-(t)\left(1 - 2\eta\sigma_{uu}\right) \\
&- i\sum_n R_{u,n}^{(b)} b_n - i\frac{\kappa_0}{2}\sum_n \sigma_{nn}G_{nu}b_u,
\end{aligned} \tag{1.6.6}$$

$$\begin{aligned}
\mathrm{i}\frac{d\sigma_{uv}}{dt} =& \sum_n J_{vn}\left(\sigma_{un} - 2\eta b_u^*\sigma_{vv}b_n\right) \\
&- \sum_n J_{nu}\left(\sigma_{nv} - 2\eta b_n^*\sigma_{uu}b_v\right) \\
&- i\sum_{n,m} R_{uv,mn}^{(\sigma)}\sigma_{mn} - i\frac{\kappa_0}{2}\sum_n \sigma_{nn}(G_{un} + G_{vn})\sigma_{uv} \\
&+ (1-\eta)K_v b_u^*\sigma_{vv}b_v - (1-\eta)K_u b_u^*\sigma_u b_v \\
&+ \mu_v^-(t)b_u^*\left(1 - 2\eta\sigma_{vv}\right) \\
&- \mu_u^*(t)\left(1 - 2\eta\sigma_{uu}\right) b_v,
\end{aligned} \tag{1.6.7}$$

$$
\begin{aligned}
\mathrm{i}\frac{dy_{uv}}{dt} =& \sum_n J_{vn}\left(1-2\eta\sigma_{vv}\right)y_{un} + \sum_n J_{un}\left(1-2\eta\sigma_{uu}\right)y_{vn} \\
&- i\sum_{n,m} R^{(y)}_{uv,mn}y_{mn} - i\frac{\kappa_0}{2}\sum_n \sigma_{nn}(G_{un}+G_{vn})y_{uv} \\
&- 2\eta\sum_n \delta_{uv}J_{vn}\left(1-2\eta\sigma_{vv}\right)y_{vn} \\
&+ \mu^-_v(t)\left(1-2\eta\sigma_{vv}\right)b_u + \mu^-_u(t)\left(1-2\eta\sigma_{uu}\right)b_v \\
&- 2\delta_{uv}\eta\mu^-_v(t)\left(1-2\eta\sigma_{vv}\right)b_v \\
&+ (1-\eta)\left(K_v\sigma_{vv}+K_u\sigma_{uu}\right)y_{uv} \\
&+ (1-\eta)\delta_{uv}K_v\left(1-\eta(3-2\eta)\sigma_{vv}\right)y_{vv}. \qquad (1.6.8)
\end{aligned}
$$

1.6.4 3rd order models

The following factorization model keeps at least 3rd order terms "whole" and factorizes all higher order terms in specific schemes. The third order is the lowest nonlinear order process in isotropic samples. Therefore, by keeping at least third order variables the "whole" previously known features should be kept and then factorization affects only higher order terms.

All the following models rely on the following form of the NEE:

$$
\begin{aligned}
\mathrm{i}\frac{db_u}{dt} =& \sum_n J_{un}b_n - 2\eta\sum_n J_{un}z_{uun} + (1-\eta)K_u z_{uuu} \\
&+ \mu^-_u(t) - 2\eta\mu^-_u(t)\sigma_{uu} \\
&- i\sum_n R^{(b)}_{u,n}b_n - i\frac{\kappa_0}{2}\sum_n \sigma_{nn}G_{nu}b_u \\
&+ b^{(5)}_u, \qquad (1.6.9)
\end{aligned}
$$

$$
\begin{aligned}
\mathrm{i}\frac{d\sigma_{uv}}{dt} =& \sum_n J_{vn}\sigma_{un} - \sum_n J_{nu}\sigma_{nv} \\
&- i\sum_{n,m} R^{(\sigma)}_{uv,mn}\sigma_{mn} - i\frac{\kappa_0}{2}\sum_n \sigma_{nn}(G_{un}+G_{vn})\sigma_{uv} \\
&+ \mu^-_v(t)b^*_u - \mu^+_u(t)b_v \\
&+ \sigma^{(4)}_{uv}, \qquad (1.6.10)
\end{aligned}
$$

$$
\begin{aligned}
\mathrm{i}\frac{dy_{uv}}{dt} =& \sum_n J_{vn} y_{un} + \sum_n J_{un} y_{vn} - \sum_n 2\eta\delta_{uv} J_{vn} y_{vn} \\
& - i\sum_n R^{(y)}_{uv,mn} y_{mn} - i\frac{\kappa_0}{2}\sum_n \sigma_{nn}(G_{un} + G_{vn}) y_{uv} \\
& + (1-\eta)\delta_{uv} K_v y_{vv} \\
& + \mu_v^-(t) b_u + \mu_u^-(t) b_v - 2\eta\delta_{uv}\mu_v^-(t) b_v \\
& + y^{(4)}_{uv},
\end{aligned} \tag{1.6.11}
$$

$$
\begin{aligned}
\mathrm{i}\frac{dz_{kuv}}{dt} =& \sum_n J_{vn} z_{kun} + \sum_n J_{un} z_{kvn} - 2\eta\delta_{uv}\sum_n J_{vn} z_{kvn} \\
& - i\sum_{k',n,m} R^{(z)}_{kuv,k'mn} z_{k'mn} \\
& - i\frac{\kappa_0}{2}\sum_n \sigma_{nn}(G_{kn} + G_{un} + G_{vn}) z_{kuv} \\
& - \sum_n J_{nk} z_{nuv} + (1-\eta)\delta_{uv} K_v z_{kvv} \\
& + \mu_v^-(t)\sigma_{ku} + \mu_u^-(t)\sigma_{kv} - 2\eta\delta_{uv}\mu_v^-(t)\sigma_{kv} \\
& - \mu_k^*(t) y_{uv} + 2\eta\mu_k^*(t) z_{kuv} b_k \\
& + z^{(5)}_{kuv}.
\end{aligned} \tag{1.6.12}
$$

Here $b^{(5)}$ and $z^{(5)}$ are the fifth order corrections, while $y^{(4)}$ and $\sigma^{(4)}$ are the fourth order corrections.

In the present case the main downside compared to simpler models is the need for $R^z_{kmn,luv}$ relaxation terms, which come from the Redfield relaxation theory. Annihilation terms are kept the same for all models.

1.6.4.1 $z\sigma$ factorization model

In the next factorization model, which is denoted as $z\sigma$ based factorization, all terms higher than 3rd order are factorized in terms of σ and lower order variables. From the set of the above-given NEE we end up with high order corrections.

$$
b^{(5)}_u = -2\eta(1-\eta) K_u \sigma_{uu} z_{uuu}, \tag{1.6.13}
$$

$$\begin{aligned}\sigma_{uv}^{(4)} =& -2\eta \sum_n J_{vn}\sigma_{vv}\sigma_{un} - 2\eta \sum_n J_{nu}\sigma_{uu}\sigma_{nv} \\ &+ (1-\eta)\left(K_v\sigma_{vv} - K_u\sigma_{uu}\right)\sigma_{uv} \\ &- 2\eta\mu_v^-(t)z_{uvv}^* + 2\eta\mu_u^+(t)z_{uuv},\end{aligned} \tag{1.6.14}$$

$$\begin{aligned}y_{uv}^{(4)} =& -2\eta \sum_n J_{un}\sigma_{uu}y_{vn} - 2\eta \sum_n J_{vn}\sigma_{vv}y_{un} \\ &+ (1-\eta)\left(K_v\sigma_{vv} + K_u\sigma_{uu}\right)y_{uv} \\ &- \eta(2\eta-3)(\eta-1)\delta_{uv}K_v\sigma_{vv}y_{vv} \\ &- 2\eta\mu_u^-(t)z_{uuv} - 2\eta\mu_v^-(t)z_{vvu} \\ &+ 4\eta^2\delta_{uv}\sum_n J_{vn}\sigma_{vv}y_{vn} + 4\eta^2\delta_{uv}\mu_v^-(t)z_{vvv},\end{aligned} \tag{1.6.15}$$

$$\begin{aligned}z_{kuv}^{(5)} =& 2\eta \sum_n J_{nk}\sigma_{kk}z_{nuv} - 2\eta \sum_n J_{un}\sigma_{uu}z_{kvn} \\ &- 2\eta \sum_n J_{vn}\sigma_{vv}z_{kun} + 2\eta\mu_k^+(t)\sigma_{kk}y_{uv} \\ &+ (1-\eta)\left(K_v\sigma_{vv} + K_u\sigma_{uu} - K_k\sigma_{kk}\right)z_{kuv} \\ &- \eta(2\eta-3)(\eta-1)\delta_{uv}K_v\sigma_{vv}z_{kvv} \\ &- 2\eta\mu_u^-(t)\sigma_{uu}\sigma_{kv} - 2\eta\mu_v^-(t)\sigma_{vv}\sigma_{ku} \\ &+ 4\eta^2\delta_{uv}\sum_n J_{vn}\sigma_{vv}z_{kvn} + 4\eta^2\delta_{uv}\mu_v^-(t)\sigma_{vv}\sigma_{kv}.\end{aligned} \tag{1.6.16}$$

The terms like $\langle \hat{b}_u^\dagger \hat{b}_v^\dagger \hat{b}_v \hat{b}_n \rangle$ are factorized like $\sigma_{vv}\sigma_{un}$, with the assumption that $\langle \hat{b}_v^\dagger \hat{b}_v \rangle$ is population and it quickly loses coherence with other terms.

1.6.4.2 zz factorization model

Alternative is to factorize all terms higher than 3rd order in terms of z and lower order terms. Compared to the $z\sigma$ factorization scheme the operator order in zz factorization is preserved. The main difference from $z\sigma$ model is then related to preserving more of the double coherence terms as these are all split apart in other models.

$$b_u^{(5)} = -2\eta(1-\eta)K_u z_{uuu}^* y_{uu}, \tag{1.6.17}$$

$$\begin{aligned}\sigma_{uv}^{(4)} =& -2\eta\sum_n J_{vn}z_{uvv}^* b_n + 2\eta\sum_n J_{nu}b_n^* z_{uuv}\\ &+(1-\eta)K_v b_u^* z_{vvv} - (1-\eta)K_u z_{uuu}^* b_v\\ &-2\eta\mu_v^-(t)z_{uvv}^* + 2\eta\mu_u^+(t)z_{uuv},\end{aligned} \tag{1.6.18}$$

$$\begin{aligned}y_{uv}^{(4)} =& -2\eta\sum_n J_{un}z_{uuv}b_n - 2\eta\sum_n J_{vn}z_{vuv}b_n\\ &-\eta(2\eta-3)(\eta-1)\delta_{uv}K_v z_{vvv}b_v\\ &+(1-\eta)K_v z_{vvv}b_u + (1-\eta)K_u z_{uuu}b_v\\ &-2\eta\mu_u^-(t)z_{uuv} - 2\eta\mu_v^-(t)z_{vvu}\\ &+4\eta^2\delta_{uv}\sum_n J_{vn}z_{vvv}b_n + 4\eta^2\delta_{uv}\mu_v^-(t)z_{vvv},\end{aligned} \tag{1.6.19}$$

$$\begin{aligned}z_{kuv}^{(5)} =& 2\eta\sum_n J_{nk}z_{nkk}^* y_{uv} - 2\eta\sum_n J_{un}z_{kuu}^* y_{vn}\\ &-2\eta\sum_n J_{vn}z_{kvv}^* y_{un} - (1-\eta)K_k z_{kkk}^* y_{uv}\\ &-2\eta\mu_u^-(t)b_k^* z_{uuv} - 2\eta\mu_v^-(t)b_k^* z_{vuv}\\ &(1-\eta)\left(K_v z_{kvv}^* + K_u z_{kuu}^*\right)y_{uv}\\ &+4\eta^2\delta_{uv}\sum_n J_{vn}z_{kvv}^* y_{vn} + 4\eta^2\delta_{uv}\mu_v^-(t)b_k^* z_{vvv}\\ &-\eta(2\eta-3)(\eta-1)\delta_{uv}K_v z_{kvv}^* y_{vv}.\end{aligned} \tag{1.6.20}$$

1.6.4.3 zn factorization

Noting the "natural" structure that come from commutation relation $\hat{g}_u = (1-2\eta\hat{\sigma}_{uu})$, and prioritizing to keep the σ_{uu}, and preserve the order of operators, for example: $\langle\hat{b}_u\hat{b}_u^\dagger\hat{b}_u\hat{b}_u^\dagger\hat{b}_u^\dagger\rangle \to b_u^*\sigma_{uu}y_{uu}$ we find a factorization scheme which should give similar results to zz scheme:

$$b_u^{(5)} \;=\; -2\eta(1-\eta)K_u b_u^*\sigma_{uu}y_{uu}, \tag{1.6.21}$$

$$\begin{aligned}\sigma_{uv}^{(4)} =& -2\eta\sum_n J_{vn}b_u^*\sigma_{vv}b_n - 2\eta\sum_n J_{nu}b_n^*\sigma_{uu}b_v \\ &+ (1-\eta)K_v b_u^*\sigma_{vv}b_v - (1-\eta)K_u b_u^*\sigma_{uu}b_v \\ &- 2\eta\mu_v^-(t)z_{vvu}^* + 2\eta\mu_u^+(t)z_{uuv},\end{aligned} \tag{1.6.22}$$

$$\begin{aligned}y_{uv}^{(4)} =& -2\eta\sum_n J_{vn}\sigma_{vv}y_{un} - 2\eta\sum_n J_{un}\sigma_{uu}y_{vn} \\ &- (1-\eta)\eta(3-2\eta)\delta_{uv}K_v\sigma_{vv}y_{vv} \\ &+ (1-\eta)\left(K_v\sigma_{vv} + K_u\sigma_{uu}\right)y_{uv} \\ &- 2\eta\mu_v^-(t)z_{vvu} - 2\eta\mu_u^-(t)z_{uuv} \\ &+ 4\eta^2\delta_{uv}\sum_n J_{vn}\sigma_{vv}y_{vn} + 4\eta^2\delta_{uv}\mu_v^-(t)z_{vvv},\end{aligned} \tag{1.6.23}$$

$$\begin{aligned}z_{kuv}^{(5)} =& -2\eta\sum_n J_{vn}b_k^*\sigma_{vv}y_{un} - 2\eta J_{un}b_k^*\sigma_{uu}y_{vn} \\ &+ 2\eta\sum_n J_{nk}b_n^*\sigma_{kk}y_{uv} + 2\eta\mu_k^+(t)\sigma_{kk}y_{uv} \\ &- 2\eta\mu_v^-(t)b_k^*\sigma_{vv}b_u - 2\eta\mu_u^-(t)b_k^*\sigma_{uu}b_v \\ &+ 4\eta^2\delta_{uv}\sum_n J_{vn}b_k^*\sigma_{vv}y_{vn} + 4\eta^2\delta_{uv}\mu_v^-(t)b_k^*\sigma_{vv}b_v \\ &+ (1-\eta)b_k^*\left(K_v\sigma_{vv} + K_u\sigma_{uu} - K_k\sigma_{kk}\right)y_{uv} \\ &- (1-\eta)\eta(3-2\eta)\delta_{uv}K_v b_k^*\sigma_{vv}y_{vv}.\end{aligned} \tag{1.6.24}$$

1.7 Optical spectra

1.7.1 Absorption and pump-probe spectra

Induced polarization in a material can be used to define spectroscopic quantities. Using expectation values, $P = \langle\hat{P}\rangle$, the induced polarization dynamics in the dipole approximation are given by:

$$\boldsymbol{P}(t) = \boldsymbol{\mu}_m b_m(t) + c.c. \tag{1.7.1}$$

All spectroscopic observables can be computed from the induced polarization. Absorption spectra are computed by calculating the Fourier transform of the induced polarization after action by the ultrashort optical field $\boldsymbol{E}(t) =$

$\boldsymbol{o}\exp(-(\Delta t)^2/2)$, centered at zero time with the Gaussian envelope[12]:

$$S_A(\omega) = \mathfrak{Im}\int_{-\infty}^{+\infty} \mathrm{d}t\,\exp(\mathrm{i}\omega t)P(t). \tag{1.7.2}$$

Vectorial properties of the field here are neglected as the J aggregate is assumed to have the geometry where all oscillators are aligned in one dimension.

Such calculated absorption spectrum does have excitation intensity dependence since the equations are non-linear. The intensity dependence disappears at low intensity, where equations can be linearized. In the linear regime we are left with a single variable in the exciton basis and the single equation:

$$i\frac{db_a}{dt} \quad = \quad J_a b_a + \mu_a^- - iR_a^b b_a. \tag{1.7.3}$$

The solution $b_a(t) = b_a(0)\exp(-iJ_a t - R_a^b t)$, yields Lorentzian lineshapes for all excitonic transitions.

Pump-probe spectroscopic signal (PP) can be calculated by numerically propagating the set of equations. The simulation (and experiment) involves two optical pulses: pump and probe. The pump pulse initiates the quantum dynamics by exciting all NEE variables. Later probe pulse performs the detection process. Three different sets of induced polarizations has to be computed for the following cases: when both pump and probe pulses are on ($P_{pp}(t)$), when only pump pulse is on ($P_{pu}(t)$) and when only probe pulse is on ($P_{pr}(t)$) in order to extract the differential transient signal:

$$\begin{aligned} S_{pp}(\omega) \simeq & \mathfrak{Im}\int \mathrm{d}t\,\exp(\mathrm{i}\omega t)\,(P_{pp}(t) \\ & -P_{pu}(t) - P_{pr}(t)) \end{aligned} \tag{1.7.4}$$

NEE equations can be solved either in real space (site) basis or in exciton basis.

1.7.2 2DES and Phase cycling

Two-dimensional electronic spectroscopy (2DES) allows to visualize excitation dynamics and correlations in chromophoric aggregates[11–14]. Various types of two-dimensional spectroscopy[48–50] have proven to be an outstanding utility for determining material quantum properties with time and frequency resolutions not limited by Heisenberg inequality. The chronologically ordered three

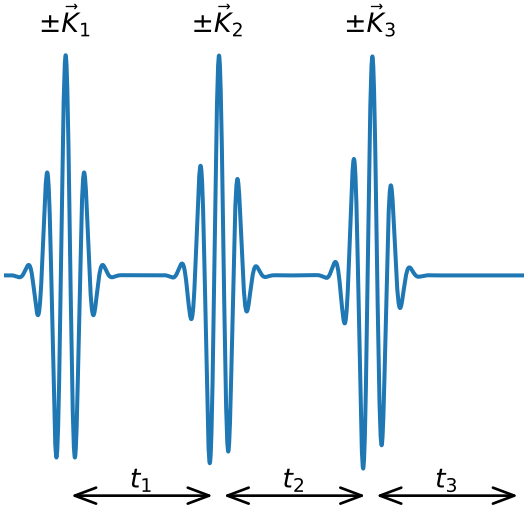

Figure 1.7.1: Diagram of pulses for generating 2DES signal

excitation pulses (characterized by wave vectors K_1, K_2, K_3) induce nonlinear response at least third order in the incoming field. The induced nonlinear polarization at a signal wave vector $\pm K_1 \mp K_2 + K_3$ is then detected by a heterodyne detection (by applying an additional pulse for detection timing) as a function of time delays between the neighboring pulses, (t_1, t_2, t_3) (shown in figure 1.7.1), the extra time point is the detection time which we can treat as detection pulse. Two Fourier transformations, with respect to the two t_1 and t_3 delays between pulses, project the signal onto two frequencies (ω_1, ω_3) in two dimensions and reveals exciton evolution, which becomes a function of the so-called t_2 waiting or delay time, which follows exciton populations and intraband coherences.

At a strict perturbative limit explicit disentanglement of the signal becomes possible which has gained the notion "density matrix tomography"[10,51,52]. As already mentioned, the external field intensity can be used to magnify the response and to reveal weak resonances.

The situation changes for large intensities when $\left(\vec{\mu_i} \cdot \vec{E}\right) \cdot \Delta t \to 1$, where Δt is the time interval during which the field is on. In this case the first order $(+K_i)$, the third order $(K_i + K_i - K_i)$, the fifth order $(K_i + 2K_i - 2K_i)$, and higher processes are comparable and contribute in the same phase matching direction, i.e. during the pulse action the multi-photon absorption and emission

processes take place, which overlap. Recently it has been shown[53,54] how specific order signals can be extracted from pump-probe measurements with their proposed variant of phase cycling.

If we compare to pump-probe, in that case we have $t_1 = 0$. The addition of extra pulse compared to pump-probe allows more precise tuning of initial state of system. By allowing $t_1$to vary and applying Fourier transform over together with t_3, we acquire a "map" of dynamics. This "map" shows shows if we apply specific input frequency what specific output signal is acquired and through control of t_2 how this response evolves over time. Also it should be noted that in usual pump-probe spectroscopy case $\pm K_1 \mp K_2 + K_3$ components are not separated. These components allow of to observe specific processes. For example as was mentioned before 2D signal at $\pm 2K_1 \mp 2K_2 + K_3$ which comes at distinct spectral window has been shown to specifically excite the double-exciton energy band and detect features related to EEA[24].

For more complicated nonlinear signals, it is necessary to extract the specific phase matching wave vector contributions[55]. The Traditional approach is related to the so-called order-by-order expansion of the signal[15]. However, due to the power-law dependence of exciton populations (due to EEA), the expansion by orders in regard to the external field is not efficient. It is more convenient to make numerical integration of the equations and then perform the extraction of various phase matching components by phase cycling[34]. In a non-collinear experiment, where each optical pulse has a specific wave vector, a specific signal part can be measured in certain directions defined by wave vector superpositions. Rephasing $-\vec{K_1} + \vec{K_2} + \vec{K_3}$ and non-rephasing $\vec{K_1} - \vec{K_2} + \vec{K_3}$ configurations are used in 2DES. If all pulses are collinear, then phase cycling[56,13,57] is the most efficient approach to separate different phase matching components of the signal. We can extract the signal of interest by calculating superpositions of polarizations corresponding to various phases of individual pulses. This corresponds to the Fourier transformation according to these phase changes. We then obtain decomposed signals corresponding to distinct wave vector configurations.

The excitation optical electric field that interacts with the medium in 2DES experiment (we also drop the vector signs because they are collinear and parallel in this case) at time t can be written as:

$$\mathcal{E}(t, r) = \sum_{l=1}^{3} \mathcal{E}_l(t - t_{0l}, r). \tag{1.7.5}$$

Here

$$\mathcal{E}_l(t,r) = \boldsymbol{E}_l(t-t_{0l})\cos(\omega_l(t-t_{0l}) - K_l r) \tag{1.7.6}$$

is the full field of $l-$th pulse. Next, we denote $\Delta_l = K_l r$ as the phases of pulses, then $t_l = t_{0(l+1)} - t_{0l}$ as the delays between pulses. Due to chronological pulse ordering, the time delays are always positive $t_l \geq 0$. Delay t_3 corresponds to the time elapsed after the third excitation pulse, i.e., $t_3 \equiv t$, when $t_{03} = 0$, for convenience. The induced polarization is then obtained as the function of these parameters, $P(t) \to P(t_3, t_2, t_1, \Delta_1, \Delta_2, \Delta_3)$. The polarization is detected as a function of t_3. For the phase cycling, the phases form the lattice

$$\Delta_i = \frac{2\pi}{m_i} n_i \tag{1.7.7}$$

(where $n = 0,...,m-1$) is the phase shift of the $i-$th pulse. The five-dimensional Fourier transform is then applied: $P(t_1, t_2, t_3, \Delta_1, \Delta_2, \Delta_3) \to P(\omega_1, t_2, \omega_3, k_1, k_2, k_3)$. An integer m_i is determined to be the highest value of the wavevector $m_i K_i$ we are interested. The sampling rate must be at least double of the spatial frequency, which we want to extract in accord with the Nyquist–Shannon sampling theorem[58]. This needs to be done for each pulse, therefore we need to consider $(2m_1+1)\cdot(2m_2+1)\cdot(2m_3+1)$ samples (while many of them are conjugate to each other). In case of rephasing (or non-rephasing) four-wave mixing signal the wavevector configuration corresponds to $-\vec{K_1}+\vec{K_2}+\vec{K_3}$ (or $\vec{K_1}-\vec{K_2}+\vec{K_3}$), so $3^3 = 27$ components are necessary to compute.

We additionally studied the six-wave mixing configurations of the form $-2\vec{K_1}+2\vec{K_2}+\vec{K_3}$. In the collinear configuration the signal also appears at the same signal beam as $-\vec{K_1}+\vec{K_2}+\vec{K_3}$. To extract this component one needs $5\times5\times3 = 75$ phase cycling configurations.

While this approach requires a lot of similar calculations, on the positive side, we obtain all other wave vector combinations, up to the limit imposed by the sampling number, because of the properties of the Fourier transformation. So, by calculating $-2\vec{K_1}+2\vec{K_2}+\vec{K_3}$ signal, we also at the same time obtain other contributions: $-\vec{K_1}+\vec{K_2}+\vec{K_3}$, $\vec{K_1}-\vec{K_2}+\vec{K_3}$, as well as $2\vec{K_1}-2\vec{K_2}+\vec{K_3}$.

1.8 NEE description in Exciton basis

Changing the problem to exciton representation leads to computational stability as the exciton basis considers specific resonances and symmetries of aggregate

and reduces oscillating terms. For example, population σ_{aa} terms do not have any oscillations. Further on 5th order terms and terms that involve 3 excitations are dropped, for example terms like $\hat{b}_a^\dagger \hat{b}_b \hat{b}_c \hat{b}_d$. Fourth order terms like $\hat{b}_a^\dagger \hat{b}_b^\dagger \hat{b}_c \hat{b}_d$ are factorized into $\sigma\sigma$ in real space by keeping the population intact and then the result is transformed into the exciton basis.

The transformation is carried out by transforming each operator one by one, for example for z variable is transformed $z_{abc} = \sum_{u,v,w} \theta_{u,a}\theta_{v,b}\theta_{w,c} z_{uvw}$ and inverse relation is $z_{uvw} = \sum_{a,b,c} \theta_{u,a}\theta_{v,b}\theta_{w,c} z_{abc}$, where $\theta_{u,e}$ is the transformation coefficient between u molecular excitation and e exciton. Transformation coefficients are calculated from eigenvalue problem:

$$\sum_n J_{mn}\theta_{n,a} = J_a \theta_{m,a}, \tag{1.8.1}$$

where J_a is the a-th exciton energy. Using this approach, all terms are transformed into exciton basis and take operator expectation values as follows: $b_a = \langle \hat{b}_a \rangle$, $\sigma_{ab} = \langle \hat{b}_a^\dagger \hat{b}_b \rangle$, $y_{ab} = \langle \hat{b}_a \hat{b}_b \rangle$, $z_{abc} = \langle \hat{b}_a^\dagger \hat{b}_b \hat{b}_c \rangle$. With this the following equations describe coherent dynamics of excitons (we show transformed equations for Eqs.1.4.10-1.4.13, because there are what we used in the specific study[32]):

$$\begin{aligned} \mathrm{i}\frac{db_a}{dt} =& + J_a b_a - \sum_{bcd}(2\eta J_d - (1-\eta)K)\Lambda_{abcd} z_{bcd} \\ &+ \mu_a^-(t) - 2\eta \sum_{bcd} \Lambda_{abcd}\mu_b^-(t)\sigma_{cd} \end{aligned} \tag{1.8.2}$$

$$\begin{aligned} \mathrm{i}\frac{d\sigma_{ab}}{dt} =& + (J_b - J_a)\sigma_{ab} \\ &- \sum_{cde}(2\eta J_c - (1-\eta)K)\Lambda_{bcde}\sigma_{ae}\sigma_{dc} \\ &+ \sum_{cde}(2\eta J_c - (1-\eta)K)\Lambda_{acde}\sigma_{ce}\sigma_{db} \\ &+ \mu_b^-(t)\hat{b}_a^\dagger - 2\eta \sum_{cde}\Lambda_{bcde}\mu_c^-(t)(z_{ade})^* \\ &- \mu_{e_1}^+(t)\hat{b}_b + 2\eta \sum_{cde}\Lambda_{acde}\mu_c^+(t) z_{deb} \end{aligned} \tag{1.8.3}$$

$$
\begin{aligned}
\mathrm{i}\frac{dy_{ab}}{dt} = &+ (J_b + J_a)y_{ab} - \sum_{cd}(2\eta J_c - (1-\eta)K)\Lambda_{abcd}y_{cd} \\
&+ \mu_b^-(t)b_a + \mu_a^-(t)b_b - 2\eta\sum_{cd}\Lambda_{abcd}\mu_c^-(t)b_d \\
&- 2\eta\sum_{cde}\Lambda_{acde}\mu_c^-(t)z_{deb} - 2\eta\sum_{cde}\Lambda_{bcde}\mu_c^-(t)z_{dae} \\
&+ 4\eta^2\sum_{cdef}\Lambda^{(6)}_{abcdef}\mu_c^-(t)z_{def}
\end{aligned} \tag{1.8.4}
$$

$$
\begin{aligned}
\mathrm{i}\frac{dz_{abc}}{dt} = &+ (J_c + J_b - J_a)z_{abc} - \sum_{de}(2\eta J_d - (1-\eta)K)\Lambda_{bcde}z_{aed} \\
&+ \mu_c^-(t)\sigma_{ab} + \mu_b^-(t)\sigma_{ac} - 2\eta\sum_{de}\Lambda_{bcde}\mu_d^-(t)\sigma_{ae} \\
&- \mu_a^+(t)y_{bc}
\end{aligned} \tag{1.8.5}
$$

Here Λ is the overlap between 4 exciton wavefunctions $\Lambda_{abcd} = \sum_u \theta_{u,a}\theta_{u,b}\theta_{u,c}\theta_{u,d}$, $\Lambda^{(6)}$ is overlap between 6 wavefunctions $\Lambda^{(6)}_{abcdef} = \sum_u \theta_{u,a}\theta_{u,b}\theta_{u,c}\theta_{u,d}\theta_{u,e}\theta_{u,f}$ and $K_{abcd} = \sum_u K_u\theta_{u,a}\theta_{u,b}\theta_{u,c}\theta_{u,d}$.

Then $\mu_a^\pm = \sum_u \theta_{u,a}\mu_u^\pm$ is dipolar transition moment in exciton basis. For the case $K_u = K$ then $K_{abcd} = K\Lambda_{abcd}$.

While the system interacts with the bath, this interaction is weak. At zeroth order to this interaction the system is perfectly coherent. Adding linear relaxation and EEA leads to the following final set of equations in eigenstate basis:

$$
\mathrm{i}\frac{db_a}{dt} = \text{coherent} - R^{(b)}_{a,a}b_a - \mathrm{i}\sum_{bcd}\Gamma_{abcd}z_{bcd}, \tag{1.8.6}
$$

$$
\begin{aligned}
\mathrm{i}\frac{d\sigma_{ab}}{dt} = &+ \text{coherent} - \sum_{cd}R^{(\sigma)}_{ab,cd}\sigma_{cd} \\
&- \mathrm{i}\frac{\kappa_0}{2}\sum_{cde}\left(\Gamma_{acde}\sigma_{cd}\sigma_{eb} + \Gamma_{bcde}\sigma_{cd}\sigma_{ae}\right),
\end{aligned} \tag{1.8.7}
$$

$$\mathrm{i}\frac{dy_{ab}}{dt} = + \text{coherent} - \sum_{cd} R^{(y)}_{ab,cd} y_{cd} - \mathrm{i}\frac{\kappa_0}{2}\sum_{cde}\left(\Gamma_{acde}\sigma_{cd}y_{eb} + \Gamma_{bcde}\sigma_{cd}y_{ae}\right), \tag{1.8.8}$$

$$\mathrm{i}\frac{dz_{abc}}{dt} = + \text{coherent} - \sum_{def} R^{(z)}_{abc,def} z_{def} - \mathrm{i}\frac{\kappa_0}{2}\sum_{def}\left(\Gamma_{adef}\sigma_{de}z_{fbc} + \Gamma_{bdef}\sigma_{de}z_{afc} + \Gamma_{cdef}\sigma_{de}z_{abf}\right), \tag{1.8.9}$$

here

$$\Gamma_{abcd} = \sum_u \sum_n \theta_{u,a}\theta_{n,b}\theta_{n,c}\theta_{u,d}(\delta^{(n-n)}_{nu} + \delta_{nu}). \tag{1.8.10}$$

The bath-induced relaxation tensors[9] $R^{(b)}_a$, $R^{(\sigma)}_{abcd}$, $R^{(z)}_{abcdef}$ are defined in section 1.5. This is the most complete numerically efficient NEE model. We denote this model by the label "Ex".

The model can be slightly reduced by assuming a simpler relaxation tensor for the z variable. By taking $R^{(z)}_{abcdef} = \delta_{ad}\delta_{be}\delta_{df}\left(R^{(b)*}_a + R^{(b)}_b + R^{(b)}_c\right)$ a model with simple relaxation model is obtained, which We denote by "Ex-R".

1.8.1 Overdamped model

Additional approximation can be implemented by assuming a fast decay of intraband coherences. The coherences can then be crossed out from equations. Considering specific experiments (e.g., pump-probe measurement), the model implies that the delay times between optical pulses are longer than the decay times of molecular coherences. With this assumption we drop y variables, $\sigma_{ab},\ a \neq b$ coherences and $z_{abc},\ a \neq b$ intra-band coherences. So, for relaxation terms only secular population-related forms are considered. The full set of equations then take the form:

$$
\begin{aligned}
\mathrm{i}\frac{\mathrm{d}b_a}{\mathrm{d}t} =& + \mu_a^-(t) + (J_a - \mathrm{i}R_{a,a}^{(b)})b_a \\
& - 2\eta \sum_{bc}((1-\delta_{bc})J_b + J_c)\Lambda_{abbc} z_{bbc} \\
& + (1-\eta)\sum_{bc}(2-\delta_{bc})K\Lambda_{abbc} z_{bbc} \\
& - 2\eta \sum_{bc}\Lambda_{abcc}\mu_b^-(t)\sigma_{cc} - \mathrm{i}\frac{1}{2}k_0 \sum_{bc}\Gamma_{abbc}\sigma_{bb} b_c,
\end{aligned} \tag{1.8.11}
$$

$$
\begin{aligned}
\mathrm{i}\frac{\mathrm{d}\sigma_{aa}}{\mathrm{d}t} =& + \mu_a^-(t) b_a^\dagger - \mu_a^+(t) b_a - \mathrm{i}\sum_b R_{aa,bb}^{(\sigma)}\sigma_{bb} \\
& - 2\eta \sum_{bc}\Lambda_{aabc}(\mu_c^-(t)(z_{aab})^* - \mu_c^+(t) z_{aab}) \\
& - 2\eta \sum_{bc}\Lambda_{abbc}(\mu_c^-(t)(z_{bba})^* - \mu_c^+(t) z_{bba}) \\
& + 2\eta \sum_{b}\Lambda_{aaab}(\mu_b^-(t)(z_{aaa})^* - \mu_b^+(t) z_{aaa}) \\
& - \mathrm{i}k_0 \sum_b \Gamma_{abba}\sigma_{bb}\sigma_{aa},
\end{aligned} \tag{1.8.12}
$$

$$
\begin{aligned}
\mathrm{i}\frac{\mathrm{d}z_{aab}}{\mathrm{d}t} =& + (J_b - \mathrm{i}R_{aab,aab}^{(z)})z_{aab} + \mu_b^-\sigma_{aa}(1+\delta_{ab}) \\
& - 2\eta \sum_c (J_a + J_c - \delta_{ac}J_a)\Lambda_{aabc} z_{aac} \\
& + \sum_c (2-\delta_{bc})(1-\eta)K\Lambda_{aabc} z_{aac} - \sum_c 2\eta\Lambda_{abca}\mu_c^-\sigma_{aa} \\
& - \mathrm{i}k_0 \sum_c \Gamma_{acca}\sigma_{cc} z_{aab}(1-\delta_{ab}) - \mathrm{i}k_0\frac{1}{2}\sum_c \Gamma_{accb}\sigma_{cc} z_{bba} \\
& - \mathrm{i}k_0\frac{1}{2}\sum_{cd}\Gamma_{bccd}\sigma_{cc} z_{aad}(1+\delta_{ab}).
\end{aligned} \tag{1.8.13}
$$

Here we assumed the same anharmonicity for all chromophores, $K_u = K$. This overdamped model is denoted by OD. Like with the Ex model, we will also use OD-R, where relaxation of the z variable is simplified accordingly. Notice that the model differences are mostly related to multi-excitonic properties. The linear response of all models would be the same.

1.9 Theory summary

At low excitation conditions the multi-chromophore systems are relatively simple for modeling. The single exciton band of states can usually be calculated explicitly by either analytic or numerical Hamiltonian diagonalization. Higher resonances, available from the third order spectroscopy can be done also analytically for simple J aggregates or numerically by using e.g., the exciton-exciton scattering approach (within the NEE), or by brute force numerical diagonalization[59,15].

Modeling the highly excited resonances of nonlinear systems becomes extremely challenging, as the order-by-order expansion as well as a rotating-wave-approximation does not always hold at all. This is especially true for the EEA process[60,27,61,54,62]. Notice for example that if the excited state population follows equation ($\alpha \neq 1$)

$$\frac{dn}{dt} = -\gamma n^{\alpha}, \tag{1.9.1}$$

what is the case for EEA, where n is the exciton concentration, γ - the EEA parameter, the solution

$$n(t) = \frac{1}{\left(\frac{1}{n_0^{\alpha-1}} + (\alpha-1)\gamma t\right)^{\frac{1}{(\alpha-1)}}} \tag{1.9.2}$$

at long times is a power law function, which cannot be expanded in efficiently converging exponential series. For $\alpha > 1$ (in this work we define EEA as $\alpha = 2$; the parameter is not restricted to integer values) we find that the solution has strong tail that decays much slower than the exponential function, and only at infinite time it fully decays. In this case only the numerical solution of the equations, describing the process, can be used to calculate the observables[47].

The flexibility of NEE combined with various approximations leads to generation of many models that are suited to modeling different problems.

We have models separated by the basis they are set in (site basis or exciton basis). Another separation is the treatment of higher order dephasing and relaxation terms; the equations are numerically unstable with higher order terms in paulionic case because the relaxation derivation neglects the bosonicity/paulionicity of system.

Another split which can appear redundant at first is site and exciton basis. Ideally the change of basis should not change calculation results. But it allows

various kinds of approximations to be applied and have different numerical stability as excitons are system Hamiltonian eigenstates. The fact that EEA is defined in site basis and dephasing and relaxation in exciton basis, we get no numerical scaling benefit from basis change.

An overview of select models is given in tables 1.9.1, 1.9.2 and 1.9.3.

Table 1.9.1: Models of NEE factorization

Model	Main idea	Properties
Complete factorization	Factorize everything to the smallest block possible.	Describes coupled nonlinear oscillators and still includes some anharmonicities. Computationally the cheapest. Computational cost scale as 2th power to molecule number.
Restricted coherent state factorization(coh)	If the system remains coherent, the wavefunction description is completely valid and daggered and non-daggered operators evolve independently .	Appears to somewhat replicate higher order factorization results, but ESA sideband much weaker. and shifted more. With EEA terms is more similar to higher order factorization. Computational cost scale as 4th power to molecule number.
Direct factorization(s)	Retaining σ and using $\hat{g}_v = (1 - 2\eta\hat{\sigma}_{vv})$ as hint for factorization. Retaining σ means retaining population-induced effects, which last longer than coherences.	Results are strange and behave completely different from other models. No ESA sideband and main peak strongly shift from excitation intensity. Computational cost scale as 4th power to molecule number.

Table 1.9.2: 5th order models of NEE factorization

Model	Main idea	Properties
Fifth order $z\sigma$	Preserve third order with factorizing higher order term into population terms without preserving operator order.	Higher cost because of z relaxation terms required. ESA sideband strongly shifts from excitation intensity. Computational cost scale as 6th(4th with simplified relaxation for z) power to molecule number.
Fifth order zz	Preserve third order with keeping factorization blocks as big as possible. Preserve more double coherence terms.	Higher cost because of z relaxation terms required. Shows some erratic behavior with negative signal appearing in nonlinear absorption. Computational cost scale as 6th(4th with simplified relaxation for z) power to molecule number.
Fifth order zn	Preserve third order while and preserve operator order while factorizing with preference to populations by noting the structure that arises when deriving NEE using $\hat{g}_v = (1 - 2\eta\hat{\sigma}_{vv})$ as hint for factorization	Higher cost because of z relaxation terms required. Appears to give best results. Computational cost scale as 6th(4th with simplified relaxation for z) power to molecule number.

Table 1.9.3: Exciton basis models of NEE

Model	Main idea	Properties
Exciton basis(Ex)	Exciton basis allows additional approximations and should be numerically more stable	Better numerical stability, less oscillating terms in exciton basis and coherences decay. If EEA neglected then equations are cheaper to compute in exciton basis. Allows extra simplification by neglecting dark states and only modeling bright excitons. Computational cost scale as 6th power to molecule number.
Exciton basis overdamped(OD)	In exciton basis coherences should be short lived, by dropping most of them computational complexity can be significantly reduced	ESA is more shifted compared to normal exciton basis model. Computational cost scale as 4th power to molecule number.

2 RESULTS

Continuing the work from[9], where we extended the Nonlinear Exciton equations[39,40] (NEE) with EEA terms and showed that numerical NEE-based simulations of pump probe spectra of a molecular dimer quantitatively describe both coherent and incoherent processes as a function of excitation intensity. The natural progression of study is application of these equations to spectra calculation of larger molecular systems and calculation of higher order nonlinear spectra. In addition, there is room for improvement with generalizing the equations for both paulions and bosons with a parameter that allows smooth transition from one description to another. This is valuable as intermediate statistics of molecular electronic excitations do not strictly obey either boson or paulion statistics. In exciton basis we describe four different NEE realizations which allow very efficient calculations of the signals.

2.1 Evaluating the effect of different factorization models on nonlinear absorption

In the following we apply various factorization schemes for linear molecular aggregate of seven molecules. Study is made over several excitation intensity values, thus revealing nonlinear effects in absorption spectrum too. This way the effect of factorizing higher order terms can be seen.

2.1.1 System parameters and model

Various levels of theory will be tested on the model system, which is a linear J aggregate of seven chromophores. This is the simple linear chain of chromophores, which shows superradiant absorption, which is red shifted from the independent chromophore[5]. Parameters of the model are taken from typical tubular J aggregates[23,63]. The nearest-neighbor resonant coupling $J_{nn+1} = J_{n+1n} = -800$ cm^{-1} and ends are connected with periodic boundary conditions. Periodic conditions represent the infinitely long linear aggregate. Additionally, the diagonal Gaussian energy disorder with variance $\sigma = 100$ cm^{-1} is included to perturb the ideal symmetry of the aggregate. The excitation energy

mean value J_{nn} of all sites is set at $18000\ \mathrm{cm}^{-1}$. On-site energy anharmonicity (only needed when $\eta \neq 1$) is taken $K_{nn} = +1000\ \mathrm{cm}^{-1}$. For the quantum particle statistics, 3 different cases as considered: bosons $\eta = 0$, paulions $\eta = 1$ and the intermediate regime, $\eta = 0.5$.

For system-phonon interaction the Drude spectral density is used:

$$C''(\omega) = 2\lambda \frac{\omega\Lambda}{\omega^2 + \Lambda^2} \tag{2.1.1}$$

with $\lambda = 20\ \mathrm{cm}^{-1}$ and $\Lambda = 50\ \mathrm{cm}^{-1}$. System temperature is set at $T = 300\ \mathrm{K}$. Annihilation parameter is set to $\kappa_0 = 1000\ \mathrm{cm}^{-1}$, with direct conversion $\tau = 1/\kappa_0 \sim 5.27\mathrm{fs}$, note that annihilation does not follow exponential decay, and actual rate of decay is a function of the population itself.

As we include EEA terms, optical excitation field intensity becomes an important parameter. The optical field envelope is defined as $\boldsymbol{E}(t) = AE_0(t)$, A is the amplitude and $E_0(t)$ is the normalized envelope function

$$E_0(t) = \frac{1}{s\sqrt{2\pi}} \exp\left(-\frac{t^2}{2s^2}\right), \tag{2.1.2}$$

$$s = \frac{2\sqrt{2}}{\Delta\omega_{FWHM}\sqrt{\ln(2)}}. \tag{2.1.3}$$

The molecule transition dipole moments are taken such that

$$\mu E = \frac{A_0}{\sqrt{7}}, \tag{2.1.4}$$

where A_0 is the excitation with external optical field scaling constant. The factor of $\sqrt{7}$ is included by keeping in mind that when transforming such a system into the exciton basis, the lowest exciton has a transition dipole moment scaled as $\sqrt{N}$ where N is the number of molecules in such a system. This way allows to relate A_0 to population in lowest energy exciton approximately as $\sigma \sim A_0^2$ ignoring any saturation effects.

2.1.2 Nonliear absorption spectra

First, we present results without EEA. Starting with the 3 simplest models: restricted coherent state factorization model (Eqs 1.6.4, 1.6.5) marked as coh, direct factorization model (Eqs 1.6.6, 1.6.7, 1.6.8) marked as s and 3rd order pure unfactorized model (Eqs 1.6.9, 1.6.10, 1.6.11, 1.6.12) marked as $z3$, we present

comparison of these models with no EEA in figure 2.1.1. Here we show intensity dependent absorption spectra. Wildly different behavior between these models is seen when the field intensity is increased. For a coh model, a second peak appears and grows with the field intensity. This peak can be associated with induced excited state absorption (ESA) appearing from the already excited main exciton band into the higher levels. This ESA peak grows weakly compared to other models, as coherences are short lived so higher order terms are more suppressed with this factorization. In contrast the s model, which preserves populations, shows no extra peak, only the whole main absorption line shifts to higher energy. In addition, a change in lineshape is visible, the peak appears to be "tilted" to the blue, the blue side gets steeper with intensity while the red side gets shallower. The 3rd order model $z3$ has similar behavior as coh model except the side peak is much narrower, so has much larger amplitude. Notably the excitation intensity effects are much more pronounced for paulions, which is a much more complicated nonlinear system.

Next, the models, where factorization is performed at 4th order terms (the terms higher than 3rd order are factorized) are compared; the models are labeled as $z\sigma 4$, which corresponds to Eqs. 1.6.14, 1.6.15, $zz4$ corresponds to Eqs. 1.6.18, 1.6.19, and $zn4$ corresponds to Eqs. 1.6.22, 1.6.23, where these terms are added to $z3$ terms. Intensity dependent spectra of these models are shown in figure 2.1.2. What we find is that all three models show similar behavior as the $z3$ model, consequently, the contribution from factorization at 4th order terms is small. Main reason for this is likely because the 4th order does not "directly" contribute to polarization, where the 3rd order is dominating i.e., z in b and 5th order inside z. Even order terms appear mostly responsible for scaling of the transition dipole moment, which is again a small contribution.

The factorization can be performed at 5th order contributions. We mark 3 distinct factorization schemes for 5th order contribution: $z\sigma 5$ model (Eqs. 1.6.13, 1.6.16), $zz5$ model (Eqs. 1.6.17, 1.6.20), and $zn5$ model (Eqs. 1.6.21, 1.6.24). Wildly differing behavior between spectra with factorization schemes is visible (figure 2.1.3), however, the common feature is again related to appearance of a separate ESA peak, which grows with increasing field intensity. In the present case the ESA amplitude is again much weaker than in Fig. 2.1.2. It can be observed that some features of low order factorization models reappear in these models: for the $z\sigma 5$ model, which is the population favoring model, also the ESA peak shifts to higher energy when field intensity increases, partially mirroring the s model where the whole absorption was shifted. The $zz5$

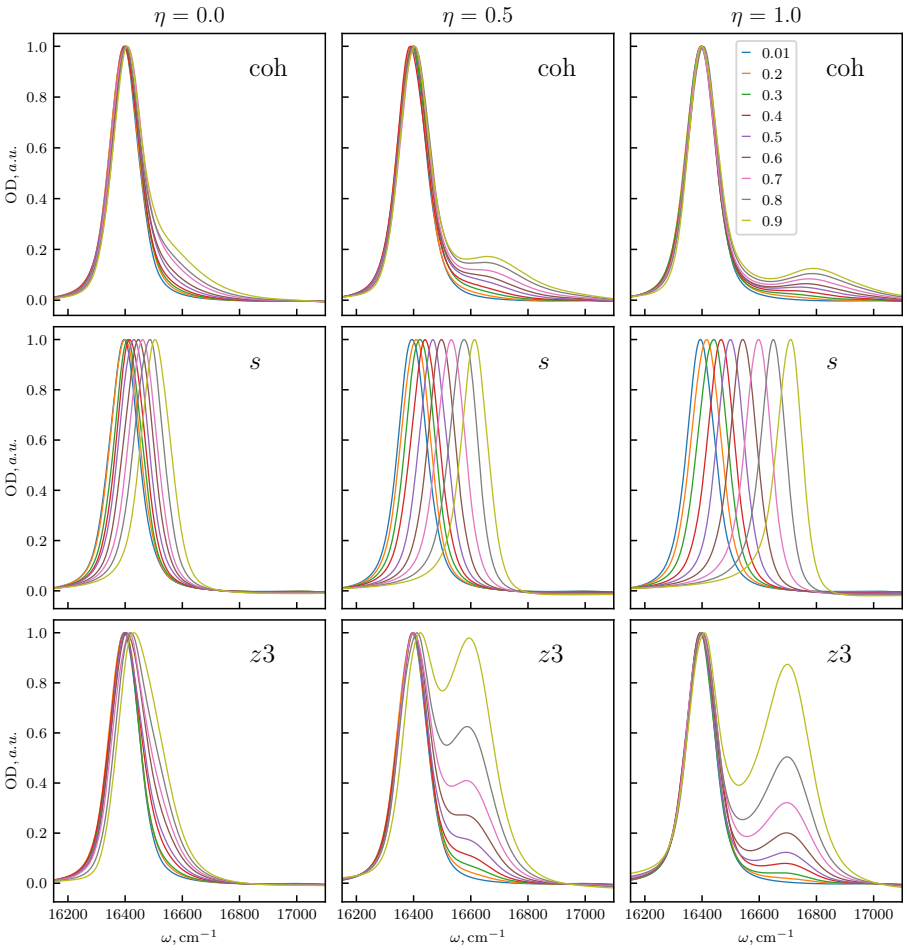

Figure 2.1.1: Absorption of J aggregate for different factorization models (*coh*, s and $z3$) at different excitation optical field intensity values, without EEA. Vertical axis represents optical density, horizontal - frequency, legend shows intensity units.

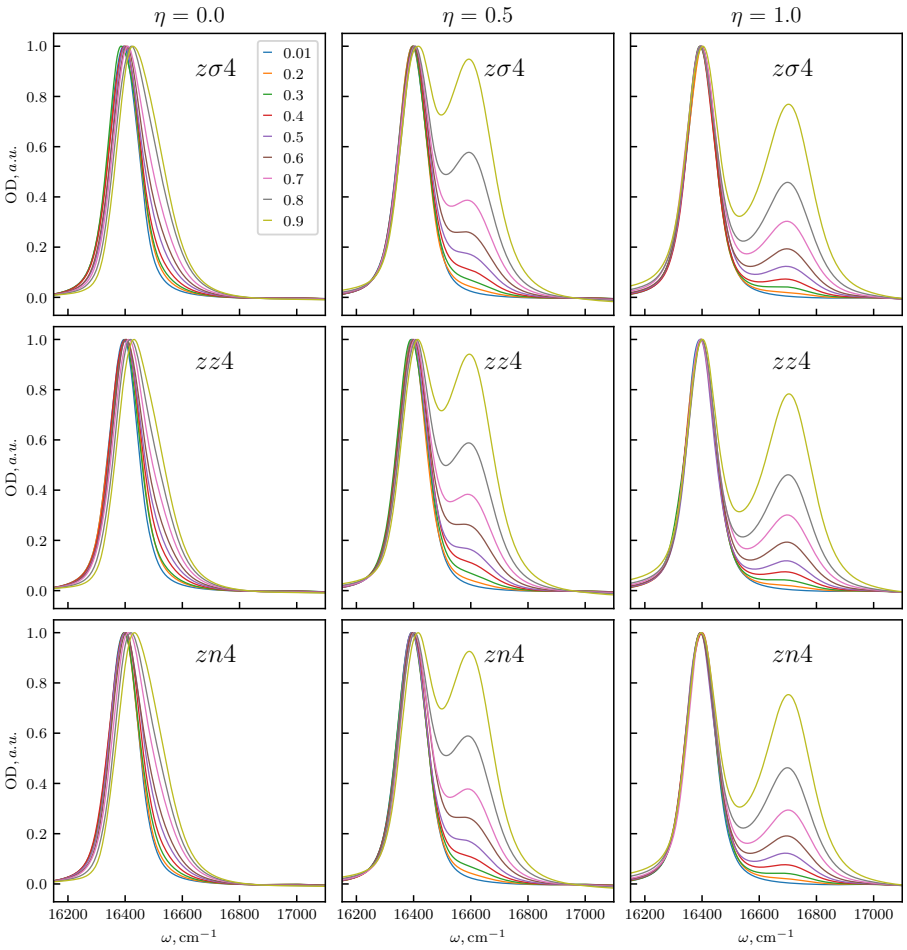

Figure 2.1.2: Absorption of J aggregate for different factorization models (z with 4th order factorized terms models) at different excitation optical field intensity values, without EEA. Vertical axis represents optical density, horizontal - frequency, legend shows intensity units.

model shows more strange behavior. It is the only case where negative value regions appear in spectra. These features should be interpreted as the induced emission contribution. The $zn5$ model appears most consistent as it shows similar behavior to $z\sigma 4$, $zz4$, $zn4$ and $z3$ models.

Next, we look at the same models with the EEA process included. Looking at the simpler models first (fig. 2.1.4) we see that EEA leads to excessive broadening of ESA features. Still, the s model is the only model which shows shift of the whole absorption band with field intensity. Additional small dip for high excitation intensities on the red side for the paulion case implies presence of induced emission as in the $zz5$ model in Fig. 2.1.3. ESA in the coherent model has significantly lower ESA intensity. The absorption spectra for model $z3$ with EEA terms are broadened, with a significant shoulder reflecting ESA.

4th order factorized models (figure 2.1.5) are similarly affected by EEA, mimicking $z3$ model. Surprisingly, the differences between different factorizations become very small.

With EEA, the 5th order models (figure 2.1.6) again differ much less between themselves and between the 4th order models. Apparently, the large broadening induced by EEA hides differences between the 4th and 5th order factorization models.

2.1.3 Discussion

Various factorizations of NEE equations are associated with different models of optical response, enhancing specific phenomena. High order terms (which were factorized) are coming from specific types of nonlinearities in the system. The research's target is to identify specific important phenomena and then to associate them with specific variables, so that specific processes can be pointed out when analyzing corresponding experiments.

First of all, it should be noted that at low intensities all models yield the same absorption spectra. (even independent of η value). This is shown in figure 2.1.7, where all the absorptions overlap, with negligible differences that come from the finite static disorder averaging.

This can be also observed from the equations, where in all models dropping out nonlinear terms (vanishing at low intensity) leads to a simple linear model defined by a single equation:

$$\mathrm{i}\frac{db_u}{dt} = J_{un}b_n + \mu_u^-(t) + iR_{un}^{(b)}b_n. \tag{2.1.5}$$

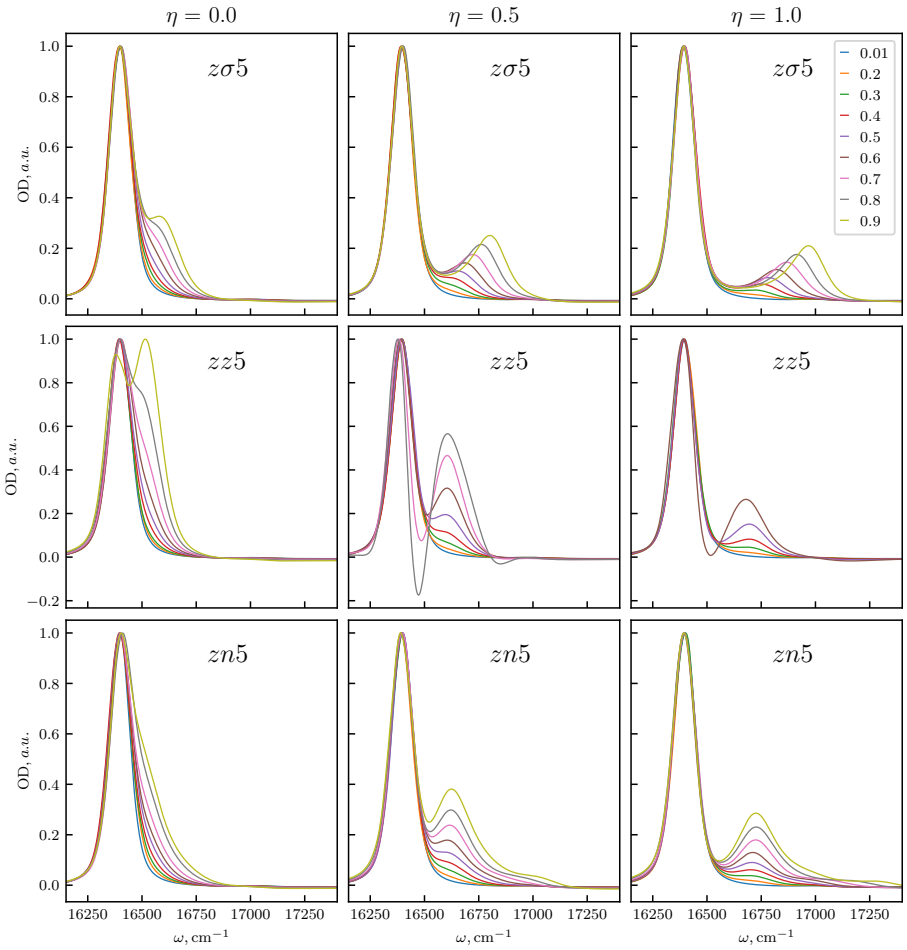

Figure 2.1.3: Absorption of J aggregate for different factorization models (z with 5th order factorized terms models) at different excitation optical field intensity values, without EEA. Vertical axis represents optical density, horizontal - frequency, legend shows intensity units.

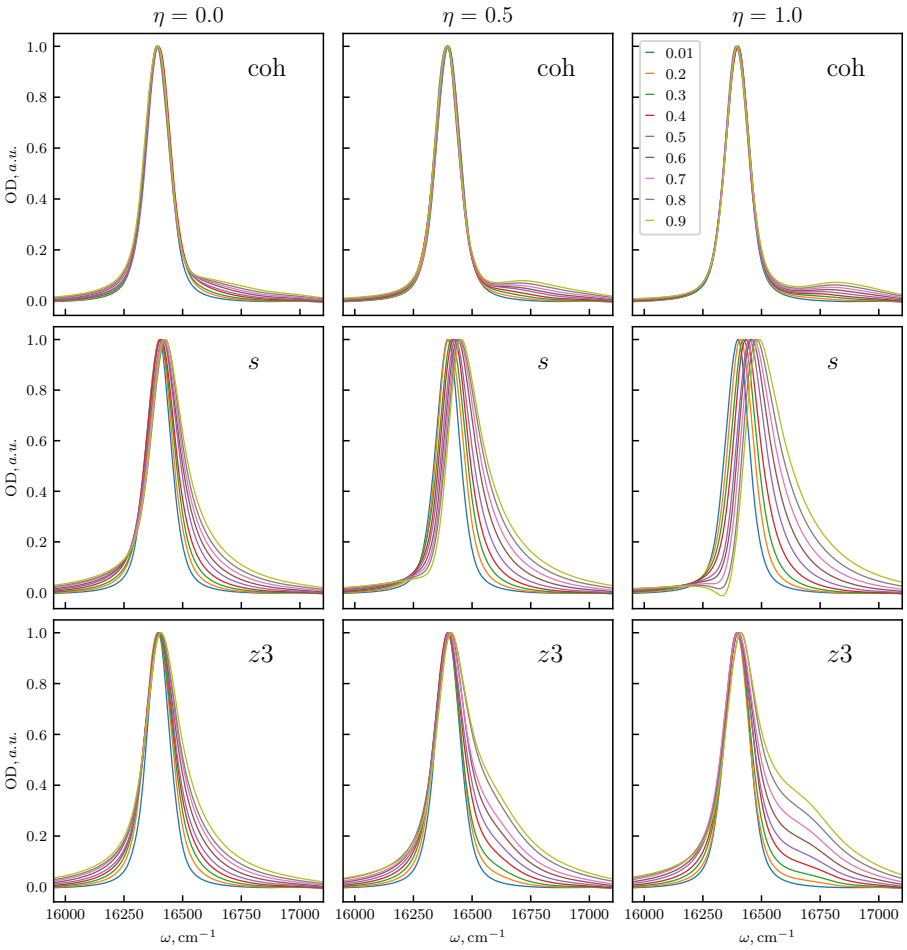

Figure 2.1.4: Absorption of J aggregate for different factorization models (*coh*, s, $z3$) at different excitation optical field intensity values, with EEA. Vertical axis represents optical density, horizontal - frequency, legend shows intensity units.

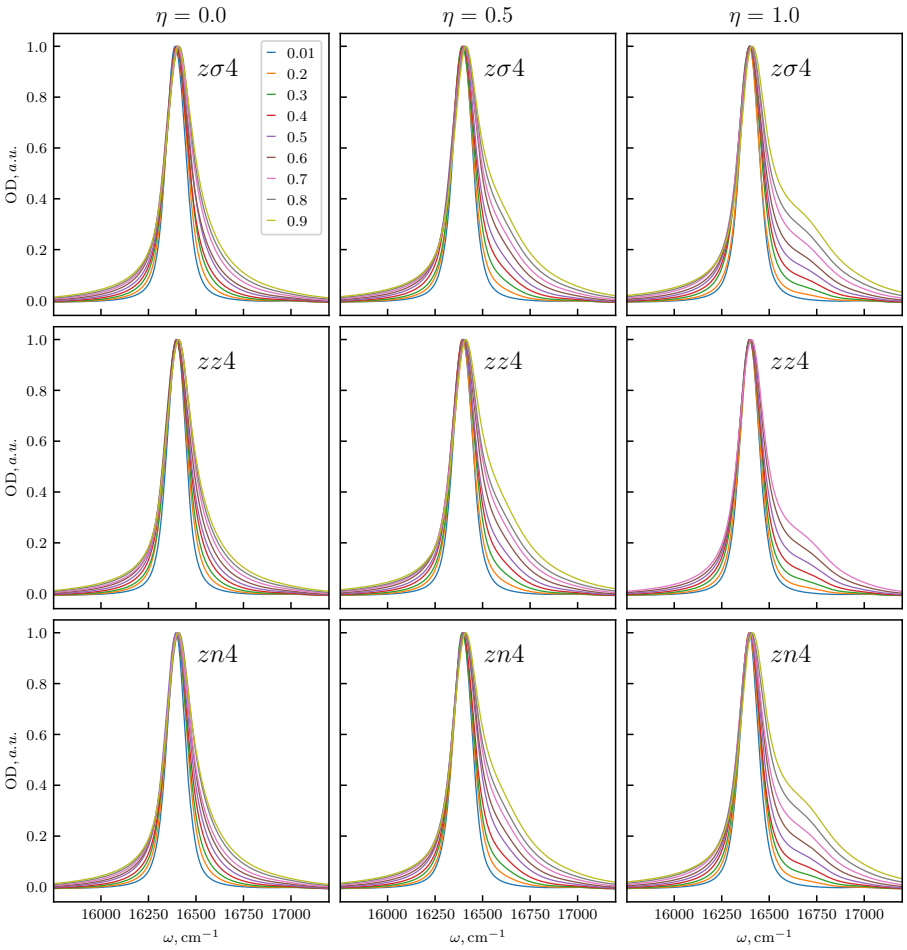

Figure 2.1.5: Absorption of J aggregate for different factorization models (z with 4th order factorized terms models) at different excitation optical field intensity values, with EEA. Vertical axis represents optical density, horizontal - frequency, legend shows intensity units.

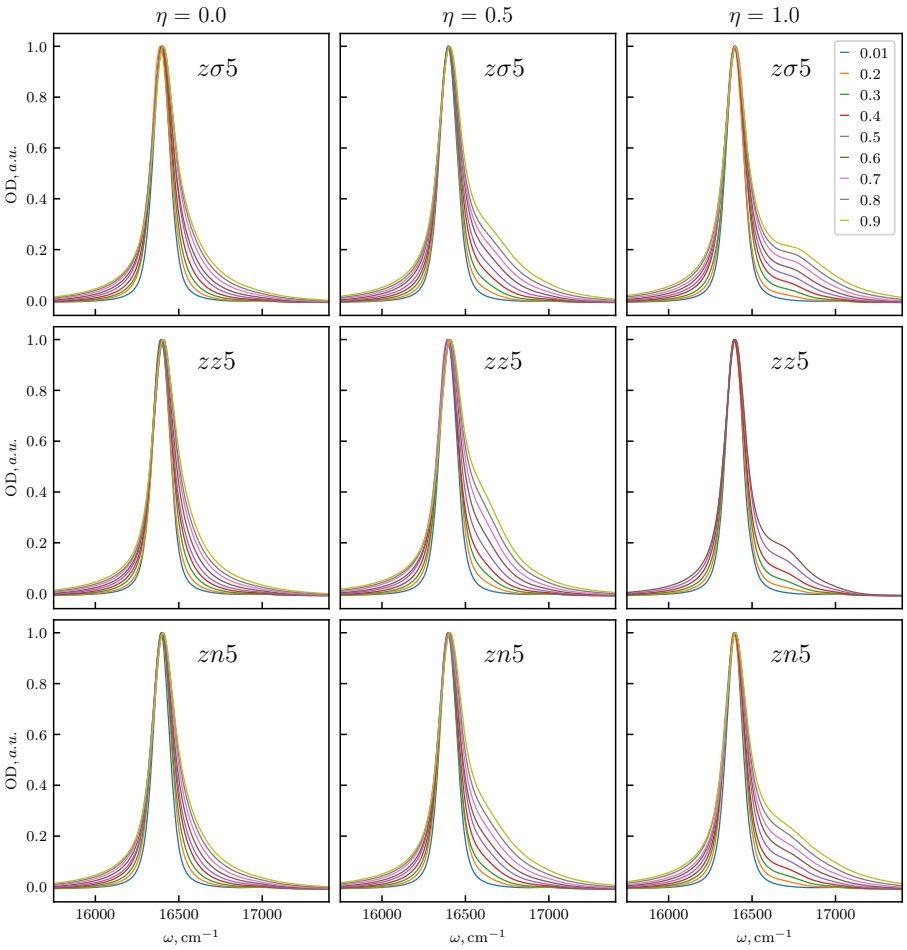

Figure 2.1.6: Absorption of J aggregate for different factorization models (z with 5th order factorized terms models) at different excitation optical field intensity values, with EEA. Vertical axis represents optical density, horizontal - frequency, legend shows intensity units.

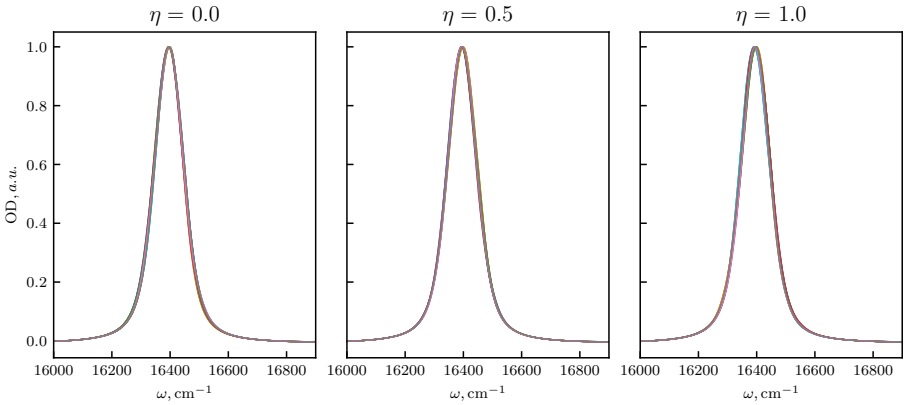

Figure 2.1.7: The absorption of all models presented for both no and with annihilation at low intensity. Vertical axis represents optical density, horizontal - frequency.

This equation is equivalent to the linear response theory. Polarization becomes directly related to $\hat{b}(t)$ time dependence, which can be solved analytically in exciton eigenstate representation. The solution then yields the single excitonic Lorentzian peak, as seen in Fig. 2.1.7.

At higher field intensity nonlinear terms become contributing. We see that most nonlinear nontrivial contributions come from odd order terms. Polarization is directly related to $\hat{b}(t)$ which relates to $\hat{b}^\dagger\hat{b}\hat{b}$ which relates to $\hat{b}^\dagger\hat{b}^\dagger\hat{b}\hat{b}\hat{b}$ which relates to 7th order similar terms, and this continues ad infinitum. In this case, the equations are limited to third and fifth order operator configurations as we assume that the EEA does not allow the creation of high excitation levels. We find that going from 3rd to 4th order the change is minimal (only intensity is affected). But going to 5th order other changes appear: ESA intensity drops to 1/3 of its intensity in third and fourth order cases.

Small but significant differences between different types of factorizations can be seen. In cases which favor populations in factorization and disregard operator order, the ESA peak position becomes dependent on excitation intensity, while when applying more rigid factorization with preserving operator order, the ESA peak position is stable over excitation intensities.

Curiously, when factorizing in bigger blocks (factorizing with third order terms instead of second order) some instability and even negative amplitudes in “absorption” spectra are seen. These negative features are related to the type of signal we consider. Note that in general we analyze the Fourier transformation of polarization decay after short excitation. As a result, both the induced

absorption and stimulated emission must be considered. The emission leads to negative features. Different spectra could be obtained by simulating high intensity CW measurement. In that case at strong excitation intensities, additional peak shifts coming from polaritonic effects should be observed.

2.2 Application of NEE for large molecular aggregates

In this study we test the application of NEE for large molecular aggregates, by looking at the resultant pump-probe spectra. What constitutes "Large" in this context is what is computational feasible to calculate in reasonable amount of time at specific level of approximation. The main approximation in this part is simulator only part of the molecular system by noting that J aggregates have only one bright (non-zero transition dipole) exciton and it is the lowest energy exciton. This means that this bright part is most important in resultant spectra. But other effects such energy transfer have indirect effects too, therefore limiting the entire system to 1 exciton from, for example, 50 molecules can lead to nonphysical results.

Another way to decrease computational complexity is dropping terms by reasoning that coherence-like terms should decay fast and populations should survive longer timescales, a type of overdamped model (OD).

Distinct levels of theory, corresponding to different sets of equations will be compared. These include Ex, Ex-R, OD, OD-R.

2.2.1 System parameters and model

Parameters for the system are taken typical of the cyanine dye aggregates[23,63]. A linear chain of seven ($M = 7$) chromophores is taken with the nearest-neighbor resonant coupling $J_{nn+1} = -800$ cm^{-1}, and diagonal Gaussian site energy disorder of $\sigma = 100$ cm^{-1}. The disorder-averaging includes 800 different runs, what is sufficient for convergence over the ensemble. The excitation energies J_{nn} of all sites is set to 18000 cm^{-1}. On-site anharmonicity parameter $K_{nn} = +1000$ cm^{-1}. For the statistics we include 3 different cases: bosons $\eta = 0$, paulions $\eta = 1$ and an intermediate regime, $\eta = 0.5$.

The optical field envelope is defined as $E_l(t) = A_l E_0(t)$, A_l is the amplitude and $E_0(t)$ is normalized Gaussian:

$$E_0(t) = \frac{1}{s\sqrt{2\pi}} \exp(-\frac{t^2}{2s^2}), \tag{2.2.1}$$

$$s = \frac{2\sqrt{2}}{\Delta\omega_{FWHM}\sqrt{\ln(2)}}. \tag{2.2.2}$$

The carrying frequency is set to lowest energy exciton $\omega_l = 16400$ cm^{-1} and the pulse width of all pulses is set to $\Delta\omega_{FWHM} = 3000$ cm^{-1}.

The energy absorbed by the aggregate depends on the number of chromophores. We want to keep excitation conditions the same between different size aggregates. The excitation electric field energy is proportional to $|E|^2$. However, the ideal J aggregate shows superradiance, where the lowest energy exciton has a transition dipole proportional to the number of molecules. The absorbed energy, which is proportional to $|\mu_e E|^2$ then scales as N^2. The absorbed energy per molecule then scales as $N^2E^2/N = NE^2$. Then by keeping this number constant we must ensure $E^2 \sim N^{-1}$, or $E \sim N^{-1/2}$.

Therefore, we set transition dipole moment as $\mu_m = \mu_0$, with $\mu_0 A_{probe} = \frac{0.01}{\sqrt{N}}$ and $\mu_0 A_{pump} = \frac{0.5}{\sqrt{N}}$. That means for the same excitation parameter we have the same conditions for J aggregates made of different number of molecules.

For the site energy fluctuations, we use a Drude spectral density (Eq. 2.1.1), with $\lambda = 20$ cm^{-1} and $\Lambda = 50$ cm^{-1}. System temperature, which affects only the relaxation rates, is set at $T = 300$ K. Regarding the interband EEA a single decay parameter characterizes the process $\kappa_0 = 1000$ cm^{-1}. Notice that this rate-dimension parameter does not correspond to the inverse annihilation time, as the EEA process is non-exponential (see Discussion section).

2.2.2 Full model comparison

First, we compare the absorption spectrum, shown in figure 2.2.1, calculated using Ex, Ex-R, OD, and OD-R models using intensity of the probe pulse ($N = 7$). The estimated exciton occupation $\sigma_{aa} \sim 10^{-4}$, so excitation intensity is low. Calculations include nonlinear contributions coming from exciton statistics, anharmonicity and EEA. As expected, all models overlap and do not affect the absorption spectrum. For reference, we additionally show the homogeneous spectra without diagonal disorder. This also confirms that in the linear regime the differences between different models of equations are minor.

The pump-probe spectrum, which originates from at least third order nonlinearities, is designed to reveal variations in absorption induced by the preexcitation. The spectrum was calculated for the pump-probe delay time of 1 ps. The pump pulse intensity is 2500 times stronger than for the absorption.

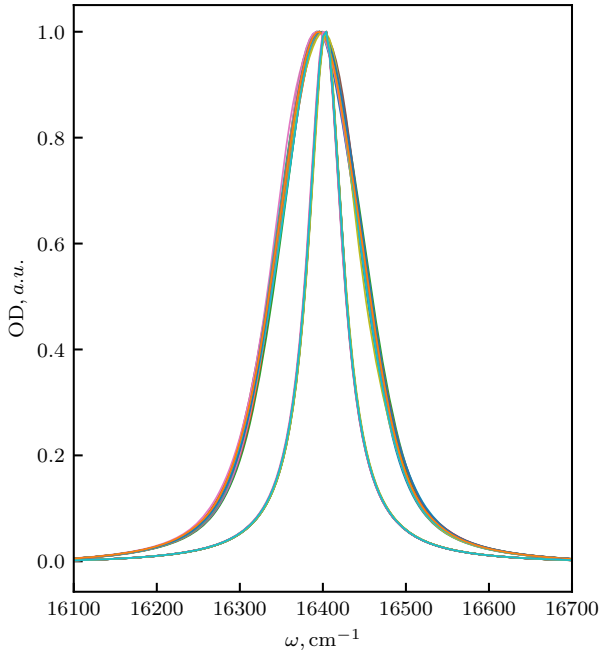

Figure 2.2.1: Absorption spectra for J aggregate of 7 molecules for models Ex, Ex-R, OD, OD-R, for cases of $\eta = 0, 0.5, 1.0$ and with and without EEA for weak excitation conditions. All models are overlapping, so they are not distinguishable and the labels to different curves are not introduced for clarity. Reference calculation results for all models without disorder are in teal (the narrow peak). Vertical axis represents optical density, horizontal - frequency.

Nonlinear spectrum cuts the linear component from the signal. While differences in absorption are negligible, the differences in PP spectrum (especially in excited state absorption region) are significant as shown in Fig. 2.2.2. The spectrum theoretically consists of three components: bleaching component, excited state emission and excited state absorption (ESA). Since in J aggregate the bright excitons are at the bottom of the exciton band, the absorbing and emitting states are the same, hence the bleaching and the excited state emission contributions overlap and form the negative band at 16400 cm^{-1}. The ESA covers the spectrum from 16500 cm^{-1} to 17000 cm^{-1} and depends on the model.

The negative band for all models is again not sensitive to the calculation model. This may be obvious for the bleaching component, which is essentially equal to the inverted absorption spectrum. The excited state emission, is a nonlinear signal, however, being related to the single-exciton characteristics is not affected by the choice of the model.

Significant differences to the model appear at the excited state absorption, which is induced by the third order terms (mainly z and related terms) when EEA is not included (1-st row). Bosonic ($\eta = 0$) and paulionic ($\eta = 1$) models have slightly shifted position of the ESA peak and as expected, the intermediate case ($\eta = 0.5$) leads to intermediate placement of the ESA peak. Comparing the OD and Ex approaches, we see that the OD model tends to slightly shift ESA band more to higher energies. The other trend that can be seen is that simplified -R relaxation models have wider ESA bands.

When EEA is enabled (Fig. 2.2.2 2-nd row) the PP spectra decays with the delay time and lineshapes change. The bleach contribution acquires left and right shoulders, marked in figure by arrows, (same as has been observed for the dimer in ref.[9]) and bleach is narrower, the ESA decays more compared to the bleach contribution.

The ESA position is fully controlled by the model. The Ex model is the most complete (including various particle correlations and the relaxation) and corresponds to the most coherent model, what applies to the systems where the relaxation is weak. Note that some factorizations have been performed, which also may affect the ESA peak position at high intensity, where triple-excitations may be expected. EEA brings the excitons down to the single-exciton level, so highly excited exciton resonances become irrelevant. Consequently, the multiple-exciton variable factorization becomes highly relevant. The Ex-R model additionally implies fast relaxation of multiple exciton con-

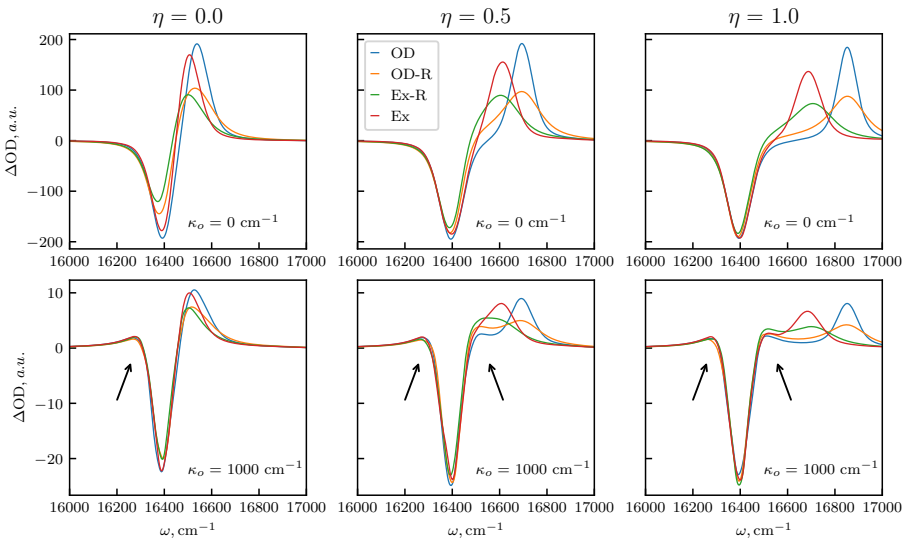

Figure 2.2.2: Pump-probe spectra for the aggregate of 7 molecules for strong pump excitation conditions at time delay 1 ps., first row - annihilation parameter $\kappa_0 = 0$, second row - $\kappa_0 = 1000$ cm^{-1}. Ex calculation for paulions was performed by including only 5 lowest exciton states, which is sufficient to fully represent the signal. Vertical axis represents optical density, horizontal - frequency.

figurations, leading to extra broadening of ESA. Finally, OD models are for the systems, experiencing the fast relaxation, when all properties are described within a single exciton band via incoherent exciton hopping (diffusion). Then ESA peaks reflect single-exciton resonances. For such systems, the signal information is preserved by dropping much of coherence terms. Hence, instead of the full Ex model calculations, which scale as N^6, the calculation may be reduced considerably down to N^4.

2.2.3 Reduced model

The scaling of the number of equations with the system size is at least N^4 for OD model, while it is N^6 for Ex model. This becomes prohibitive for large systems with thousands of molecules[64,65]. In the earlier subsection the aggregate of 7 chromophores is a relatively small system for performing full Ex model calculation. For much larger systems it is impossible to execute calculations and make comparisons.

For some types of molecular aggregates, the entire system can be described with just a few exciton states[66]. Such are the J aggregates where only a few lowest energy excitons have non-zero transition dipolar moment. Thus, we can restrict NEE to only those bright excitons and keep only the relevant variables describing them. High energy excitons in J aggregates may never be occupied and hence the corresponding variables can be dropped out. This is only applicable in exciton basis, as excitons are collective oscillations and couple to each other only via system nonlinearities and/or from relaxation/hopping which needs to be kept in mind when discarding excitons. As a result, the above presented calculations may be over-inclusive with the number of significant variables even smaller.

First, we take the same system of 7 chromophores and show in Figure 2.2.3 how fast the spectrum converges by increasing the included number of excitons starting from the lowest energy towards higher energies. It turns out that using only 1 exciton, which is the brightest one, the spectra already show bleach and ESA features, while the position of ESA is shifted from the full system of 7 excitons (in Fig. 2.2.2). The bleaching and emission components are not affected at all. ESA intensities are slightly higher. The largest deviations are for the Ex model. Increasing the number of excitons quite surprisingly, the spectra of 3 excitons appear to be converged, so the result can be achieved with a little computational effort.

Figure 2.2.4 shows the convergence of the spectra with EEA included. The

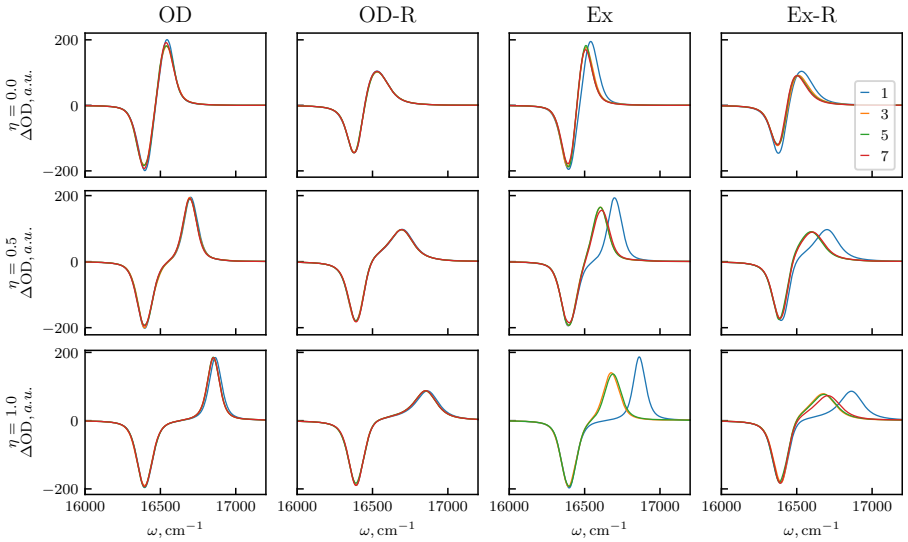

Figure 2.2.3: Convergence of the pump-probe spectra of 7 sites (at the same conditions as in Fig. 2.2.2) without annihilation. Vertical axis represents optical density, horizontal - frequency. The legend denotes the number of excitons used in calculation.

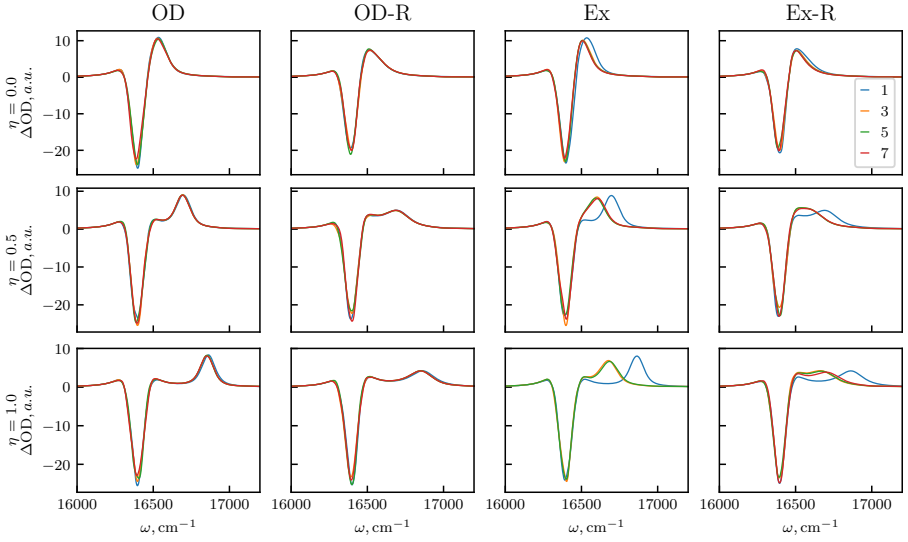

Figure 2.2.4: Convergence of the pump-probe spectra of 7 sites (at the same conditions as in Fig. 2.2.2) with EEA. Vertical axis represents optical density, horizontal - frequency. The legend denotes the number of excitons used in calculation.

convergence with the number of excitons is essentially also very fast so that the three excitons are sufficient to include for proper PP spectrum representation.

To understand how this translates to larger systems, next we made calculations for 15 and for 50 chromophores. The convergence of all theoretical models is similar. We thus present only the OD-R model (in Fig. 2.2.5). This model for larger systems produces PP spectra that closely matches higher level models with small computational cost. Compared to the case of 7 molecules we may notice more pronounced absolute intensity variation between different models at different values of η. Apart from that the spectra are very fast converging.

For a system of 50 sites the spectra converge, but this time we cannot calculate the full system of 50 excitons. An interesting point is that with more molecules ESA position becomes independent on η value, likely because of the entropic factor, where the combination excitations become much more abundant than the overtone-type excitations.

2.2.4 Discussion

NEE are very flexible to contain all necessary nonlinear properties. However, the number of equations describing various resonances depends on the excitation intensity. As the excitation intensity increases, the relevant number of variables in coherent conditions exponentially grow up. At the same time the number of excitations increases, thus the splitting between adjacent resonances diminishes. Effectively the system turns into a classical nonlinear oscillator system, which is very effective even for complicated systems, such as carbon nanotubes[47].

Direct numerical solution of NEE equations leads to additional benefit compared to order by order response function calculations. An arbitrary high order nonlinearities become directly incorporated and optical pulse overlap are included automatically.

Our proposed theoretical models in exciton basis can be used to increase calculation efficiency depending on the system parameters (and on the excitation regime). Comparing calculations (the timing tests were made on a PC) times between approximations we take $\eta = 0.5$ for 7 site aggregate. The full Ex calculation takes - 215 s, Ex-R - 214 s, OD - 4 s, OD-R - 4 s: these are the single runs for a single configuration of diagonal disorder. The absolute time is irrelevant (as different PCs would cause different times), however the computation time ratio between full Ex model and OD case is close to $7 \cdot 7 = 49$, hence, the

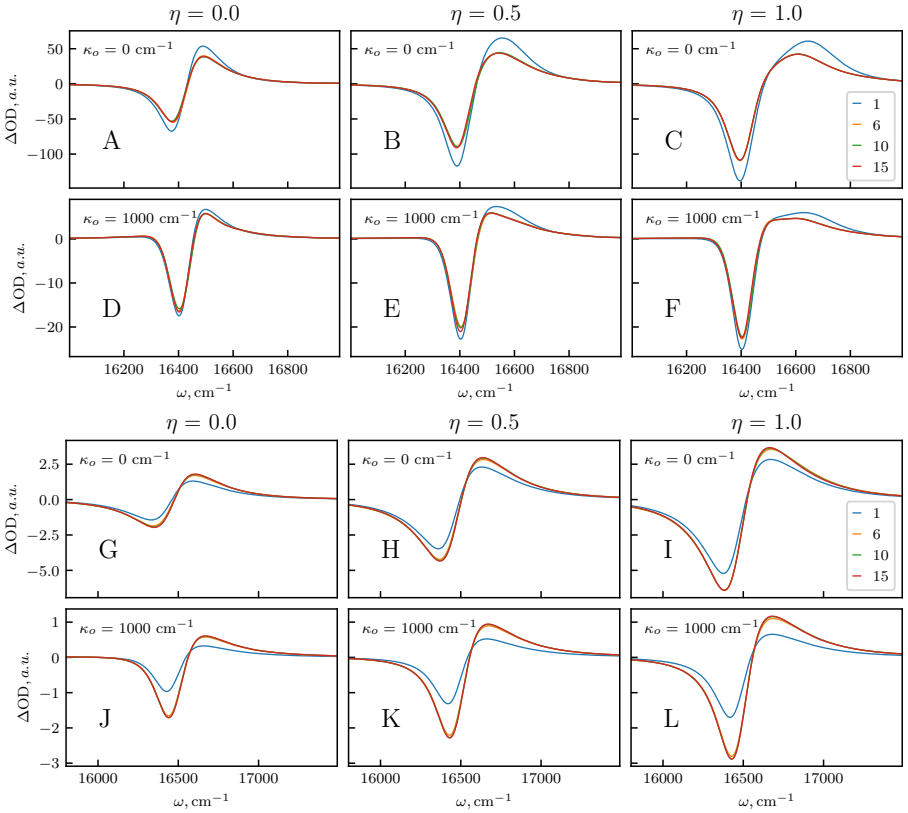

Figure 2.2.5: Pump-probe spectra for aggregates of 15 (A–F) and 50 molecules (G-L) in the exciton basis for the OD-R model, for A,B,C,G,H,I annihilation parameter is 0, D,E,F,J,K,L with EEA rate $\kappa_0 = 1000$ cm^{-1}. Vertical axis represents optical density, horizontal - frequency. The legend denotes the number of excitons used in calculation.

overdamped approximation makes calculation 2 orders faster. Essentially, the overdamped model allows to reduce the computational scaling from N^6 to N^4 where N is the number of molecules.

The highly nonlinear properties are mostly affecting the ESA peak (shape and position) in PP. The same would be the case for more advanced multidimensional spectroscopy techniques. We have shown that changing the model regimes as well as damping (linear relaxation and NEE) considerably affects the peak, and these properties can be employed to understand and control the whole spectrum of the system under consideration.

Truncation of the system depends on the relation between exciton dephasing and splitting of adjacent exciton states. This is effectively supported by EEA, which annihilates exciton pairs, thus reducing the need for high resonances. Accordingly, higher than double exciton resonances are barely created and can be neglected when EEA is in place. For example the triple excitations (characterized by $\langle \hat{b_n^3} \rangle$, $\langle \hat{b_n^\dagger} \hat{b_n^3} \rangle$, $\langle \hat{b_n^{2\dagger}} \hat{b_n^3} \rangle$, $\langle \hat{b_n^{3\dagger}} \hat{b_n^3} \rangle$ and similar or higher orders) on the same chromophore become highly unlikely because of EEA, which quenches such states. So, the excitation "accumulation" on the same chromophore is disregarded. On different chromophores excitations are possible but are independent. So $\langle \hat{b_n^\dagger} \hat{b_k^{j\dagger}} \hat{b_n} \hat{b_k^i} \rangle \approx \langle \hat{b_n^\dagger} \hat{b_n} \rangle \langle \hat{b_k^{j\dagger}} \hat{b_k^i} \rangle$. In this case higher-than triple products of operators can be neglected, what allows to close the hierarchy of equations.

Such truncation is not applicable for systems such as H aggregates. H type aggregates (in contrast to J type) have bright exciton at the highest energy. Thus, such systems are excited in a state that is far from steady state, exhibit a lot of energy transfer effects and coherence effects. While overdamped model accounts for population transfer, the coherences are neglected. J aggregates exhibit less change after excitation as the system is already close to the steady state. The only way the higher energy excitons in J aggregate can be reached is through thermalization as excitations redistribute from the only bright exciton to higher energy excitons.

2.3 Application of NEE for calculation of high order 2D spectra

In this part we apply NEE to calculate 3rd and 5th order 2DES (two dimensional electronic spectroscopy). We limit this analysis to dimer and trimer systems. To extract highly nonlinear 2D signals we apply the phase cycling method[34].

2.3.1 System parameters and model

For study of EEA effect on 2DES spectra we use two simple model systems: a chromophoric dimer and a trimer. Both systems consist of identical chromophores. Their single chromophore excitation energy is taken as a reference and is placed at 0 cm^{-1}. So, all the spectra are presented with respect to that value. The resonant coupling, for the dimer, is taken as $J_{12} = -200$ cm^{-1}, while for the trimer we have a chain with $J_{12} = J_{23} = J_{31} = -200$ cm^{-1}.

We calculate both cases of exciton statistics: paulions and bosons. In the case when particles are boson, we set anharmonicity parameter as $K = 500$ cm^{-1}. For paulions the parameter K is not relevant.

For system-bath interaction we use a Drude spectral density (Eq. 2.1.1), where the correlation decay rate $\Lambda = 50$ cm^{-1}, and the reorganization energy $\lambda = 10\,\text{cm}^{-1}$, and we take the room temperature conditions, $k_B T = 200\,\text{cm}^{-1}$. Static disorder was not included to reveal the fine structure of the spectrum.

As we include EEA terms, optical excitation field intensity becomes an important parameter. The optical field envelope is defined as $\boldsymbol{E}_l(t) = A_l E_0(t)$, A_l is the amplitude, which can be tuned, and $E_0(t)$ is the normalized envelope function

$$E_0(t) = \frac{1}{\tau\sqrt{2\pi}} \exp\left(-\frac{t^2}{2\tau^2}\right), \tag{2.3.1}$$

where τ is the time domain Gaussian standard deviation of the normalized pulse. The width of all pulses is set to $\tau = 6$ fs. In 2DES the first 2 pulses set up the non-equilibrium system and the 3rd pulse reads the system state. Note that $A\mu E_0(t)$ has dimension of energy cm^{-1}, we will consider that $E_0(t)$ carries dimensional qualities and $A\mu$ is then dimensionless. With this and knowing that $\int E_0(t)\mathrm{d}t = 1$, i.e. dimensionless, we can parametrize the amplitude for the two first pulses as strong excitation $A\mu = \frac{0.9}{\sqrt{N}}$ and for the last (detection) pulse (weak deexcitation) $A\mu = \frac{0.01}{\sqrt{N}}$, where N is number of chromophores; the factor related to the number of chromophores is required to keep the excitation intensity consistent between dimer and trimer, as both are J type systems, where only the lowest-energy exciton has non-zero transition dipole moment, which is $\sqrt{N}\mu_0$, where μ_0 is the single chromophore transition dipole moment. The transition dipole moment for all molecules is the same $\mu = \mu_0$. Note that the chosen envelope of pulse implies the bandwidth limited pulses.

In this section we used the model described by Eqs. 1.4.10-1.4.13, with simpler relaxation terms for z equation. The model used explicitly drops out 3 excitation terms. This was done to simplify the interpretation of 2DES spec-

tra. The effects of higher order terms on 2DES spectra need to be studied in a separate study.

2.3.2 $\vec{K_1} - \vec{K_2} + \vec{K_3}$ 2DES spectra dynamics of a paulionic chromophoric dimer

A symmetric dimeric J-type paulionic system has two single-excitonic states, which are separated by energy gap $2J_{12}$ related to resonance interchromophoric interaction. In the absence of an environment, the lower-energy state is optically bright, while the higher-excitonic peak is optically dark. There is also a single double-exciton state, with energy equal to the sum of the chromophore excitation energies. The linear absorption spectrum of the dimer would show a single peak, corresponding to the bright exciton.

Third order nonlinear spectra additionally involve the excited state absorption, where the double-exciton state becomes involved. The non-rephasing ($\vec{K_1} - \vec{K_2} + \vec{K_3}$) 2DES spectra for paulionic dimer is presented in Fig. 2.3.1. The figure shows $\vec{K_1} - \vec{K_2} + \vec{K_3}$ 2DES spectra for 3 different annihilation values: $\kappa_0 = 0$ cm^{-1} - no annihilation, 1 cm^{-1} - small EEA parameter value, and 100 cm^{-1} - large EEA parameter value. Notice that the annihilation parameter values do not explicitly correspond to annihilation times as the annihilation process is not exponential, thus annihilation time cannot be assigned. For each case, the 2DES spectra were calculated at multiple t_2 delay times.

The well-known third-order features of the dimer are observed on the left column at short delay time in Fig. 2.3.1. The low energy diagonal peak ($\omega_1 = \omega_3 = -200$ cm^{-1}) corresponds to the low energy exciton in the dimer, and the cross-peaks show coherences in the system. The cross-peak, which is above the diagonal (a weak peak at $\omega_1 = -200$ cm^{-1}, $\omega_3 = 200$ cm^{-1}) is opposite from the diagonal peak by sign and shows excited state absorption. The other potential cross-peak ($\omega_1 = 200$ cm^{-1}, $\omega_3 = -200$ cm^{-1}) is invisible since the corresponding higher energy exciton (at $+200$ cm^{-1}) is optically dark.

Little change is observed over the delay time t_2. Since the diagonal peak corresponds to the lowest energy exciton, there is no significant relaxation happening; One additional little cross-peak at ($\omega_1 = 200$ cm^{-1}, $\omega_3 = -200$ cm^{-1}) becomes visible at long delay time. Its intensity grows because of excitation thermalization dynamics. Notice that while the higher exciton is dark, the high intensity of the excitation pulse takes the system away from perturbative excitation regime and excitations are pushed into the dark excited state; later these relax slowly into the bright state and we obtain slight growth of spectral inten-

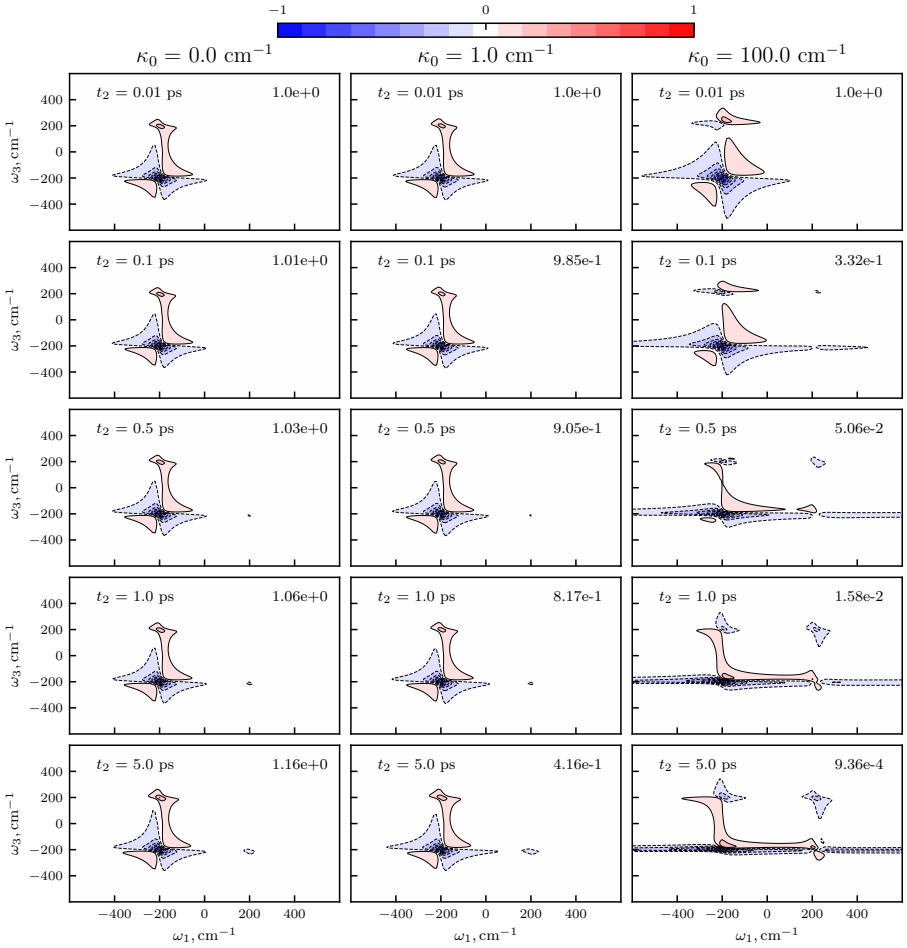

Figure 2.3.1: $\vec{K}_1 - \vec{K}_2 + \vec{K}_3$ 2DES spectra of J type dimer ($J_{12} = -200$ cm^{-1}) for paulions at various delay times t_2 and for various EEA parameter values. In each subfigure the top left corner has the delay time, top right the amplitude in relation to top row amplitudes that are set to 1. At the very top of the figure colorbar is given, for each subfigure the amplitude of colorbar should be taken as amplitude (negative and positive) given in the subfigure.

sities even without EEA terms.

If EEA is turned on (small annihilation parameter value) the peaks decay over time and peak shapes are broader. No other substantial changes appear, however, with further increase of the annihilation parameter all cross-peaks become stronger with respect to the diagonal peak at short delay times ($t_2 = 0.5$, 1 ps delay) and decays over longer times are more severe. A striking feature is that at these delay times the diagonal peak at $\omega_1, \omega_3 = +200$ cm^{-1} becomes observable, which was optically dark without annihilation. For very short delay times ($t_2 = 0.01$, 0.1 ps) the lineshapes are significantly broader. At long delay times the lower diagonal peak gets broadened along ω_1 and broadening in ω_3 decreases to the same levels as with no annihilation. This is related to the fact that with the delay time the system returns to lower excited levels (due to EEA), where lineshapes are smaller. Additionally, for a large EEA parameter value the excited state absorption peak gets an extra feature (blue slightly shifted from the red) which is related to contribution from an additional quantum pathway, where three interactions take place with K_2 pulse. This pathway does not contribute without EEA at a unique position.

2.3.3 $2\vec{K_1} - 2\vec{K_2} + \vec{K_3}$ 2DES spectra dynamics of the paulionic chromophoric dimer

Next, we study the fifth order signal at $2\vec{K_1} - 2\vec{K_2} + \vec{K_3}$. Annihilation is a fifth order process to the optical field therefore it should have more pronounced effect in $2\vec{K_1}-2\vec{K_2}+\vec{K_3}$ 2DES signal compared to $\vec{K_1}-\vec{K_2}+\vec{K_3}$ signal[67,68,24].

However, the excitonic dimer is a highly nonlinear system even without EEA, so the fifth order signal is generated when $\kappa = 0$ due to the Pauli exclusion. The result is shown in Fig. 2.3.2 on the first column. Comparing the $2\vec{K_1} - 2\vec{K_2} + \vec{K_3}$ to $\vec{K_1} - \vec{K_2} + \vec{K_3}$ signal for a chromophoric dimer we see the effect of paulionicity: the paulions forbid double excitation on a single chromophore, so the signal is at ($\omega_1 = 0$ cm^{-1}, $\omega_3 = \pm 200$ cm^{-1}), showing the presence of the double exciton created by $2K_1$ excitation. The time evolution is slow as well. There is the overall peak intensity decay apparently from a simplified model of Markovian relaxation, which excessively damps z variable.

When EEA is enabled, we see a few significant changes. Additional peaks appear along $\omega_1 = -400$ cm^{-1} at $\omega_3 = \pm 200$ cm^{-1}. The features along $\omega_1 = -400$ cm^{-1} can be associated with two-time excitation of the lower-energy exciton (note that there is neither exciton state at -400 cm^{-1}, nor dou-

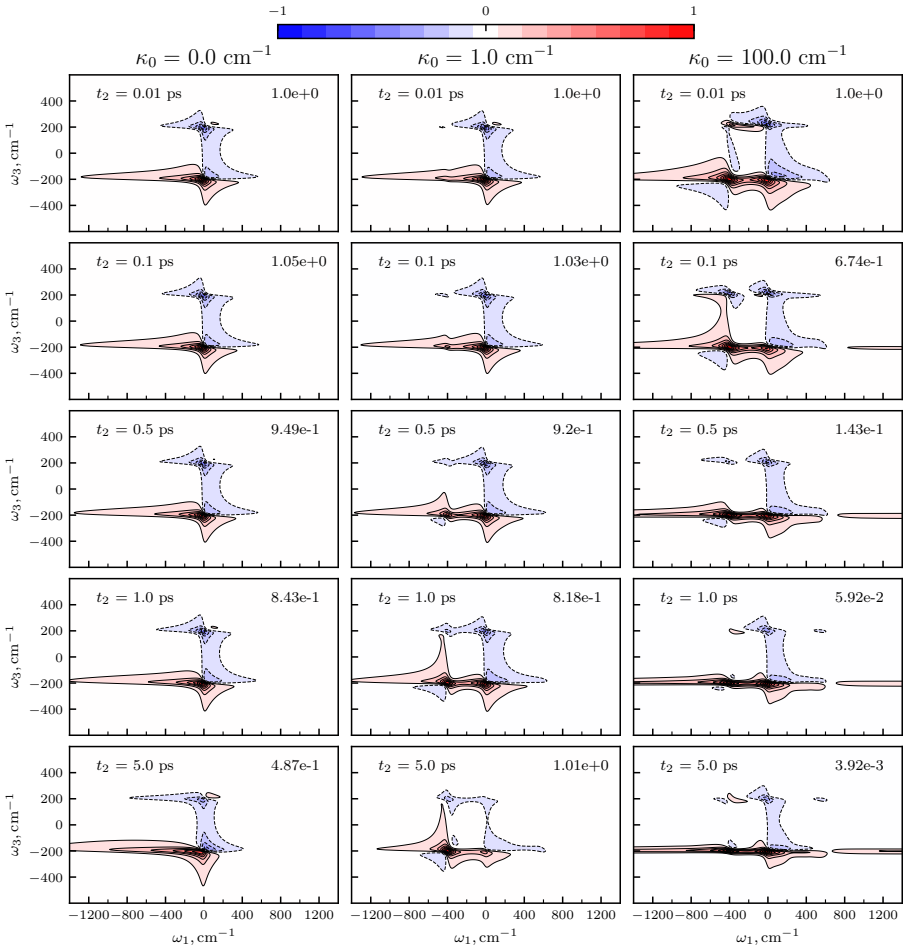

Figure 2.3.2: $2\vec{K}_1 - 2\vec{K}_2 + \vec{K}_3$ 2DES spectra of J type dimer ($J_{12} = -200\,\mathrm{cm}^{-1}$) for paulions at various delay times t_2 and for various EEA parameter values. See fig. 2.3.1 for markings description.

ble exciton at this position). These new peaks grow in intensity over the delay time compared to the peaks along $\omega_1 = 0$. The reason why we have these features appear can be related to the EEA process taking place during the excitation events. EEA is a local chromophoric process and likely eliminates exciton-imposed symmetries even during the pulses actions. As a result, the action of $2\vec{K}_1$ creates the *excitons* two times resulting in doubling the excitonic coherence. This is a pure feature of the NEE form.

For large EEA everything decays, but at different parameter values. The features at $\omega_1 = -400$ cm^{-1} are more intensive while quickly decaying, and other features are broader in general, but for longer delay times the features decay and become narrow in ω_3. The lineshapes are significantly distorted at long delay times compared to the case without EEA.

For large EEA the peak along $\omega_1 = +400$ cm^{-1} appears; its origin is the same as the peak along $\omega_1 = -400$ cm^{-1}. However, the peak along $\omega_1 = +400$ cm^{-1} is additionally related to "opening" of the dark exciton. The EEA, being the local chromophoric process, destroys excitonic system symmetry and mends the exciton characteristics by opening the dark transitions.

2.3.4 $\vec{K}_1 - \vec{K}_2 + \vec{K}_3$ 2DES spectra dynamics of the trimer

A paulionic chromophoric dimer is the smallest system, where aggregate features are included, however, its double exciton band consists of a single state. In larger systems the double-exciton band is also a band of states. So next we check whether the above-mentioned properties are observed for a chromophoric trimer, which in principle has three doubly excited states. Notice that for our system the structure of the double-exciton band is the same as for the single-exciton band: one state is at -400 cm^{-1} and two degenerate states are at $+200$ cm^{-1}. The $\vec{K}_1 - \vec{K}_2 + \vec{K}_3$ 2DES non-rephasing spectra of the paulionic trimer is shown in figure 2.3.3. Only the lowest energy exciton is bright. In the 2DES spectrum for $\kappa_0 = 0$ we see the single diagonal peak and excited state absorption at $\omega_3 = 0$ cm^{-1}, that show coherence between the chromophores. At long t_2 delay a cross-peak at $\omega_1 = 0$ cm^{-1}is induced in the same way as for the dimer. Decay of peaks is turned on by switching on the EEA. With a larger annihilation parameter, the decay intensifies (especially of the diagonal peak) and cross-peaks become more resolvable. Like the dimer case, the features which were forbidden without EEA are magnified by EEA again via breaking of excitonic symmetries.

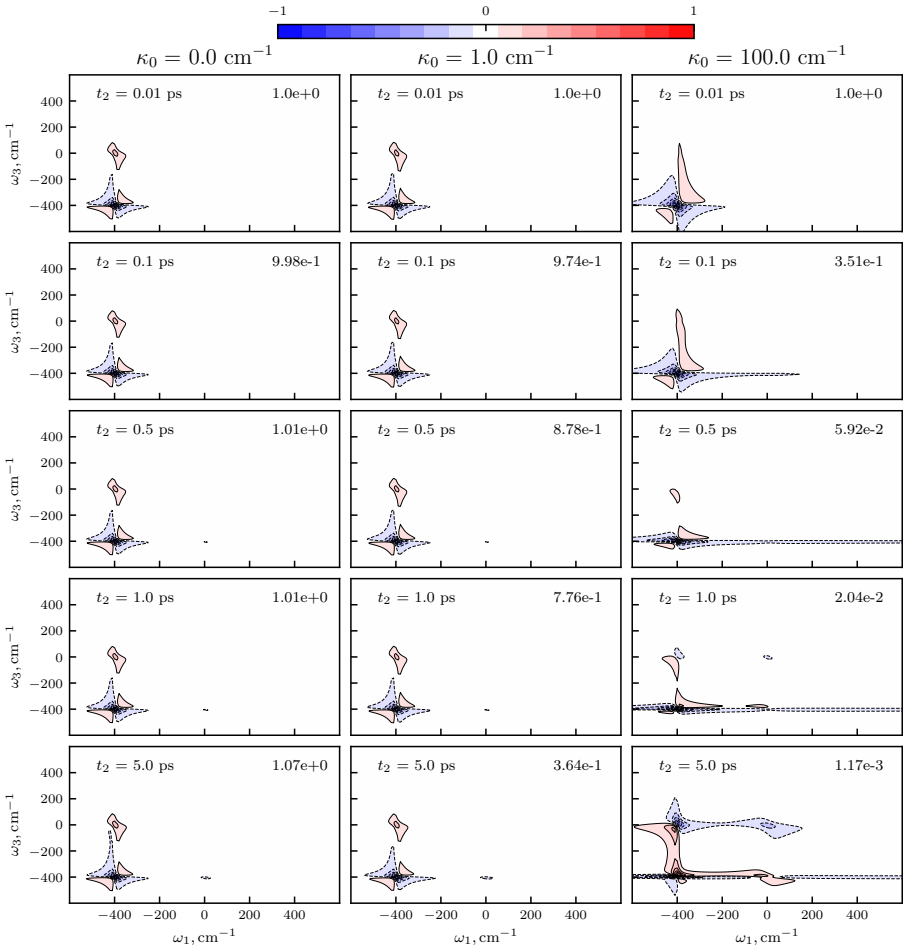

Figure 2.3.3: $\vec{K}_1 - \vec{K}_2 + \vec{K}_3$ 2DES spectra of J type trimer ($J_{12} = J_{23} = J_{31} = -200$ cm^{-1}) for paulions at various delay times t_2 and for various EEA parameter values. See fig. 2.3.1 for markings description.

2.3.5 $2\vec{K}_1 - 2\vec{K}_2 + \vec{K}_3$ 2DES spectra dynamics of a trimer

$2\vec{K}_1 - 2\vec{K}_2 + \vec{K}_3$ 2DES spectra for the trimer is shown in figure 2.3.4. The effects in general mirror the features which were observed for the dimer. For the no-annihilation case, the features are along $\omega_1 = -400$ cm^{-1}, which corresponds to the lowest energy double exciton creation. The peak at $\omega_3 = -400$ cm^{-1} corresponds to the main exciton and $\omega_3 = 0$ cm^{-1} corresponds to coherence between single and double excitons.

Since the overall features resemble the dimer, only one bright exciton determines most of the features. The peak decay with the delay time becomes considerably faster with annihilation enabled and we see additional spectral peaks appearing along $\omega_1 = -800$ cm^{-1}; same tendency as observed for the dimer along $\omega_1 = -400$ cm^{-1}. These features appear at a position where two-time excitation of the bright exciton occurs. Again, the annihilation introduces decay of excitons during the excitation process and re-excitation of the excitons takes place. For large annihilation parameter values the lineshapes along ω_3 get smeared out and at short delay times the peaks get broadened symmetrically, while for longer delay time the peak intensities redistribute due to uneven annihilation across the exciton band.

2.3.6 $\vec{K}_1 - \vec{K}_2 + \vec{K}_3$ 2DES spectra for bosons

Next, we present the same type of spectra that were made for paulions, but for the boson case. For the dimer, the $\vec{K}_1 - \vec{K}_2 + \vec{K}_3$ bosonic spectra are shown in figure 2.3.5. The main difference from the paulions is that the cross-peaks related to the correlations between excitons are not visible in boson case. Strong excited state absorption shows up at around ($\omega_1 = -200$ cm$^{-1}, \omega_3 = 0$ cm^{-1}) and is shifted by about half the anharmonicity value from the main peak ($\omega_1 = -200$ cm$^{-1}, \omega_3 = -200$ cm^{-1}) and consists of blended chromophore overtone excitation and a combination band excitation. These features are mirrored at around $\omega_1 = 0$. For the case with no EEA, we see slight decay of the signal in contrast with slight growth in paulion case. The difference is that in boson case in NEE there is no population-dependent transition dipole anharmonicity (in general transition dipole moment terms are multiplied by $(1 - 2\eta\hat{\sigma}_{uu})$ in Eqs. 1.4.5-1.4.8). For large EEA parameter values, we see spectra significantly broadened with larger decay over delay time.

For the trimer, the $\vec{K}_1 - \vec{K}_2 + \vec{K}_3$ spectra are shown in figure 2.3.6. We see the same trend as in the dimer case (note the figure does extend to positive ω_3;

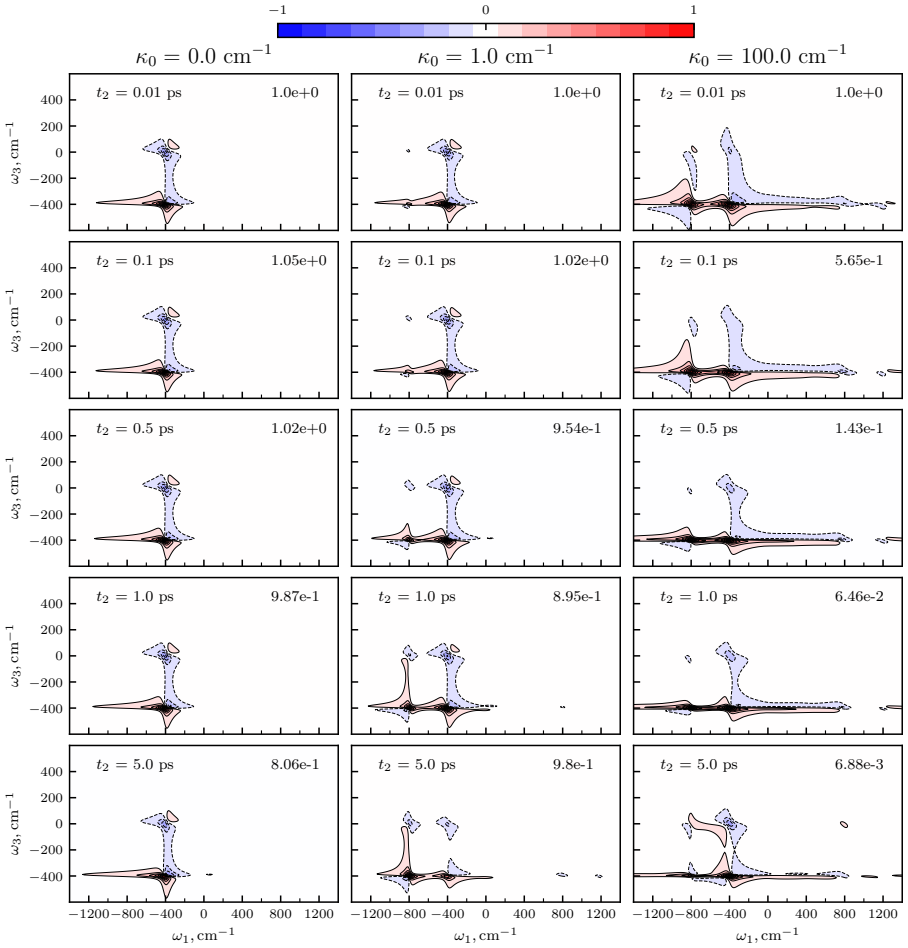

Figure 2.3.4: $2\vec{K}_1 - 2\vec{K}_2 + \vec{K}_3$ 2DES spectra of J type trimer ($J_{12} = J_{23} = J_{31} = -200$ cm^{-1}) for paulions at various delay times t_2 and for various EEA parameter values. See fig. 2.3.1 for markings description.

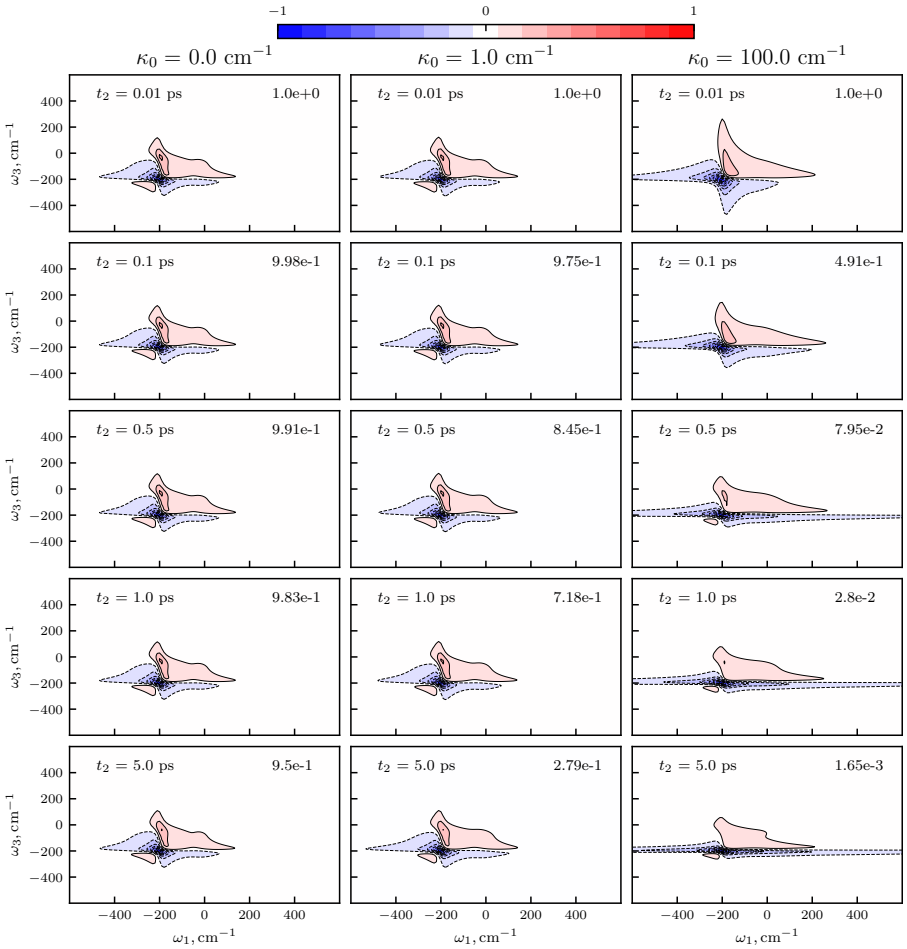

Figure 2.3.5: $\vec{K_1} - \vec{K_2} + \vec{K_3}$ 2DES spectra of J type dimer ($J_{12} = -200\ \mathrm{cm}^{-1}$) for bosons at various delay times t_2 and for various EEA parameter values. See fig. 2.3.1 for markings description.

there are no features visible in there). The differences are the main diagonal peak is at ($\omega_1 = -400$ cm$^{-1}, \omega_3 = -400$ cm^{-1}), and the cross-peaks are closer to the diagonal peak, compared to the dimer case.

2.3.7 $2\vec{K}_1 - 2\vec{K}_2 + \vec{K}_3$ 2DES spectra for bosons

The $2\vec{K}_1 - 2\vec{K}_2 + \vec{K}_3$ signal is more complex for bosons as shown in figures 2.3.7 and 2.3.8. For bosons the chomophoric overtone state is not forbidden, and it dominated the spectra giving peaks, for the dimer at ($\omega_1 \approx -300$ cm$^{-1}, \omega_3 \approx -200$ cm^{-1}) and for the trimer at ($\omega_1 \approx -700$ cm$^{-1}, \omega_3 \approx -400$ cm^{-1}). The lineshapes are slightly broader compared to paulions.

In the dimer case we observe additional peaks at ($\omega_1 \approx 700$ cm$^{-1}, \omega_3 \approx -200$ cm^{-1}) which correspond to excitation of another double exciton, which is not available for the paulions. This feature gets weaker compared to the main feature with EEA enabled, due to double exciton quenching.

For the trimer, additional peaks, corresponding to excitation of other double excitons (along $\omega_1 \approx -800$ cm^{-1}), are weaker compared to the dimer case. Same as in the dimer case this feature decays when EEA is enabled, but we see additional features at ($\omega_1 = 1200$ cm$^{-1}, \omega_3 = -400$ cm^{-1}) which shows contributions from even other excitons. A trimer system has 3 double excited states of which only one is visible at low excitation intensity. With increased excitation intensity effects from other double excited states become visible.

2.3.8 Discussion

Phase cycling has been used for disentangling various phase matching components. The downside of this approach when applied to calculations is that it requires repeated calculations multiple times for phase shifts. The upside is that the system of equations is preserved and does not need to be rearranged using order by order expansion methods (which do not work in this case since EEA leads to non-exponential dynamics). Also, computationally phase cycling is easy to parallelize, so it is very efficient.

We see that inclusion of EEA terms affects 2D spectra significantly. The most basic phenomena introduced by inclusion of EEA is the decay of spectral features over the delay time, which can be observed when the EEA is active. Additionally, EEA affects peak linewidth. With increased EEA parameter value cross-peaks are enhanced, even the peaks that should be dark and have no transition dipole moment become visible. For the $2\vec{K}_1 - 2\vec{K}_2 + \vec{K}_3$ signal

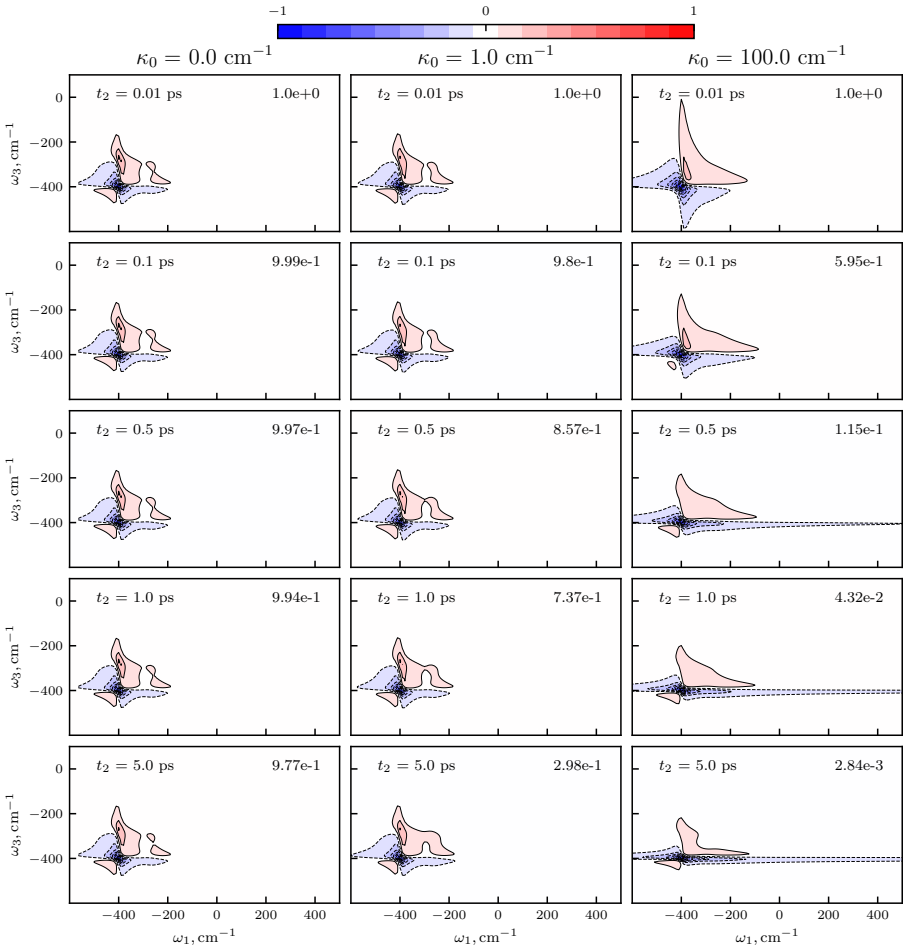

Figure 2.3.6: $\vec{K}_1 - \vec{K}_2 + \vec{K}_3$ 2DES spectra of J type trimer ($J_{12} = J_{23} = J_{31} = -200$ cm^{-1}) for bosons at various delay times t_2 and for various EEA parameter values. See fig. 2.3.1 for markings description.

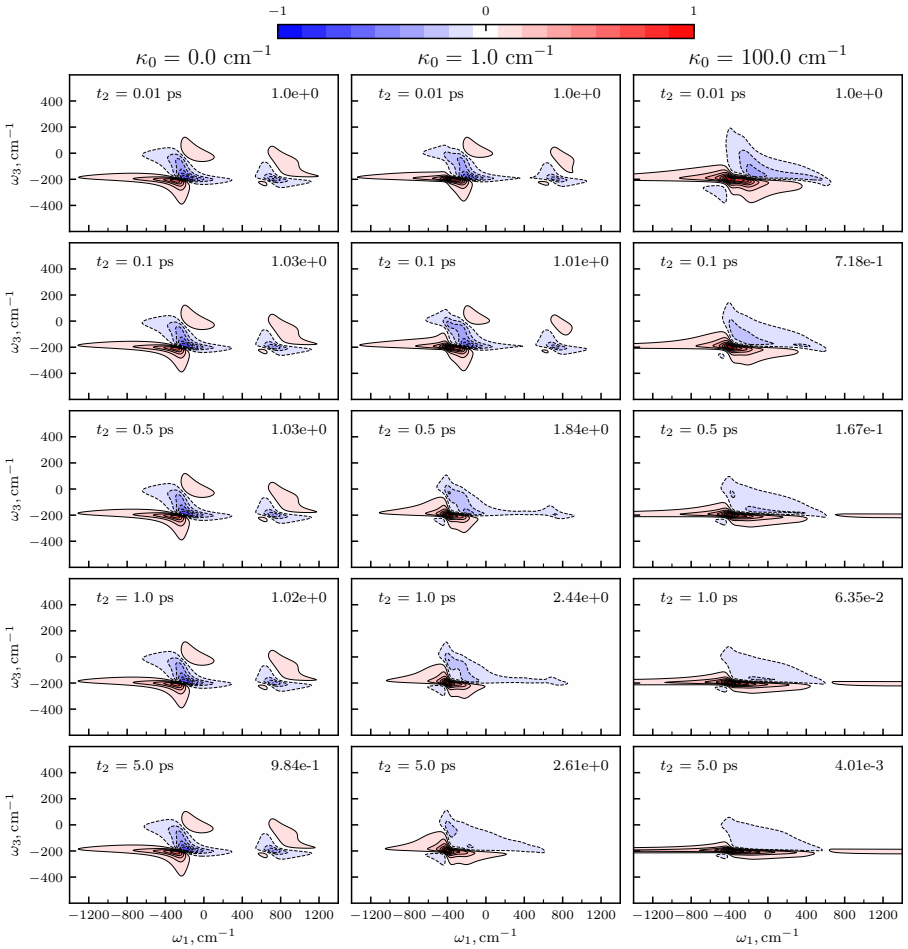

Figure 2.3.7: $2\vec{K}_1 - 2\vec{K}_2 + \vec{K}_3$ 2DES spectra of J type dimer ($J_{12} = -200$ cm^{-1}) for bosons at various delay times t_2 and for various EEA parameter values. See fig. 2.3.1 for markings description.

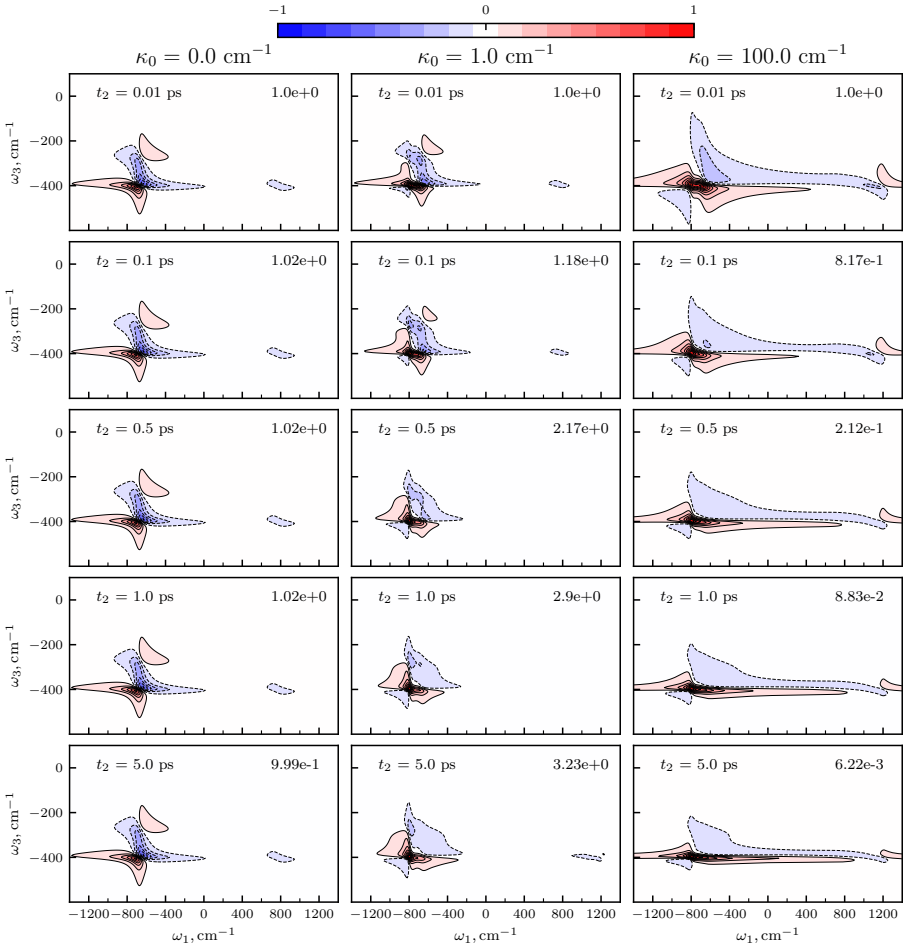

Figure 2.3.8: $2\vec{K}_1 - 2\vec{K}_2 + \vec{K}_3$ 2DES spectra of J type trimer ($J_{12} = J_{23} = J_{31} = -200$ cm^{-1}) for bosons at various delay times t_2 and for various EEA parameter values. See fig. 2.3.1 for markings description.

we also find peaks associated with forbidden transitions as well as with double resonances. An additional feature related to high intensity excitations is related to deviations from the perturbative excitation regime. In this case an excitation does not necessarily correspond to transition between specific system levels. Instead, specific resonances may be initiated during the excitation process, which follow different symmetry selection rules from exciton. This is the main reason why dark excitons become populated. Then they relax into bright states and give time dependent features at non-standard positions.

Indeed, in perturbative treatment, the material Hamiltonian eigenstates (excitons in our model) are stationary states when the optical field is switched off; the field introduces only transitions between these states. However, when the external field is on continuously, the full stationary Hamiltonian has additional stationary system-field interaction. Even if the material Hamiltonian is diagonal (in e.g., exciton representation), the full stationary system-field Hamiltonian in this case would be not diagonal and its new stationary states are denoted by polaritons[69]. Correspondingly their selection rules are different compared to excitons.

In our case the optical field is impulsive, and in the excitation process when the field is on, our system momentarily enters non-perturbative polaritonic regime when even the dark excitons (which are dark when the field is off) turns to be open for excitation. This symmetry breaking is explicitly defined by population-scaled transition dipoles in Eqs. 1.4.5-1.4.8, i. e. at high occupation numbers $\mu_n(t) \to (1 - 2\eta\sigma_{nn})\mu_n(t)$.

This feature leads to counterintuitive behavior in $\vec{K_1} - \vec{K_2} + \vec{K_3}$ spectra for paulions when specific spectral features grow with the delay time in case with no EEA. Such growth is related to additional occupation of the bright exciton by slow relaxation of population from the dark exciton, being populated during the excitation process. The nature of this is clearer when we see how the exciton populations behave after single-pulse excitation (like in pump-probe scheme). We show exciton population dynamics in figures 2.3.9, for high excitation intensity, and 2.3.10, for low excitation intensity, for a dimer with the same parameters. The most interesting case is for paulions at high excitation intensity. We see that the lowest energy exciton (which is bright by exciton selection rules) becomes saturated when pumping and the second exciton (which is dark by exciton selection rules) acquires population. The other cases show that boson populations do not show such saturation and behave the same way, independent of excitation intensity except only scaled. We also observe the

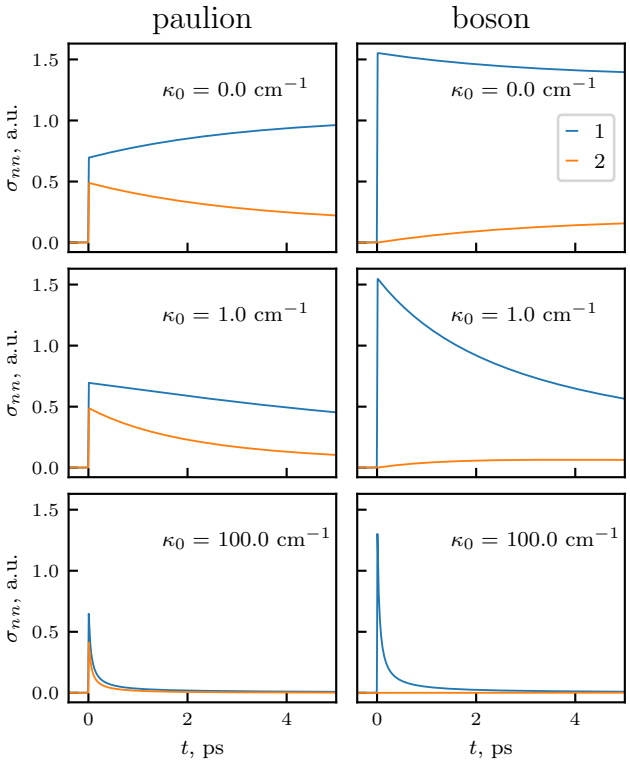

Figure 2.3.9: Population dynamics of a molecular dimer ($J_{12} = -200$ cm^{-1}), in high excitation regime after a single pump-type excitation. System parameters are the same as the parameters of the dimer in this chapter. Shown populations are in exciton basis where legend shows the exciton, i. e. the bright lower-energy exciton σ_{11}, and the dark higher-energy exciton σ_{22}. The optical pulse intensity parameter $A\mu = 0.9$.

nonexponential decay induced by EEA.

Additional resonances also emerge at high excitation intensity and remain even when the field is off. For example, a paulionic dimer would have two excitons with energies -200 cm^{-1} and $+200$ cm^{-1} and double excitation, which is at the sum of the single exciton energies (0 in the present case). The spectra features would be at $\omega_1 = 0$ cm^{-1}(paulions forbid double excitation on same site) and $\omega_3 = -200$ cm^{-1}, yet we observe feature at ($\omega_1 = -400$ cm^{-1}, $\omega_3 = -200$ cm^{-1}) that grows with the delay time relative to the other spectral features as the whole spectrum decays. For the trimer we have features in the same spirit appearing at ($\omega_1 = -400$ cm^{-1}, $\omega_3 = -200$ cm^{-1}) , and the features at $\omega_1 = -200$ cm^{-1} are partially replicated at $\omega_1 = -400$ cm^{-1}.

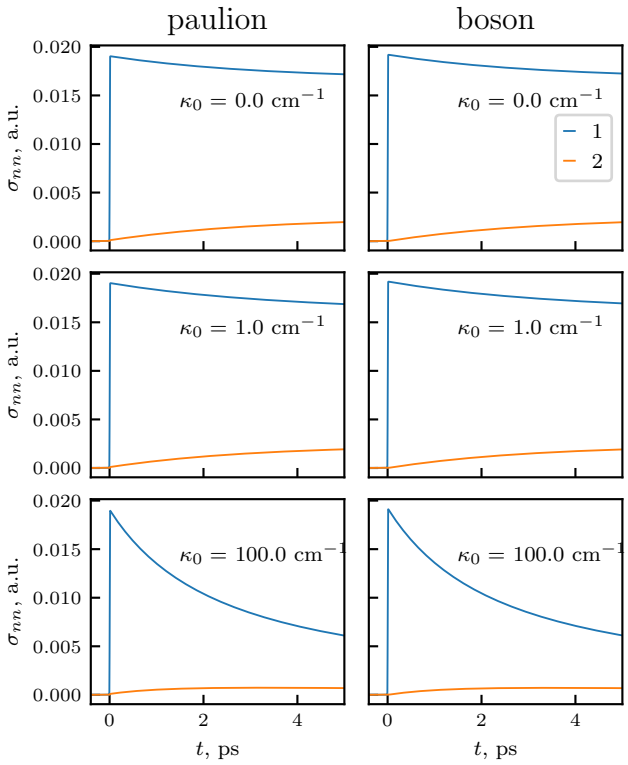

Figure 2.3.10: Population dynamics of a molecular dimer ($J_{12} = -200\,\mathrm{cm}^{-1}$), in low excitation regime after a single pump-type excitation. System parameters are the same as the parameters of the dimer in this chapter. Shown populations are in exciton basis where legend shows the exciton, i. e. the bright lower-energy exciton σ_{11}, and the dark higher-energy exciton σ_{22}. The optical pulse intensity parameter $A\mu = 0.1$.

These high-intensity related features could be explicitly demonstrated by using the NEE formalism. Notice that in Eqs. 1.4.5-1.4.8 in operator notation not only all transition dipoles have additional population-related scaling as described above, but the resonant couplings can be also considered as scaled by populations $J_{nm} \rightarrow (1 - 2\eta\sigma_{nn})J_{nm}$. This severely affects excitonic resonances at high excitation intensity. These specific features of the NEE equations lead to very fine effects in various 2D spectra. Overall, the spectra become very sensitive to paulionicity, anharmonicity, EEA and excitation intensity and various experiments have to be examined very carefully to capture these specific processes.

Bosonic systems in general exhibit similar 2DES spectra features with few exceptions. In the $2\vec{K_1} - 2\vec{K_2} + \vec{K_3}$ case the features which were along $\omega_1 = -400$ cm^{-1}for the paulion dimer are overshadowed by overtone excitations in bosons case. Another difference is the appearance of new high energy peaks of other double-excitons that decay with enabled EEA. Overall, at high excitation intensity all features reflect the anharmonicity parameter $K-$induced presence of negative-positive doublet implying the existence of possible absorption from an arbitrary excited state. These features represent anharmonic ladder scheme of boson states.

We chose the parameters for the model system to represent a variety of systems. For the squaraine dimers the coupling values, for example in ref. [70], range from -350 cm^{-1}to -650 cm^{-1}. J-aggregates have even larger values [63], while the coupling between the special pair in the photosynthetic reaction center of photosystem II [71] is around 150 cm^{-1}. So, our set of couplings fall within this wide range. Bath parameters were tuned to have narrow enough lineshape to see details. In general, the main effect of annihilation in experiments is the nonexponential decay of spectral features. This decay depends on initial excitation intensity and in our case a single annihilation parameter. In addition, the geometry of nearest neighbors of each molecule should also be considered. We believe the realistic value should fall between the small values we chose and the large value. As a comparison, for a specific double walled molecular tubular J-aggregate annihilation happens on a timescale of picoseconds [23], which coincides with our calculations.

In our case the optical field is impulsive, and in the excitation process when the field is on, our system momentarily enters non-perturbative polaritonic regime when even the dark excitons (which are dark when the field is off) turn to be open for excitation. This symmetry breaking is explicitly defined

by population-scaled transition dipoles in Eqs. 1.4.5-1.4.8, i. e. at high occupation numbers $\mu_n(t) \to (1 - 2\eta\sigma_{nn})\mu_n(t)$.

This feature leads to counterintuitive behavior in $\vec{K_1} - \vec{K_2} + \vec{K_3}$ spectra for paulions when specific spectral features grow with the delay time in the case with no EEA. Such growth is related to additional occupation of the bright exciton by slow relaxation of population from the dark exciton, being populated during the excitation process. The nature of this is more clear when we observe how the exciton populations behave after single-pulse excitation (like in pump-probe scheme). We show exciton population dynamics in figures 2.3.9, for high excitation intensity, and 2.3.10, for low excitation intensity, for a dimer with the same parameters. The most interesting case is for paulions at high excitation intensity. We see that the lowest energy exciton (which is bright by exciton selection rules) becomes saturated when pumping and the second exciton (which is dark by exciton selection rules) acquires population. The other cases show that boson populations do not show such saturation and behave the same way, independent of excitation intensity except only scaled. We also observe the nonexponential decay induced by EEA.

In this work we apply a phenomenological description of the EEA[9]. We could achieve a more explicit description of the EEA by adding Hamiltonian terms that would couple single and double excitation bands (terms that do not preserve the number of excitations): $\left[I_{m\alpha}\hat{b_m}\right]\hat{Q_\alpha}$, $\left[I'_{mn\alpha}\hat{b_m^\dagger}\hat{b_m}\hat{b_n}\right]\hat{Q_\alpha}$ and etc., here $\hat{Q_\alpha}$ is the coordinate operator of the α bath oscillator, $I_{m\alpha}$ and $I'_{mn\alpha}$ are coupling coefficients between bath oscillators and excitation bands. These terms require further study to determine if the modeled EEA behavior is computationally feasible to apply in practice and if it corresponds to the experiments.

Additionally, here we have made an approximation by neglecting triple excitation terms in equations (e.g., *bbb* and their Hermitian conjugates). It can be argued that at the high excitations these terms should be needed. However, at higher excitation intensity the EEA process becomes dominant, and excitations are efficiently quenched so triple excitations, and their corresponding resonances are not generated. Effects of these terms require additional study.

3 CONCLUSIONS

1. We have shown that NEE can be very efficiently factorized in real space and then truncated in eigenstate space. As a result, a highly nonlinear spectra of very large molecular chromophore aggregates can be calculated quite efficiently. The ESA peak is the most sensitive to the nonlinear properties and must be studied to determine system properties at high excitation conditions.

   As already noted, the main reason factorization is included is to close the hierarchy of equations due to limited computational resources. The mathematically exact approach is given by infinite hierarchy of equations, which cannot be implemented in calculations. However, the "best" factorization method does not exist - different factorization approaches enhance different phenomena. For example, one of the simplest the direct factorization model can be used if only shift of absorption line with excitation intensity is observed. Including z variable may be important, if separate excited state absorption line is observed.

   Different types of factorization lead to distinct simplification of equations which lead to efficient and fast computations. The simplest set of equations certainly leads to very fast calculations. Alternatively, some other types lead to instabilities: note that the $zz5$ model fails to converge for high intensity cases. The reason why instabilities are seen could be related to the fact that the commutation-induced symmetry is preserved with lower order terms, while factorizations may break this symmetry, for example, in case $\langle \hat{b}^\dagger \hat{b}^\dagger \hat{b}\hat{b} \rangle \rightarrow \langle \hat{b}^\dagger \hat{b} \rangle \langle \hat{b}^\dagger \hat{b} \rangle$ both $\hat{b}\hat{b}$ and $\hat{b}^\dagger \hat{b}^\dagger$ get broken and double-excitation characteristics implied by commutation relations is disregarded, but in case $\langle \hat{b}^\dagger \hat{b}^\dagger \hat{b}\hat{b} \rangle \rightarrow \langle \hat{b}^\dagger \hat{b}^\dagger \hat{b} \rangle \langle \hat{b} \rangle$ the breaking is introduced only partially and imbalance between various terms could be introduced, which may lead to diverging solutions.

   In section 2.2 NEE has been used in the exciton basis, which made them very efficient for the J aggregate. This is a rather favorable system for the exciton model since mostly the lowest energy exciton is optically bright. However, including only one exciton in the description leads to

incorrect ESA peak. By including just a few exciton states, the ESA peak converges. This implies that double-exciton resonances are not simple single-exciton product states, however, only several energetically close excitons are sufficient to correctly represent the double-exciton resonances. Accordingly, this implies that only excitons which are close in energy do interact.

Additional factor regarding the one-exciton approach deficiency is due to thermal activation of excitons. Notice that in thermal equilibrium the k_BT range of exciton band will be populated. It is then a matter of how many excitons are within this range. This is also defined in exciton basis and cannot be done in chromophore basis.

2. We introduce NEE with new commutation relation for generalized particles. And we test the case of $\eta = 0.5$ which falls between paulions and bosons. The obtained solution show properties are in middle of paulion and boson properties. In calculated absorption and pump probe spectra cases spectra we observe that the ESA band shift is in between the paulionic and bosonic cases, when comparing spectra.

3. Differences between different equation models become smoothed out by including EEA (section 2.1). Coherent and direct factorization schemes stand out and show more significant differences from others. While the spectra become much more similar with EEA, instability from the zz model at high intensity remains. But the instability becomes apparent for larger intensities compared to the case with no annihilation.

   It is shown that absorption spectra of molecular systems can be enhanced by additional features at high excitation intensities. This can be addressed using non-perturbative propagation of NEE. The equations must be closed for numerical implementation, and there are many ways to close them. The most interesting approach relies on factorization of various highly nonlinear terms in NEE. Different types of factorizations may enhance various processes, what can be utilized in specific applications of NEE. The whole analysis becomes even less complicated when including EEA, because EEA does not allow for creation of highly excited states. Therefore, EEA diminished differences between different schemes of factorization. As a result, the NEE application to the systems with EEA is efficient and the calculations can rely on simple equations.

4. Increasing EEA parameter strongly affects 2DES cross-peaks (section 2.3): even the peaks that should be dark and should have no transition dipole moment may become visible. For the $2\vec{K}_1 - 2\vec{K}_2 + \vec{K}_3$ signal we find peaks associated with forbidden transitions as well as with double resonances. These features are related to deviations from the perturbative excitation regime. In this case an excitation does not necessarily correspond to transition between specific system levels. Instead, specific resonances may be initiated during the excitation process, which follow molecular symmetry selection rules compared to exciton. This is the main reason why dark excitons become populated. Then they relax into bright states and give time dependent features at non-standard positions.

   Indeed, in perturbative treatment, the material Hamiltonian eigenstates (excitons in our model) are stationary states when the optical field is switched off; the field introduces only transitions between these states. However, when the external field is on continuously, the full transient Hamiltonian has additional stationary system-field interaction. Even if the material Hamiltonian is diagonal (in e.g., exciton representation), the full transient system-field Hamiltonian in this case would be not diagonal and its new stationary states are denoted by polaritons[69]. Correspondingly their selection rules are different compared to excitons.

   In our case the optical field is impulsive, and in the excitation process when the field is on, our system momentarily enters non-perturbative polaritonic regime when even the dark excitons (which are dark when the field is off) turn to be open for excitation. This symmetry breaking is explicitly defined by population-scaled transition dipoles in Eqs. 1.4.5-1.4.8, i. e. at high occupation numbers $\mu_n(t) \to (1 - 2\eta\sigma_{nn})\mu_n(t)$.

5. NEE together with phase cycling yields polarization in a generic way which is the basic quantity describing various types of spectra (section 2.3). The presented highly nonlinear NEE equations together with phase cycling thus can be applied to study wide variety of spectroscopy techniques. The phase cycling allows simple extraction of various phase matching directions. Numerical solution of NEE includes explicit excitation pulse properties. It thus includes and properly accounts for pulse overlap effects. These effects add contributions that arise from non-time-ordered interactions even when the pulse centers are ordered, due to finite

pulse duration. The approach was efficiently used for third-to-fifth order spectra calculations. For example for signal $m_1K_1 + m_2K_2 + m_3K_3$ would require calculating $(2|m_1| + 1)\cdot(2|m_2| + 1)\cdot(2|m_3| + 1)$ phase shifted samples and 5D Fourier transform would be applied (2 dimensions for t_1 and t_3, the rest for every wave mixing wave vector).

SANTRAUKA

Įvadas

Molekuliniai agregatai yra sistemos pasižyminčios savitomis elektroninių sužadinimų ir sužadintos būsenos dinamikų savybėmis. Šios sistemos yra svarbios fotosintetiniuose šviesos surinkimo ir energijos pernešimo vyksmuose, kurie turi didelę svarbą gamtoje[1,2]. Esant tinkamoms sąlygoms, molekuliniai agregatai gali susiformuoti ir iš sintetinių dažų molekulių. Tai suteikia galimybę projektuoti ir tirti kvantinius reiškinius, kurie priklauso nuo chromoforo savybių bei jų kiekio[3–7]. Norint suprasti, valdyti ir nuspėti molekulinių agregatų spektroskopiniuose eksperimentuose optines savybes, reikia koordinuoti ir plėtoti teoriją su modeliavimu.

Chromoforinis dimeras yra mažiausia sistema, kuri atkartoja molekulinio agregato savybes[8–10]. Agregatų sugerties juostos yra pasislinkusios lyginant su nesąveikaujančiais chromoforais. Taip yra dėl rezonansinės sąveikos tarp agregatą sudarančių chromoforų. Sužadintos būsenos sugertis (ESA) gali būti stebima net ir kai agregato molekulės aprašomos kaip dviejų lygių sistemos. Tokių modelinių sistemų savybės galima patikimai modeliuoti ir vieno sužadinimo lygyje, atsižvelgiant į sudėtingą aplinkos struktūrą, kuri veda prie nemarkovinės eksitonų relaksacijos. Tačiau, kai molekulių skaičiaus daug didesnis ir esant dideliam žadinimo intensyvumui nėra trivialu modeliuoti chromoforinių agregatų spektrus. Pagrindinė to priežastis yra eksponentiškas skaičiavimo laiko didėjimas didinant molekulių skaičių agregate bei atsižvelgiant į sužadinimų skaičių esant netrivialiam žadinimo intensyvumui.

Dvimatė elektroninė spektroskopija (2DES) yra įprastas įrankis, kuris suteikia galimybę stebėti koreliacijas ir sužadinimų dinamikas chromoforiniuose agregatuose[11–14]. Trys laike surikiuoti žadinimo impulsai (aprašomi pagal jų bangos skaičiaus vektorius K_1, K_2, K_3) sukuria bent trečios eilės netiesinį atsaką medžiagoje. Tada indukuota netiesinė poliarizacija detektuojama heterodininės detekcijos metodu(taikomas papildomas impulsas matavimo metu) ties bangos skaičiaus vektoriaus kryptimi $\pm K_1 \mp K_2 + K_3$. Poliarizacija tada yra nuo laiko tarpų (t_1, t_2, t_3) tarp laike gretimų žadinimo impulsų ir detektavimo priklausanti funkcija. Poliarizacijai taikoma dvimatė Furje transformacija t_1 ir

t_3 atžvilgiu ir signalas projektuojamas į ω_1, ω_3 dažnius dvimatėje erdvėje, likusi t_2 trukmė arba kitaip vadinama vėlinimo trukmė leidžia stebėti sužadinimo užpildų dinamikas bei intrajuostinius koherentiškumus.

Signalą galima tirti, trikdžių teorijos rėmuose, ir analitiškai[12,15]. Bet tada sužadinimų skaičius turi būti mažas, todėl optinio lauko intensyvumas taip pat turi būti mažas. Galima suskaičiuoti kiek kvantų dalyvauja atitinkamuose reiškiniuose ir nustatyti sąveikos eilę optinio žadinimo lauko atžvilgiu. Ir atskirti pagal eiles, bet tai įmanoma, kai sužadinimų skaičius yra pakankamai mažas.

Tačiau, esant didesniam žadinimo intensyvumui, aukštesnės eilės žadinimo impulso lauko atžvilgiu negalime išskirti skirtingų vyksmų. Trikdžių eilutė nekonverguoja ir žadinimo sukelti įvairūs skirtingos eilės efektai pasireiškia įvairaus tipo signaluose, kurie įprastai siejami su žemesnės eilės matavimais. Tai gali lemti klaidinga spektrinių matavimų interpretaciją, todėl reikalinga neartutinis apdorojimas.

Trečios eilės lauko atžvilgiu, įprastoje žadinimo-zondavimo schemoje[16], matuojamo signalo intensyvumas auga tiesiškai didinant žadinimo pulso intensyvumą. Žadinimo lauko intensyvumas matavimuose yra dažnai naudojamas pasiekti geresnį signalo triukšmo santykį, o ne kaip parametrą įtakojantį signalą. Jei signalą sudaryto tik trečios eilės nariai, tada tik signalo intensyvumas priklauso nuo žadinimo intensyvumo. Bet didėjant sužadinimų tankiui pasireiškia papildomi, aukštos eilės lauko atžvilgiu, procesai susieti su eksitono-eksitono sąveika. Tam tikri fizikiniai vyksmai kinta, dėl aukštesnių netiesinių procesų, keičiantis sužadinimų tankiui medžiagoje, kuris priklauso nuo žadinimo lauko intensyvumo.

Eksitono-eksitono anihiliacija (EEA) yra vienas iš procesų, kuris stipriai priklauso nuo sužadinimų tankio[17–21,9,22]. Šis procesas yra vidinės konversijos pasekmė, kai stipriai sužadintas chromoforas, rezonansinis dvigubam kvantiniam sužadinimui, užgesina vieną sužadinimą ir relaksuoja į žemiausią sužadintą būseną, to pasekoje lieka viengubas kvantinis sužadinimas. Eksitonų gesimo kinetikos dideliuose molekuliniuose agregatuose gali suteikti informacijos apie eksitonų difuziją[23]. Persidengiantys aukštesnės eilės procesai (penktos ir aukštesnės eilės) pasireiškia, kai įvyksta dvi papildomos sąveikos su žadinimo impulsais. Tačiau buvo parodyta, kad 2D signalas kryptimis $\pm 2K_1 \mp 2K_2 + K_3$, sužadina dvigubų sužadinimų juostą ir leidžia stebėti su EEA susietas ypatybes[24]. Tačiau norint paaiškinti šių spektrinių ypatybių smulkiai struktūrą yra reikalingi tolesni tyrimai.

Eksitonų sąveika su aplinkos virpesiniais laisvės laipsniai (fononais) sukelia

eksitonų lokalizaciją (dėl statinės netvarkos) ir relaksaciją (dinaminės fliuktuacijos)[19]. Jau minėta EEA atsiranda dėl virpesinių sąveikų netiesiniame sužadinimų režime[25,20,26,22]. Šie reiškiniai slopina eksitonų formavimąsi. Molekulinėse sistemose fononai dažniausiai yra vietiniai virpesiai (arba statinė diagonali netvarka), kurie veikia chromoforų žadinimų energijas be jokių erdvinių koreliacijų. Taip moduliuoja chromoforų žadinimo energijas ir išderina chromoforus nuo stabilių rezonansų. Todėl, kai atsižvelgiame į visus vietinius ir nevietinius efektus, lygčių negalima trivialiai supaprastinti keičiant bazę į delokalizuotą eksitonų bazę.

Į virpesinius laisvės laipsnius atsižvelgiama netiesiogiai taikant Redfield relaksacijos teoriją. Šioje relaksacijos teorijoje virpesiniai laisvės laipsniai yra aprašomi kaip begalinis harmoninių osciliatorių rinkinys, kuris sąveikauja su sistema. Ši sąveika tarp sistemos ir aplinkos yra laikoma maža, tada jos atžvilgiu taikoma antros eilės trikdžių teorija. Darydami prielaidą, kad aplinka yra markovinė (atmetami atmintis efektai), aplinką apdorojame kaip suderintinio lauko teorijoje, osciliatoriai yra "užšaldomi" šiluminiame vidurkyje, kuris apibrėžtas aplinkos temperatūros. Taip gaunamas Redfield relaksacijos teorijos aprašymas.

Lygtys neartutiniam spektrų skaičiavimui (sąveikaujančių elektroniniam osciliatorių rinkiniui) buvo išvestos taikant Netiesinių eksitonų lygčių (NEE) formalizmą. Neartutiniai metodai generuoja begalines lygčių hierarchijas, kurių bendrai negalima išspręsti analitiškai[27]. NEE generuoja begalinę sukabintų lygčių hierarchiją. Praktiniams skaičiavimams yra reikalingos prielaidos, kurios pagrindžia šio hierarchijos uždarymą tam tikru lygiu. Priklausomai ar pridedame ar išimame EEA narius galime daryti prielaidas apie koks yra efektyvus sužadinimų skaičius sistemoje. Tada galime atrinkti narius susietus su labai dideliu sužadinimų skaičiumi ir juos galime faktorizuoti, tai yra, perrašyti, kaip mažesnės eilės narių sandaugą. Bet dėl sistemos ypatybių ir nuo spektroskopinio matavimo tipo lygčių narių negalime faktorizuoti bet kaip. Hierarchijos uždarymui reikia atmesti tam tikros eilės narius narius arba juos faktorizuoti. To pasekoje lygčių rezultatai gali būti netikėti: diverguojantys sprendiniai, nefizikiniai efektai ar išvis svarbių efektų pametimas. Todėl reikia atlikti įvairių faktorizavimo schemų analizę. Tačiau, esant dideliam sužadinimų skaičiui, faktorizacija gali leisti teisingai įvertinti daugiakvantines sumines vidutines spektrines savybes, kurių kitais metodais nepavyktų įvertinti.

Vienas iš būdų išvengti eksponentinio skaičiavimo kaštų augimo yra apriboti sužadinimų skaičių. Tai reiškia, kad apsiribojame labiausiai pasireiškiančiais

netiesiniais procesais, apsiribojame silpno sužadinimo lygiu. Kitas supaprastinimas yra apsiriboti tik ryškiais eksitonais, kuriuos galime įvertinti iš pasirinktos sistemos simetrijų. Tam pereiname iš molekulinės/mazgų bazės į eksitoninę bazę, kur dėl sistemos simetrijų gali būti tik keli optiškai pasiekiami rezonansai iš visų galimų būsenų. Tai leidžia efektyviai sumažinti problemos dydį ir net begalinio dydžio agregatai gali būti "išspręsti" analitiškai[30].

Šiame darbe tiriami stipriai netiesiniai efektai netiesinės sugerties, žadinimo-zondavimo ir 3-5 eilės 2DES spektruose chromoforiniams agregatams[31–33].

Aprašome kaip EEA įtraukimas į NEE paveikia 2D spektrus skirtinguose bangų maišymosi lygiuose[31]. 2D spektrų analizėje apsiribojame dimerų ir trimerų sistemomis. Siekiant išskirti stipriai netiesines 2D signalų komponentes, buvo panaudotas fazių moduliavimo metodas[34] . Su EEA 2D spektruose atsiranda reikšmingi skirtumai, kurie gali būti paaiškinami dinamišku eksitonų simetrijos pažeidimu.

Taip pat, tiesiniam chromoforų agregatui, palyginame keletą faktorizacijos tipų[33] , nuo mažo iki didelio žadinimo lauko intensyvumo, skaičiuodami paprastą sugerties spektrą. Parodome, kad esant dideliam žadinimo intensyvumui matoma papildoma indukuota sugertis ir šios savybes stipriai priklauso nuo sistemos netiesiškumų ir tuo pačiu nuo faktorizacijos tipo. Tai galima panaudoti specifiniuose taikymuose atitinkamoms molekulinėms sistemoms.

Ir tiriame NEE lygčių elgseną su EEA nariais J tipo agregatams, kai sprendžiame lygtis su tik dalimi iš visų eksitonų[32]. Tam skaičiuojame žadinimo zondavimo spektrus esant skirtingiems optinio žadinimo lauko intensyvumams. Parodome, kaip spektrai sukonverguoja naudojant tik kelis eksitonus skaičiavimuose.

Disertacijos tikslai ir užduotys

1. Ištirti netiesinių eksitonų lygčių pritaikomumą didelėms molekuliniams agregatams.

2. Įvertinti skirtingų NEE aproksimacijų ribas vykdant simuliacijas.

3. Ištirti NEE pritaikymo galimybes aukštesnės eilės netiesinių spektrų skaičiavime.

Ginamieji teiginiai

1. NEE faktorizavimas ir molekulinės sistemos perrašymas į eksitoninę bazę ir bazės nukirpimas įgalina efektyvų netiesinių spektrų skaičiavimą J tipo agregatams sudarytiems iš didelio molekulių kiekio.

2. Netiesinės eksitonų lygtys leidžia aprašyti apibendrintas daleles ir paulionus ir bozonus su vienu parametru, kuris leidžia tolygiai pereiti nuo vieno aprašymo prie kito.

3. EEA narių įtraukimas suvienodina skirtingų NEE modelių rezultatus.

4. EEA ir sistemos netiesiškumai įgaliną eksitonų simetrijos pažeidimą dėl lokalios procesų prigimties, kas pasireiškia papildomais signalais spektre tarsi susietais su tariamais "tamsiais" eksitonais.

5. Fazių moduliavimo metodas leidžia efektyviai išskirti skirtingas stipriais netiesinio 2DES spektro dalis.

Teorijos apžvalga

J agregatai

Šiame darbe mūsų modelinės sistemos bus J agregatai. idealizuotas tiesinis agregatas yra sistema sudaryta iš identiškų molekulių grandinės. Šios molekulės turi tik artimiausio kaimyno sąveiką ir ši sąveika yra vienoda visoms molekulėms. Taip pat visos molekulės agregate turi vienodą šuolio dipolinį momentą. Šie šuolio dipoliniai momentai yra nukreipti atitinkama kryptimis molekulių grandinės ašies atžvilgiu. Jei šuolio dipoliniai momentai yra statmeni molekulių grandinės ašiai tada tokia sistema vadinama H agregatu. Jei šuolio dipoliniai momentai yra lygiagretūs molekulių grandinės ašiai tada tokia sistema vadinama J agregatu. Dėl šių sąvybių tik viena tikrinė būsena turi nenulinį šuolio dipolinį momentą, tai yra "šviesi". J agregate šis eksitonas yra mažiausios energijos. Šią J agregatų savybę išnaudosime spektrų skaičiavimų spartinimui

Frenkelio eksitonų modelis molekuliniam agregatui

Molekulinė sistema yra sudaryta iš keleto chromoforinių molekulių. Chromoforai molekulės, kurios jautrios optiniui elektriniui laukui. Molekulės šiuo

atvejus yra supaprastintos į 2 (paulionai) ar 3 ir daugiau (bozonai) lygių sistemas su specifine žadinimo energija J ir anharmoniškumu parametru K (kai molekulė sužadinama daugiau nei vieną kartą). Sąveika su šviesa yra aprašoma šuolio dipoliniu momentu $\boldsymbol{\mu}_m$. Sąveiką tarp skirtingų molekulių didžiąja dalimi sudaro rezonansinė elektrostatinė sąveika, kurią galima išreikšti kaip kuloninę dipolis-dipolis sąveika. Tam yra reikalinga prielaida - molekulių dydis mažesnis nei atstumas tarp molekulių.

Molekulinė sistema aprašoma Frenkelio eksitonų hamiltonianu:

$$\begin{aligned} H &= \sum_{m,n} J_{mn}\hat{b}_m^\dagger \hat{b}_n + \frac{1}{2}\sum_m K_m \hat{b}_m^{\dagger 2}\hat{b}_m^2 \\ &\quad + \sum_m \mu_m^-(t)\hat{b}_m^\dagger + \sum_m \mu_m^+(t)\hat{b}_m. \end{aligned} \tag{1}$$

indeksai m, n žymi skirtingus osciliatorius (chromoforus) esančius ant skirtingų saitų. Matricos J_{mn} diagonalūs nariai yra elektroninių šuolių energijos ($m = n$), likę nariai ($m \neq n$) yra rezonansinės sąveikos, K_m yra $m-$tojo osciliatoriaus anharmoniškumas, $\hat{b}_m^\dagger$ ($\hat{b}_m$) yra sukūrimo (išnykimo) operatoriai m osciliatoriui. Bendrai K turėtų būti 4 rango tenzorius, $K_{mnkl}\hat{b}_m^\dagger \hat{b}_n^\dagger \hat{b}_k \hat{b}_l$, atvaizduojantis įvairius anharmoninių pataisų tipus, pavyzdžiui rezonansinės sąveikos pataisa dėl užpildos, K_{mnnl} ir elektrochrominiai poslinkiai dėl užpildos, K_{mnnm}. Tačiau mes šiuo atveju paliekame tik diagonalius narius.

Suminis optinis laukas sudarytas iš žadinimo impulsų sužymėtų pagal l. Sistemos-lauko sąveiką nusako skaliarinė sandauga tarp optinio elektrinio lauko ir chromoforo šuolio dipolinio momento $\boldsymbol{\mu}_m$:

$$\mu_m^\pm(t) = \sum_l \boldsymbol{\mu}_m \cdot \boldsymbol{E}_l(t - t_{0l}) \exp(\pm \mathrm{i}\omega_l(t - t_{0l}) \mp \mathrm{i}\boldsymbol{K}_l\boldsymbol{r}), \tag{2}$$

kuris apibrėžia eksitono sukūrimo ir išnykimo amplitudes; taip pat buvo panaudota besisukančios bangos aproksimacija, kur kiekvieno eksitono sukūrimo/išnykimo procesas susietas su atitinkamu optiniu dažniu. $\boldsymbol{E}_l(t)$ yra impulso gaubtinės funkcija. t_{0l} yra impulso centro laikas, o ω_l - nešantysis dažnis.

Apibendrintas komutacinis sąryšis

Daugiadalelinės statistikos aprašomos specifiniu komutaciniu sąryšiu. Paulionams[35,36] šis sąryšis yra:

$$[\hat{b}_n, \hat{b}_m^\dagger] = \delta_{mn}(1 - 2\hat{b}_m^\dagger \hat{b}_n). \tag{3}$$

Šitas komutacinis sąryšis draudžia kelių sužadinimų buvimą viename chromofore. Toks modelis aprašo dviejų lygių elektroninį osciliatorių. Tuo tarpu bozonams komutacinis sąryšis yra:

$$[\hat{b}_n, \hat{b}_m^\dagger] = \delta_{mn}, \tag{4}$$

šiuo atveju yra galimi keliagubi chromoforo sužadinimai. Mes sutraukiame šiuos 2 aprašymus į bendrą komutacinį sąryšį:

$$[\hat{b}_n, \hat{b}_m^\dagger] = \delta_{mn}(1 - 2\eta\hat{b}_m^\dagger \hat{b}_n), \tag{5}$$

kur $\eta = 0$ atitinka bozonus ir $\eta = 1$ - paulionus. Ir leidžiame parametrui η kisti nuo 0 iki 1.

Čia mes pridėjome parametrą, kuris leidžia pereiti nuo vieno aprašymo į kitą. Bet sužadinimų savybės tarp dviejų kraštinių atvejų (paulionų ir bozonų) nėra patikrintos. Todėl toliau šalia skaičiavimų paulionams ir bozonams, atliksime papildomus skaičiavimus ir "vidurinei" parametro vertei $\eta = 0.5$. Šitas pasirinkimas leis įvertinti ar rezultatai yra fizikiniai ir konverguoja. Taip pat parodome kaip šis atvejis dera su paulionais ir bozonais.

Čia mes laikome molekules kaip vientisus vienetus, bet jos yra daugiaelektroninės sistemos. Todėl nei paulioninis, nei bozoninis aprašymas nėra visiškai teisingas molekulinės sistemos elektroniniams sužadinimams. Molekulinei chromoforai gali būti sužadinami į aukštesnes būsenas, o šuolio dipoliniai momentai neseka pilnai harmoninio osciliatoriaus schemos. Todėl šis papildomas paulioniškumo parametras gali leisti geriau atvaizduoti molekulines sistemas.

Koherentinės eksitonų dinamikos - Netiesinės eksitonų lygtys

Kvantinė mechanika turi kelias formuluotes[37,38]. Netiesinės eksitonų lygtys remiasi Heisenbergo atvaizdavimu. Heisenbergo atvaizdavime visą priklausomybė nuo laiko yra operatoriuose ($\hat{A_H}(t)$), o būsena ($|\psi(0)\rangle$) yra pastovi, nepriklausanti nuo laiko ir atitinka pradines sąlygas. Kitoks yra Šriodingerio atvaizdavimas, kur ($\hat{A}_S$) pastovūs (juose yra tik išreikšta priklausomybė nuo

laiko, jei hamiltonianas priklauso), o visa likusi laiko įtaka yra sutalpinta į būseną ($|\psi(t)\rangle$) . Vidutinė vertė Heisebergo atvaizdavime yra:

$$\langle \hat{A}(t)\rangle = \langle \psi(0)|\hat{A}_H(t)|\psi(0)\rangle$$

Judėjimo lygtys Heisenbergo atvaizdavime, kai hamiltonianas tiesiogiai nuo laiko nepriklauso, yra suskaičiuojamos iš komutacinio sąryšio:

$$\mathrm{i}\frac{d\hat{A}}{dt} = [\hat{A}, \hat{H}]. \tag{6}$$

čia $\hat{A}$ yra pasirinktas operatorius Heisenbergo atvaizdavime.

Tikslas yra suskaičiuoti kaip molekulinė sistema atsako į išorinį optinį elektrinį lauką. Tai aprašo poliarizacija. Poliarizacijos operatorius:

$$\hat{\boldsymbol{P}} = \sum_n \boldsymbol{\mu}_n \hat{b_n} + \sum_n \boldsymbol{\mu}_n^\dagger \hat{b}_n^\dagger,$$

kurio vidutinė vertė:

$$\langle \boldsymbol{P}(t)\rangle = \sum_n \boldsymbol{\mu}_n \langle \hat{b_n}\rangle + \sum_n \boldsymbol{\mu}_n^\dagger \langle \hat{b}_n^\dagger\rangle.$$

Nuo mažiausios eilės operatoriaus, $\hat{b}_n$, diferencialinių lygčių sistema sugeneruojama, kuri vadinama NEE[39,40]. Čia laikome $\overline{h} = 1$, tada dažnis yra kaip energijos atitikmuo. Įvedame sudėtinius operatorius: $\hat{\sigma}_{uv} = \hat{b}_u^\dagger \hat{b}_v$, $\hat{y}_{uv} = \hat{b}_u \hat{b}_v$, $\hat{z}_{uv} = \hat{b}_k^\dagger \hat{b}_u \hat{b}_v$ bei $\hat{g}_u = (1 - 2\eta\hat{\sigma}_{uu})$. Ir surandame kelias pirmąsias NEE lygtis:

$$\mathrm{i}\frac{d\hat{b}_u}{dt} = \sum_n J_{un}\hat{g}_u\hat{b}_n + (1-\eta)K_u\hat{b}_u^\dagger\hat{g}_u\hat{y}_{uu} + \mu_u^-(t)\hat{g}_u, \tag{7}$$

$$\begin{aligned}\mathrm{i}\frac{d\hat{\sigma}_{uv}}{dt} =& \sum_n J_{vn}\hat{b}_u^\dagger\hat{g}_v\hat{b}_n - \sum_m J_{mu}\hat{b}_m^\dagger\hat{g}_u\hat{b}_v \\ &+ (1-\eta)K_v\hat{b}_u^\dagger\hat{\sigma}_{vv}\hat{b}_v - (1-\eta)K_u\hat{b}_u^\dagger\hat{\sigma}_{uu}\hat{b}_v \\ &+ \mu_v^-(t)\hat{b}_u^\dagger\hat{g}_v - \mu_u^+(t)\hat{g}_u\hat{b}_v,\end{aligned} \tag{8}$$

$$
\begin{aligned}
\mathrm{i}\frac{d\hat{y}_{uv}}{dt} =& \sum_n J_{vn}\hat{g}_v\hat{y}_{un} + \sum_n J_{un}\hat{g}_u\hat{y}_{vn} \\
&- 2\eta\delta_{uv}\sum_n J_{vn}\hat{g}_v\hat{y}_{vn} \\
&+ (1-\eta)\left(K_v\hat{\sigma}_{vv} + K_u\hat{\sigma}_{uu}\right)\hat{y}_{uv} \\
&+ (1-\eta)\delta_{uv}K_v\left(1-\eta\left(3-2\eta\right)\hat{\sigma}_{vv}\right)\hat{y}_{vv} \\
&+ \mu_v^-(t)\hat{g}_v\hat{b}_u + \mu_u^-(t)\hat{g}_u\hat{b}_v - 2\eta\delta_{uv}\mu_v^-(t)\hat{g}_v\hat{b}_v, \qquad (9)
\end{aligned}
$$

$$
\begin{aligned}
\mathrm{i}\frac{d\hat{z}_{kuv}}{dt} =& \sum_n J_{vn}\hat{b}_k^\dagger\hat{g}_v\hat{y}_{un} + \sum_n J_{un}\hat{b}_k^\dagger\hat{g}_u\hat{y}_{vn} \\
&- 2\eta\delta_{uv}\sum_n J_{vn}\hat{b}_k^\dagger\hat{g}_v\hat{y}_{vn} - \sum_m J_{mk}\hat{b}_m^\dagger\hat{g}_k\hat{y}_{uv} \\
&+ (1-\eta)\hat{b}_k^\dagger\left(K_v\hat{\sigma}_{vv} + K_u\hat{\sigma}_{uu} - K_k\hat{\sigma}_{kk}\right)\hat{y}_{uv} \\
&+ (1-\eta)\delta_{uv}K_v\hat{b}_k^\dagger\left(1-\eta\left(3-2\eta\right)\hat{\sigma}_{vv}\right)\hat{y}_{vv} \\
&+ \mu_v^-(t)\hat{b}_k^\dagger\hat{g}_v\hat{b}_u + \mu_u^-(t)\hat{b}_k^\dagger\hat{g}_u\hat{b}_v \\
&- 2\eta\delta_{uv}\mu_v^-(t)\hat{b}_k^\dagger\hat{g}_v\hat{b}_v - \mu_k^+(t)\hat{g}_k\hat{y}_{uv}. \qquad (10)
\end{aligned}
$$

Ši hierarchija yra begalinė. Tam, kad lygtis būtų galima spręsti bent skaitmeniškai, šią hierarchiją reikia uždaryti. Pirmiausia reikia suskaičiuoti vidutines operatorių vertes, šiame darbe vidutinės vertės yra žymimos nuimant operatoriaus kepurėlės ženklus $b_u(t) = \langle\hat{b}_u\rangle$, $\sigma_{uv}(t) = \langle\sigma_{uv}\rangle$, $y_{uv}(t) = \langle y_{uv}\rangle$, $z_{kuv}(t) = \langle z_{kuv}\rangle$.

Šiose lygtyse matome kokį vaidmenį atlieka η parametras. Matome jo įtaką anharmoniškumui $(1-\eta)K_u$ ir užpildų sotinimuisi per šuolio dipolinio momento pernormavimą $(1-2\eta\sigma_{uu})\,\mu_u^-(t)$. Tarpiniu atveju $\eta = 0.5$, dar turime užpildų sotinimosi efektus (paulionai), bet leidžiame aukštesnius sužadinimus, su žadinimo energijos anharmoniškumu (bozonai).

Tiesinė relaksacija

Pateikta formuluotė dar neatsižvelgia į išsifazavimo ir relaksacijos procesus. Teisingam šių procesų aprašymui modelį reikia išplėsti įtraukiant aplinkinius (fononai) laisvės laipsnius[41]. Lygtys su dideliu operatorių skaičiumi turi atspindėti daugiaeksitonias koreliacijas, kur pasireiškia platus relaksacijos

vyksmų diapazonas. Relaksacijos procesui turi būti išpildyti atitinkami reikalavimai. Svarbiausias yra pilnos tikimybės išlaikymas vieno eksitono būsenų juostoje, nes eksitono gyvavimo trukmė yra daug ilgesnė lyginant su eksitonų relaksacija juostos viduje.

Aplinka yra pridedama kaip begalinis harmoninių osciliatorių rinkinys, kurie tiesiškai sukabinti su chromoforais. Tai įprastai yra aprašoma tokio tipo sistemos-aplinkos sąveikos nariu hamiltoniane:

$$\hat{H}_{SB} = \frac{1}{2}\sum_{m}\sum_{\alpha}\left[c_{m\alpha}\hat{b}_m^{\dagger}\hat{b}_m\right]\hat{Q}_{\alpha} + h.c.; \tag{11}$$

čia Q_α yra koordinatė priklausant $\alpha-$tajam aplinkos osciliatoriui, $c_{m\alpha}$ yra sąveikos stipris. Toliau, mes taikome įprastą prielaidą, kiekvienas chromoforas aplink save turi savo vietinę aplinką, statistinės savybės visiems saitams yra vienodos ir statistiškai nepriklausomos. Heisenbergo atvaizdavime, dėl aplinkos poveikio, hamiltoniano elementai svyruoja.

Relaksacijai aprašyti, antroje eilėje sistemos-aplinkos sąveikos atžvilgiu, naudojame markovinę sekuliarią Redfield relaksacijos teoriją (MSRT)[42,15,43,44]. Pradedame nuo bendros išraiškos kombinuotam sistemos ir aplinkos tankio operatoriui W. Pritaikius Borno ir Markovo aproksimacijas (aplinka išlieka šiluminėje pusiausvyroje ir svyravimų koreliacijos greitai gęsta) redukuotam tankio operatorius, turime dinamikas:

$$\frac{\mathrm{d}\hat{\rho}(t)}{\mathrm{d}t} = -\mathrm{i}\left[\hat{H}_0, \hat{\rho}(t)\right] - R^{(\rho)}\hat{\rho} \tag{12}$$

kur $R^{(\rho)}$ yra relaksacijos superoperatorius, aprašytas[43]

$$\begin{aligned} R^{(\rho)}\hat{\rho} = \int_0^{\infty}\mathrm{d}\tau\sum_{n}\{&\hat{\sigma}_{nn}\mathcal{G}(\tau)\hat{\sigma}_{nn}\mathcal{G}(-\tau)\hat{\rho}C_n(\tau) \\ &+ \hat{\rho}\mathcal{G}(\tau)\hat{\sigma}_{nn}\mathcal{G}(-\tau)\hat{\sigma}_{nn}C_n^{*}(\tau) \\ &- \hat{\sigma}_{nn}\hat{\rho}\mathcal{G}(\tau)\hat{\sigma}_{nn}\mathcal{G}(-\tau)C_n^{*}(\tau) \\ &-\mathcal{G}(\tau)\hat{\sigma}_{nn}\mathcal{G}(-\tau)\hat{\rho}\hat{\sigma}_{nn}C_n(\tau)\}, \end{aligned} \tag{13}$$

kur $\mathcal{G}(\tau) = \exp\left(-\mathrm{i}\hat{H}_0 t\right)$ propogatorius susietas su $\hat{H}_0 = \sum_{m,n} J_{mn}\hat{b}_m^{\dagger}\hat{b}_n$(teisinė $\hat{H}$ dalis, tada galima lengvai suskaičiuoti $\mathcal{G}(t)$),

$\hat{\sigma}_{nn} = \hat{b}_n^\dagger \hat{b}_n$

$$C_n(\tau) = \sum_\alpha \frac{c_{n\alpha}^2}{2} \left(\coth \frac{\beta\omega_\alpha}{2} \cos\omega_\alpha t - \mathrm{i} \sin\omega_\alpha t \right) \tag{14}$$

yra hamiltoniano svyravimų koreliacijos funkcija saitui n , $C_n(\tau) = \langle H_{SB,n}(t) H_{SB,n}(0) \rangle$ (čia laužtiniai skliaustai nurodomas ansamblinis vidurkinimas, visų chromoforų virpesių charakteris laikomas vienodas) ir ω_α yra aplinkos osciliatoriaus dažnis, kur $\hat{H}_{SB} = \sum_n \hat{\sigma}_{nn} H_{SB,n}(\tau)$. Lygtyje 13 taikome molekuliniams agregatams įprastą prielaidą, skirtingų saitų virpesiai yra nekorialiuoti (visos kitokio tipo koreliacijų funkcijos yra nykstamos). Laikome $C_n(t) = C(t)$ visus vienodus.

Aukštesnės eilės lygčių nariams šį aprašymą galime papildomai supaprastinti laikant koherentiškumus nepriklausomais, pavyzdžiui $R_{abcabc}^{exc(z)} = (R_a^{(b)})^* + R_b^{(b)} + R_c^{(b)}$.

Eksitono-eksitono anihiliacija

EEA yra procesas, kuris įgalina netiesinį sužadinimo užpildos gesimą. Šiame darbe EEA aprašymui naudojame fenomenologinį tarpjuostinį relaksacijos procesą iš ankstesnės publikacijos[9]. Esant dideliam žadinimo intensyvumui turėtume daugiadalelinių sužadinimų, tačiau EEA procesas slopina sužadinimus. Šis procesas atspindi molekulinį vidinės konversijos vyksmą, kai molekulė yra dvigubai sužadinama į aukštas molekulines būsenas. Mes galime naudoti mūsų formalizmą, kai vidinės konversijos procesas yra greitas lyginant su tarp molekuline eksitonų šuoliavimo sparta. Tada EEA procesas gali būti atvaizduotas kaip nekoherentinis nuo atstumo priklausanti šuolis $\alpha(|\boldsymbol{r}_m - \boldsymbol{r}_n|)\hat{b}_m^\dagger \hat{b}_m \hat{b}_n^\dagger \hat{b}_n \rightarrow \hat{b}_n^\dagger \hat{b}_n$, kur $m \neq n$, $\alpha(|\boldsymbol{r}_m - \boldsymbol{r}_n|) \equiv \alpha(r_{mn})$ yra proceso amplitudė priklausanti nuo atstumo tarp saitų m ir n. Esant mažai tarpmolekulinei sąveikai, funkciją $\alpha(r_{mn})$ galime laikyti kaip Förster sužadinimo pernešimo spartą[21,26]. Jei saitai supakuoti tikroje erdvėje tankiai, taip, kad artimiausio kaimyno atstumą galima apibrėžti. Tada proceso spartą saitui m galime susietu su artimiausiais kaimynais, $\alpha(r_{mn}) = \kappa_0 \delta_{mn}^{(n-n)}$. Čia $\delta_{mn}^{(n-n)}$ yra lygus 1, kai m ir n yra artimiausi kaimynai, ir 0 kitais atvejais, o κ_0 yra anihiliacijos parametras.

Reikia atkreipti dėmesį, šis gesimo kanalas prisideda prie gyvavimo trukmės išplitimo visiems susijusiems koherentiškumams. Pagal gerai žinomą išraišką: gesimo sparta koherentiškumui mn, susijusi su gyvavimo trukme, yra

$\tau_{mn}^{-1} = (k_{mm} + k_{nn})/2$[43], kur $k_{mm} = \kappa_0 \sum_{\mathrm{n-n}} \sigma_{nn}$ yra suma per artimiausius kaimynus.

Tada EEA elgsena NEE lygtyse įtraukiama su tokios formos nariais[9]:

$$\frac{\mathrm{d}A_{nk...}}{\mathrm{d}t} = \ldots - \frac{\kappa_0}{2} \sum_m \sigma_{mm}(G_{mn} + G_{mk} + ...)A_{nk...}. \tag{15}$$

Čia kairėje lygties pusėje $nk...$ atvaizduoja apibendrintą indeksų rinkinį, o dešinėje atitinkamai pusėje kiekvienam indeksui turime po narį G_{mn}, kur $G_{mn} = (\delta_{mn}^{(n-n)} + \delta_{mn})$, kuris turi ir papildomą saito savąją anihiliacija. Ši schema atitinka kitus modelius, tai yra $dn/dt \sim -n^2$, kuris buvo panaudotas žadinimo zondavimo spektrų analizei ir patvirtintas eksperimentų (pavyzdžiai literatūroje[18,25]).

NEE lygčių uždarymas skaitiniams skaičiavimams

Uždaryti (tam tikru pasirinktu lygiu) NEE lygčių hierarchiją naudojame aukštesnės eilės narių faktorizavimą. Tai leidžia supaprastinti lygtis ir sumažinti jų skaičiavimo kaštus. Tačiau gali pašalinti ar pridėti naujus efektus į spektroskopinius rezultatus. Faktorizacijos pavyzdys:

$$\langle \hat{b}_k^\dagger \hat{b}_n^\dagger \hat{b}_k \hat{b}_n \hat{b}_n \rangle = \sigma_{kk} z_{nnn} \tag{16}$$

kai neatsižvelgia į operatorių eiliškumą, kas yra svarbu, kaip $k = n$. Tačiau, kai $k \neq n$ galime atskirti $k-$tojo chromoforo užpildą ir lieka $n-$tojo chromoforo charakteristikos. Tuo tarpu kitokia faktorizacija, kuri yra labiau priimtina kitokiai indeksų kombinacijai:

$$\langle \hat{b}_n^\dagger \hat{b}_n^\dagger \hat{b}_m \hat{b}_m \hat{b}_l \rangle = y_{nn}^* y_{mm} b_l. \tag{17}$$

Čia operatorių eiliškumas išsaugomas, bet kitas svarbus skirtumas, visi nariai yra koherentiškumai. Tikėtina, kad nariai susieti su užpildomis (faktorizavimo pavyzdys lygtyje 16) išliktų ilgiau lyginant su faktorizavimu į koherentiškumus. Abiem atvejais neįskaitomas dar vienas efektas, kai $k = n = m = l$, kur tada $\langle \hat{b}_n^\dagger \hat{b}_n^\dagger \hat{b}_n \hat{b}_n \hat{b}_n \rangle$ yra koherentiškumas tarp antro ir trečio molekulinio sužadinimo. Kintamasis $\hat{b}_n \hat{b}_n \hat{b}_n$ yra trigubo sužadinimo koherentiškumas ir šį faktorizuojant mes netenkame susietų rezonansų. Šie rezonansai gali priklausyti nuo sistemos paulioniškumo ar bozoniškumo.

Taip pat aukštos eilės narių faktorizavimas leidžia išvengti poreikio skai-

čiuoti relaksacijos spartos šiems nariams. Mažos eilės nariams Redfield nariai gali būti lengvai išreikšti eksitoninėje bazėje. Saitinė bazėje šie nariai yra nepatogūs ir greitai tampa sunkiai suskaičiuojami didėjant eilei.

Sugerties ir žadinimo zondavimo spektrai

Medžiagoje indukuota poliarizacija gali būti naudojama aprašyti spektroskopinius dydžius. Naudojant vidutines vertes $P = \langle \hat{P} \rangle$, indukuotos poliarizacijos dinamika dipolio aproksimacijoje užrašoma taip:

$$\boldsymbol{P}(t) = \boldsymbol{\mu}_m b_m(t) + c.c. \tag{18}$$

Visi stebimi spektroskopiniai dydžiais gali būti įvertinti iš poliarizacijos. Sugerties spektras suskaičiuojamas pritaikius Furje transformacija poliarizacijai po poveikio labai trumpu optiniu lauku $\boldsymbol{E}(t) = \boldsymbol{o} \exp(-(\Delta t)^2/2)$, centruoto nulio laiku su gausine gaubtine[12]:

$$S_A(\omega) = \mathfrak{Im} \int_{-\infty}^{+\infty} \mathrm{d}t \exp(\mathrm{i}\omega t) P(t). \tag{19}$$

Čia atmetėme vektorines savybes, nes J agregate laikome visų molekulių šuolio dipolinius momentus išdėstytus vienoje dimensijoje.

Tokia suskaičiuota sugertis turi priklausomybę nuo žadinimo intensyvumo, nes lygtys nėra tiesinės. Esant pakankamai mažam žadinimo intensyvumui, priklausomybė nuo žadinimo intensyvumo išnyksta. Tokiu atveju lygtis galima ištiesinti. Eksitoninėje bazėje tiesiniame režime lieka tik vienas kintamasis ir viena lygtis:

$$i\frac{db_a}{dt} \quad = \quad J_a b_a + \mu_a^- - iR_a^b b_a. \tag{20}$$

Šios lygties sprendinys yra $b_a(t) = b_a(0) \exp(-iJ_a t - R_a^b t)$, turime lorencinės linijos formas visiems eksitoniniams šuoliams.

Žadinimo-zondavimo (PP) spektroskopinis signalas gali būti suskaičiuotas skaitiškai sprendžiant lygčių rinkinį. Žadinimo-zondavimo modeliavime (ir eksperimente) yra du optiniai impulsai: žadinimo ir zondavimo. Žadinimo impulsas, sužadindamas visus NEE narius, inicijuoja kvantinę dinamika. O vėlesniu laiku zondavimo impulsas atlieka detektavimo procesą. Visumoje turi būti suskaičiuoti trys skirtingi poliarizacijos rinkiniai: kai abu žadinimo ir zon-

davimo impulsai įjungti ($P_{pp}(t)$), kai tik žadinimo impulsas įjungtas ($P_{pu}(t)$) ir kai tik zondavimo impulsas ($P_{pr}(t)$). Tada galime suskaičiuoti skirtuminį signalą:

$$S_{pp}(\omega) \simeq \Im\mathfrak{m} \int \mathrm{d}t \exp(\mathrm{i}\omega t) \left(P_{pp}(t) - P_{pu}(t) - P_{pr}(t)\right) \tag{21}$$

NEE lygtis galime spręsti ir tikros erdvės (saito) bazėje arba eksitoninėje bazėje.

2DES ir fazės moduliavimo metodas

Pereinant nuo žadinimo zondavimo spektrų turime sudėtingesnius 2D elektroninius spektrus (2DES)[11–14]. Lyginant 2DES su žadinimo zondavimo spektrais turime 2 žadinimo impulsus. Todėl 2DES eksperimentas aprašomas 4 laiko taškais: pirmas impulsas, antras impulsas, trečias impulsas (charakterizuojami banginiais vektoriais K_1, K_2, K_3) ir matavimo taškas. Toliau apibrėžiame 3 vėlinimo laikus. Šie yra (t_1, t_2, t_3), pavyzdinė diagrama pateikta 1 paveiksle. 2DES tipas priklauso nuo krypties kurioje signalas buvo matuotas $\pm K_1 \mp K_2 + K_3$, kuri yra banginių vektorių kombinacija. Atliekamos dvi Furje transformacijos, t_1 ir t_3 atžvilgiu ir signalas projektuojamas į du dažnius (ω_1, ω_3) dviejose dimensijose. Tai atskleidžia eksitonų evoliuciją, kuri tampa t_2 vėlinimo laiko funkcija, ir leidžia sekti eksitonų užpildas ir koherentiškumus.

Lyginant su žadinimo zondavimo eksperimentu turėtume atvejį $t_1 = 0$. Papildomas žadinimo impulsas lyginant su žadinimo zondavimo eksperimentu leidžia tikslesnį sistemos pradinės būsenos derinimą. Leisdami t_1 kisti, atlikus Furje transformacija šiam ir t_3, mes turime dinamikų "žemėlapį". Šis "žemėlapis" parodo kaip atsakas pasikeičia kai taikome specifinį žadinimo dažnį. Ir kaip šis atsakas keičiasi laike keičiant t_2 vėlinimo laiką. Taip pat įprastiniame žadinimo zondavimo eksperimente $\pm K_1 \mp K_2 + K_3$ komponentės nebūna išskirtos. Šios komponentės leidžia stebėti atitinkamas procesus. Pavyzdžiui 2D signalas ties $\pm 2K_1 \mp 2K_2 + K_3$[24] yra susietas su dvigubų sužadinimų juosta ir atskleidžia EEA ypatybes.

Sudėtingesniems netiesiniams signalams reikia išskirti komponentes atitinkančias tam tikras bangų maišymosi kryptis[55]. Tradicinis metodas yra signalo skleidimas žadinimo lauko eilėmis[15]. Tačiau dėl laipsninės priklausomybės nuo eksitonų užpildos (dėl EEA), skleidimas išorinio lauko atžvilgiu

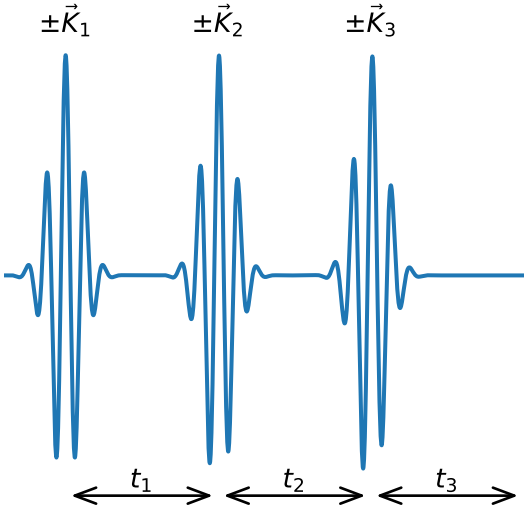

1 pav.: 2DES signalo žadinimo impulsų schema.

nėra efektyvus. Patogiau integruoti lygtis skaitmeniškai ir išskirti skirtingų signalo komponenčių atskyrimą taikant fazių moduliavimo metodą[34]. Nekolineriame eksperimente, kur kiekvienas optinis impulsas turi specifinį bangos skaičiaus vektorių, signalo komponentes galima išmatuoti skirtingomis kryptimis apibrėžtomis bangos skaičiaus vektoriaus superpozicijomis. Perfazuojančios $-\vec{K_1}+\vec{K_2}+\vec{K_3}$ ir neperfazuojančio $\vec{K_1}-\vec{K_2}+\vec{K_3}$ konfigūracijos yra naudojamos 2 dimensijų elektroninėje spektroskopijoje (2DES). Jei visi impulsai kolinearūs, tada fazės moduliavimo metodas[56,13,57] yra efektyviausias įrankis atskirti skirtingas signalo komponentes. Galime išskirti dominantį signalą skaičiuodami įvairių poliarizacijų superpoziciją skirtingomis konfigūracijomis. Tai daroma taikant Furje transformaciją fazės poslinkių atžvilgiu. Taip gaunamos atskiros signalo komponentės, atitinkančios skirtingas banginio skaičiaus vektoriaus konfigūracijas. Šiam metodui reikia daug panašių skaičiavimų, bet iškart atskiriami visų banginio skaičiaus vektorių kombinacijų indėliai ir skaičiavimus paprasta lygiagretinti. Kiek indėlių gauname yra apribota kiek skirtingų poslinkių fazių buvo paimta, dėl Furje transformacijos savybių. Todėl skaičiuodami signalą $-2\vec{K_1}+2\vec{K_2}+\vec{K_3}$ turime ir kitus indėlius: $-\vec{K_1}+\vec{K_2}+\vec{K_3}$, $\vec{K_1}-\vec{K_2}+\vec{K_3}$, ir $2\vec{K_1}-2\vec{K_2}+\vec{K_3}$.

NEE lygtys eksitoninėje bazėje

Perrašant lygtis į eksitoninę bazę, lygtys yra skaitmeniškai stabilesnės. Eksitonė bazė atsižvelgia į agregato specifinius rezonansus ir simetrijas, bei sumažina svyruojančius narius. Pavyzdžiui užpildos nariai σ_{aa} neturiu svyravimų šioje bazėje. Taip pat eksitoninėje bazėje papildomai atmetame 5 eilės narius ir narius, kurie atitinka trigubus sužadinimus. Pavyzdys nario su trimis sužadinimais $\hat{b}_a^\dagger \hat{b}_b \hat{b}_c \hat{b}_d$. Ketvirtos eilės nariai, kaip $\hat{b}_a^\dagger \hat{b}_b^\dagger \hat{b}_c \hat{b}_d$ faktorizuojami į $\sigma\sigma$ mazginėje bazėje ir tada transformuojami į eksitoninę bazę.

Transformacija į eksitoninę bazę atliekama transformuojant kiekvieną indeksą atskirai, pavyzdžiui, z transformuojamas $z_{abc} = \sum_{u,v,w} \theta_{u,a}\theta_{v,b}\theta_{w,c} z_{uvw}$, atvirkščias sąryšis $z_{uvw} = \sum_{a,b,c} \theta_{u,a}\theta_{v,b}\theta_{w,c} z_{abc}$, kur $\theta_{u,e}$ yra transformacijos koeficientas tarp u molekulinio sužadinimo ir e eksitono. Transformacijos koeficientai suskaičiuojami iš tikrinių verčių uždavinio:

$$\sum_n J_{mn}\theta_{n,a} = J_a \theta_{m,a},$$

kur J_a yra a-tojo eksitono energija. Taip visi lygčių nariai transformuojami į eksitoninę bazę.

Šitas modelis yra 3 eilės pilniausias skaitmeniškai efektyvus NEE modelis. Ši modelį žymime “Ex”.

Modelį dar galima truputį sumažinti, taikant paprastesnį relaksacijos tenzorių z kintamajam. Imant $R^{(z)}_{abcdef} = \delta_{ad}\delta_{be}\delta_{df}\left(R_a^{(b)*} + R_b^{(b)} + R_c^{(b)}\right)$ modelis su paprastesne relaksacija gaunamas, šis modelis žymimas “Ex-R”.

Perslopintas modelis

Lygtims eksitoninėje bazėje galima taikyti papildomą aproksimaciją, laikant, kad koherentiškumai greitai gęsta. Narius su koherentiškumu tada galima pašalinti iš lygčių. Turint omenyje tam tikrus spektroskopinius eksperimentus, šis perslopintas modelis priima, kad vėlinimo laikai tarp optinių impulsų yra ilgesni nei molekulių koherentiškumų gesimo trukmės. Su šia prielaida atmetame y narius, $\sigma_{ab},\ a \neq b$ koherentiškumus ir $z_{abc},\ a \neq b$ tarpjuostinius koherentiškumus. Atitinkamai paliekami tik su užpildomis susieti sekuliarų užpildos nariai. Perslopintą modelį žymime “OD”. Kaip ir buvo su Ex modeliu turime ir “OD-R”, kur z kintamojo relaksacija supaprastinta. Lyginant su eksitoniniu modelius, skirtumai tarp modelių yra susija su daugiaeksitoninėmis savybėmis. Visų modelių tiesinis atsakas būtų vienodas.

Esant mažo žadinimo sąlygoms, daugiachromoforines sistemas yra palyginti lengvą modeliuoti. Vieno eksitono juostos būsenas dažnai galima suskaičiuoti analitiškai ar skaitmeniškai diagonalizuojant hamiltonianą. Aukštesnius rezonansus, kuriuos galima pasiekti trečios eilės spektroskopijoje, irgi galima suskaičiuoti. Arba analitiškai paprastiems J agregatams arba skaitmeniškai taikant, pavyzdžiui eksitono-eksitono skaidos metodą (NEE aprašyme), ar vadinamu "brute force" skaitmeniniu diagonalizavimu.[59,15].

Stipriai sužadintų rezonansų modeliavimas netiesinėms sistemos yra labai sudėtingas. Skleidimas eilėmis ir besisukančios bangos aproksimacijos ne visada yra taikytinos. Kaip pavyzdžiui EEA procesui[60,27,61,54,62]. Jei sužadintos būsenos užpildos dinamika aprašoma tokio tipo lygtimi ($\alpha \neq 1$):

$$\frac{dn}{dt} = -\gamma n^{\alpha}, \tag{22}$$

kaip ir yra EEA atveju, čia n yra sužadinimų koncentracija/užpilda, γ - EEA parametras. Tada sprendinys,

$$n(t) = \frac{1}{\left(\frac{1}{n_0^{\alpha-1}} + (\alpha-1)\gamma t\right)^{\frac{1}{(\alpha-1)}}} \tag{23}$$

ilguose laikuose, yra funkcija, kurios negalime efektyviai išskleisti konverguojančia eksponenčių eilute. Kai $\alpha > 1$ (šiame darbe laikome EEA $\alpha = 2$; bendrai šis parametras nebūtinai sveikas skaičius) turime, kad sprendinys turi ilgą uodega, kuri gęsta lėčiau nei eksponentinė funkcija. Tokia funkcija užges pilnai tik begaliniame. Tokiu atveju stebimų dydžių skaičiavimui galime naudoti tik skaitmeninius lygčių sprendinius, kurie aprašo procesus[47].

NEE lygčių lankstumas kartu su įvairiomis skirtingomis aproksimacijomis leidžia sugeneruoti daugybę modelių, kurie gali būti pritaikyti įvairiems modeliavimo uždaviniams.

Mes išskiriame modelius pagal kurioje bazėje apibrėžti (saitinėje ar eksitoninėje bazėse). Kita atskirtis yra pagal kaip susitvarkoma su aukštesnės eilės išsifazavimo ir relaksacijos nariais. Lygtys yra skaitmeniškai nestabilios su aukštesnės eilės relaksacijos nariais paulionų atveju, nes pilnas relaksacijos narių išvedimas neatsižvelgia į sistemos bozoniškumą ir paulioniškumą.

Papildimas suskirstymas į saitinę ir eksitoninę bazę iš pirmo žvilgsnio gali atrodyti beprasmis. Iš principo bazės pakeitimas neturėtų keisti skaičiavimo

rezultatų. Bet tai leidžia taikyti skirtingo pobūdžio aproksimacijas, bei pasižymi skirtingomis skaitinio modeliavimo stabilumo savybėmis, nes eksitonai yra sistemos hamiltoniano tikrinės būsenos. Kadangi EEA yra apibrėžta saitinėje bazėje, tuo tarpu išsifazavimas ir relaksacija - eksitoninėje bazėje, bazės pakeitimas nekeičia skaičiavimo kaštų augimo nuo saitų skaičiaus.

Nedidelė pasirinktų modelių apžvalga yra pateikta lentelėse 1, 2 ir 3.

Rezultatų apžvalga

Tęsiamas darbas nuo[9], kur mes išplėtėme Netiesines eksitonų lygtis[39,40] įtraukdami eksitono-eksitono anihilacijos narius. Ten buvo suskaičiuoti molekulinio dimero žadinimo zondavimo spektrai taikant NEE lygtis. Tai leido kiekybiškai aprašyti sistemoje koherentinius ir nekoherentinius procesus kaip funkcija nuo žadinimo intensyvumo. akivaizdūs sekantys žingsniai buvo tirti lygčių pritaikymą didesnėms molekulinėms sistemoms, bei didesnės eilės netiesinių spektrų skaičiavimams. Taip pat dar papildomas galimybė buvo apibendrinti lygtis ir paulionams ir bozonams su parametru, kuris leidžia tolydžiai pereiti iš vieno aprašymo į kitą. Toks aprašymas yra vertingas, nes molekulinių elektroninių sužadinimų tarpinė statistika griežtai neseka nei bozono, nei paulionų statistikos. Eksitonų bazėje aprašome 4 skirtingas NEE realizacijos, kurios įgalina efektyvius signalo skaičiavimus.

Įvairių faktorizacijos modelių poveikis netiesiniams sugerties spektrams

Pritaikome įvairias faktorizacijos schemas tiesiniam molekuliniams agregatui sudarytam iš septynių molekulių. Atliekama analizė su keletu skirtingų žadinimo intensyvumo verčių, taip išryškinant netiesinius reiškinius ir sugerties spektre. Tai leidžia ištirti, kokį poveikį turi kiekvienos faktorizacijos schemos taikymas.

Pirma mes apžvelgiame rezultatus, kai lygtys yra be EEA narių. Pradedant su trimis paprasčiausiais modeliais: apribotos koherentinės būsenos, tiesioginės faktorizacijos ir tik 3 eilės nefaktorizuotu modeliai. Su šiais modeliass suskaičiuojame nuo žadinimo intensyvumo priklausančius sugerties spektrus. Modeliai elgėsi labai skirtingai, kai didinamas žadinimo intensyvumas. Apribotos koherentinės būsenos modelio atveju, didinant žadinimo intensyvumą, atsiranda antra juosta. Šią juostą galime susieti su sužadintos būsenos sugertimi (ESA), atsirandančią, kai sužadinti eksitonai sužadinami į dar aukštesnį lygmenį. Ši ESA juosta auga lėtai lyginant su kitas modeliais nes, koherentiš-

1 lentelė: NEE faktorizavimo modeliai.

Modelis	Pagrindinis principas	Apžvalga
Pilna faktorizacija	Viskas faktorizuojama iki mažiausio struktūrinio elemento	Aprašo sukabintus netiesiniu osciliatorius ir dar lygtyse yra netiesiškumų. Skaičiavimo kaštų atžvilgiu, pats pigiausias modelis. Skaičiavimo kaštai auga, kaip 2 laipsnio funkcija nuo molekulių skaičiaus.
Apribotos koherentinės būsenos faktorizacija (coh)	Jei sistema išlieka koherentinė, banginės funkcijos aprašymas galioja, sujungtiniai ir nesujungtiniai operatoriai evoliucionuoja nepriklausomai.	Atrodo dalinai atkartoja aukštesnių eilių faktorizacijų rezultatus, bet ESA šoninė juosta yra daug silpnesnė ir labiau paslinkta. Su EEA nariais labiau supanašėję su aukštesnių eilių faktorizacijų rezultatais. Skaičiavimo kaštai auga, kaip 4 laipsnio funkcija nuo molekulių skaičiaus.
Tiesioginė faktorizacija (s)	Išlaikome σ ir naudojame $\hat{g}_v = (1 - 2\eta\hat{\sigma}_{vv})$ kaip užuominą faktorizacijai. Išlaikydami σ išlaikome vyksmus susijusius su užpilda, kurie gyvuoja daug ilgiau nei koherentiškumai.	Skaičiavimo rezultatai yra keisti ir elgęsi kitaip lyginant su kitais modeliais. Nėra ESA šoninės juostos, o pagrindinė smailė šiame modelyje stipriais slenka nuo žadinimo impulso intensyvumo. Skaičiavimo kaštai auga, kaip 4 laipsnio funkcija nuo molekulių skaičiaus.

2 lentelė: NEE faktorizavimo 5 eilės modeliai.

Modelis	Pagrindinis principas	Apžvalga
Penktos eilės $z\sigma$	Išlaikyti trečią eilę ir faktorizuoti aukštesnės eilės narius į užpildos narius neišlaikant operatorių eiliškumo.	Didesni skaičiavimo kaštai, nes yra reikalingi z relaksacijos nariai. ESA šoninės juosta stipriai slenka nuo žadinimo intensyvumo. Skaičiavimo kaštai auga, kaip 6 (4 jei naudojama paprastesnė z relaksacija) laipsnio funkcija nuo molekulių skaičiaus.
Penktos eilės zz	Išlaikyti trečią eilę ir faktorizuoti aukštesnės eilės narius didžiausiais galimais nariais. Išlaiko daugiau dvigubų koherentiškumų narių.	Didesni skaičiavimo kaštai, nes yra reikalingi z relaksacijos nariai. Elgęsi keistai atsiranda neigiamas signalas netiesinėje sugertyje. Skaičiavimo kaštai auga, kaip 6 (4 jei naudojama paprastesnė z relaksacija) laipsnio funkcija nuo molekulių skaičiaus.
Penktos eilės zn	Išlaikyti trečią eilę ir faktorizuoti aukštesnės eilės narius su polinkiu į populiacijos narius, išlaikant struktūrą, kuri atsiranda išvedant NEE ir naudojant $\hat{g}_v = (1 - 2\eta\hat{\sigma}_{vv})$ kaip užuomina faktorizavimui.	Didesni skaičiavimo kaštai, nes yra reikalingi z relaksacijos nariai. Su šiuo modeliu rezultatai atrodo geriausiai. Skaičiavimo kaštai auga, kaip 6 (4 jei naudojama paprastesnė z relaksacija) laipsnio funkcija nuo molekulių skaičiaus.

3 lentelė: NEE modeliai eksitonų bazėje.

Modelis	Pagrindinis principas	Apžvalga
Eksitonų bazė (Ex)	Eksitonų bazės įgalina taikyti papildomas aproksimacijas ir turėtų būti skaitmeniškai stabilesnė.	Geresnis skaitinis stabilumas, nes eksitoninėje bazėje yra mažiau osciliuojančių nariu ir koherentiškumai gęsta. Jei EEA neįskaitomas, lygčių skaičiavimo kaštai mažesni eksitonų bazėje. Leidžia papildomas aproksimacijas atmetant tamsias būsenas ir modeliuojant tik šviesius eksitonus. Skaičiavimo kaštai auga, kaip 6 laipsnio funkcija nuo molekulių skaičiaus.
Perslopinta eksitoninė bazė (OD)	Eksitoninėje bazėje koherentiškumai gyvavimo laikas trumpas. Atmetant koherentiškuma lygtis galima ženkliai sumažinti.	Lyginant su paprastu eksitoniniu modeliu, ESA juosta yra labiau paslinkta. Skaičiavimo kaštai auga, kaip 4 laipsnio funkcija nuo molekulių skaičiaus.

kumai gyvuoja trumpai ir aukštesnės eilės nariai slopinami šioje faktorizacijoje. Tuo tarpu tiesioginės faktorizacijos atveju, kur turime išlaikytus užpildos narius, nėra papildomos juostos, tik šiuo atveju bendra sugerties juosta slenka į didesnes energijas, kai didiname žadinimo intensyvumą. Taip pat stebimas juostos formos pokytis, visa juosta yra tarsi pakrypusi į aukštesnės energijos pusę. Aukštesnės energijos šonas statėja didinant žadinimo intensyvumą, tuo tarpu žemesnės energijos šoną plokštėja. Trečios eilės modelis elgėsi panašiai kaip ir apribotos koherentinės būsenos modelis. Tuo tarpu, ESA juosta yra ženkliai siauresnė ir daug intensyvesnė. Efektai susieti su žadinimo intensyvumo labiau pasireiškia paulionams, kurių lygtyse yra daugiau netiesinių narių.

Toliau palyginame modelius, kur faktorizacija buvo taikyta 4-tos eilės nariams. Palyginant sugerties spektrus, visi elgesi kaip 3 eilės modelis, to pasekoje matome - 4-tos eilės narių indėlis yra mažas. To priežastis, 4-tos eilės lygčių nariai neprisideda "tiesiogiai" prie poliarizacijos, kur yra 3 eilės netiesinis narys z yra viduje b ir 5 eilės narys yra z viduje. Visi lyginės eilės yra atsakingi už šuolio dipolinio momento pernormavimą.

Pereinant prie modelių, kur buvo faktorizuoti 4 ir 5 eilės nariai. Turime 3 atskiras faktorizacijos schemas: $z\sigma 5$ modelis, $zz5$ modelis, ir $zn5$ modelis. Lyginant šių modelių netiesinius sugerties spektrus, stebimi ženklūs skirtumai, kurie ryškėja didinant žadinimo intensyvumą (pav. 2). Tačiau stebime bendrą ypatybę - ESA juostą, kuri augi didinant žadinimo intensyvumą. Šiuo atveju ESA amplitudė yra ženkliai mažesnė lyginant su 4-eilės ir tuo pačiu 3-eilės atveju. Be to pastebime reiškinių pastebėtų mažos eilės modeliams pasireiškimą: $z\sigma 5$ modelis, kur dominuoja užpildos, ESA smailė slenka link didesnių energijų, kai didinamas žadinimo intensyvumas. Tai atkartoja tiesioginės faktorizacijos savybes, kur slinko visas spektras. Tuo tarpu $zz5$ modelio rezultatai elgėsi keistai. Tai vienintelis modelis, kurio sugerties spektruose stebima neigiamo intensyvumo sritis. Tai būtų galima interpretuoti kaip stimuliuotos spinduliuotės indėlį. Modelis $zn5$ elgėsi, kaip būtų tikimasi ir rodo panašią sugerties elgsena, kaip ir ketvirtos eilės modeliai, bei trečios eilės modelis.

Toliau lyginame visus tuos pačius modelius, bet dabar su anihiliacijos nariais. Paprastuose modeliuose įtraukus EEA narius stipriai išplinta ESA juosta. Tiesioginės faktorizacijos atveju su EEA vis dar matomas spektro slinkimas didinant žadinimo intensyvumą. Nedidelis įdubimas spektro šone, esant dideliam žadinimo intensyvumui yra indukuotos emisijos ženklas. Tai galima, paulionų atveju, matyti $zz5$ modelio spektre (Pav. 2). Apribotos koherentinės būsenos faktorizacijos atveju ESA juostos intensyvumas ženkliai sumažėjo. O

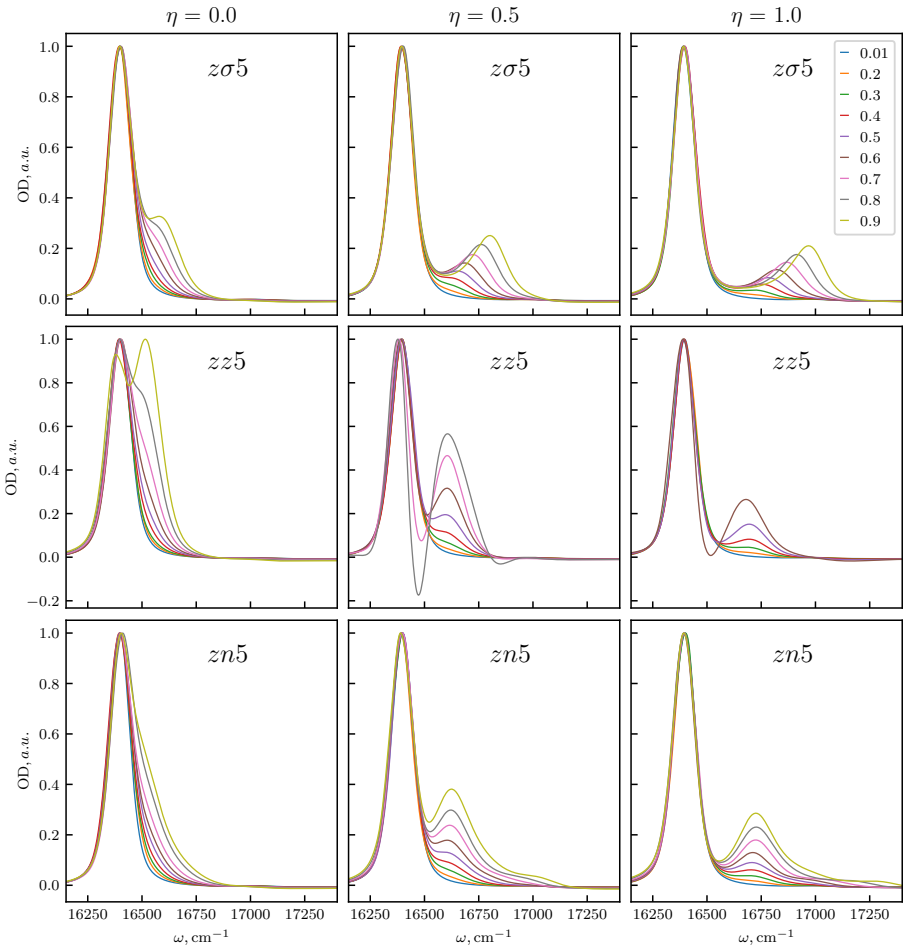

2 pav.: J agregato sugerties spektrai skirtingiems faktorizacijos modeliams be EEA, esant skirtingiems žadinimo lauko intensyvumams. Vertikalioje ašyje pateiktas optinis tankis, horizontalioje - dažnis, o legendoje - žadinimo intensyvumas.

$z3$ modelio atveju sugerties spektras labiau išplitęs, su ženkliu ESA pečiu.

Ketvirtos eilės elgęsi panašiai su EEA nariais, atkartoja $z3$ modelį. Su EEA nariais skirtumai tarp modelių tapo maži.

Su anihiliacijos nariais skirtumai tarp 5 eilės modelių yra daug mažesni (Pav. 3) ir lyginant su 4 eilės modeliais. Didelis juostos išplitimas paslepia skirtumus tarp 4 ir 5 eilės faktorizacijos modelių.

NEE taikymas dideliems molekuliniams agregatams

Kitas žingsnis yra ištirti NEE taikymą dideliems molekuliniams agregatams. Tyrimą atlikome skaičiuodami žadinimo zondavimo spektrus. "Didelis" nėra konkretus dydis, todėl tai siejame kokio dydžio agregatas yra dar suskaičiuojame skaitmeniniais metodais per praktiškai naudingą laiko trukmę. Šioje dalyje mes tyrimą apribojame taikydami aproksimacija modeliuodami tik dalį sistemos eksitoninėje bazėje, nes eksitonai yra delokalizuotos būsenos turinčios indėlį iš visų molekulių, parinkdami tik šviesius eksitonus(nenuliniu šuolio dipoliniu momentu). Tik dalies eksitonų modeliavimą pagrindžiame atkreipdami dėmesį į J agregatų savybes. J agreguose dėl simetrijos tik žemiausios energijos eksitonas turi šuolio dipolinį momentą. Todėl šis šviesus eksitonas turi svarbiausią vaidmenį spektruose. Bet kiti vyksmai, tokie kaip energijos pernešimo turi netiesioginį poveikį spektrams. Todėl visos sistemos apribojimas į vieną eksitoną, kai, pavyzdžiui, visa sistema yra sudaryta iš 50, gali duodi nefizikinius rezultatus.

Dar kitas būdas sumažinti skaičiavimo kaštus yra atmesti narius, turint omenyje koherencijų tipo nariai turėtų greitai gesti ir užpildos gyvuoti ilgiau. Taip turime perslopintą modelį (OD).

Palyginsime skirtingus teorijos lygius, kurie atitinka skirtingus lygčių rinkinius. Tai bus modeliai Ex, Ex-R, OD, OD-R.

Pilnų eksitoninių modelių palyginimas

Pirmiausiai mes palyginame suskaičiuotus sugerties spektrus, naudojant Ex, Ex-R, OD ir ODR modelius, su dviem skirtingais zondavimo impulso intensyvumais. Kai žadinimo intensyvumas mažas, eksitonų užpilda yra $\sigma_{aa} \sim 10^{-4}$. Skaičiavimai įskaito netiesinius indėlius: eksitonų statistika, anharmoniškumą ir EEA. Parodome, kad visų modelių sugertys yra identiškos, kai žadinimo intensyvumas mažas. Taip patvirtiname, kai esame tiesiniame režime, skirtumai tarp modelių nykstami.

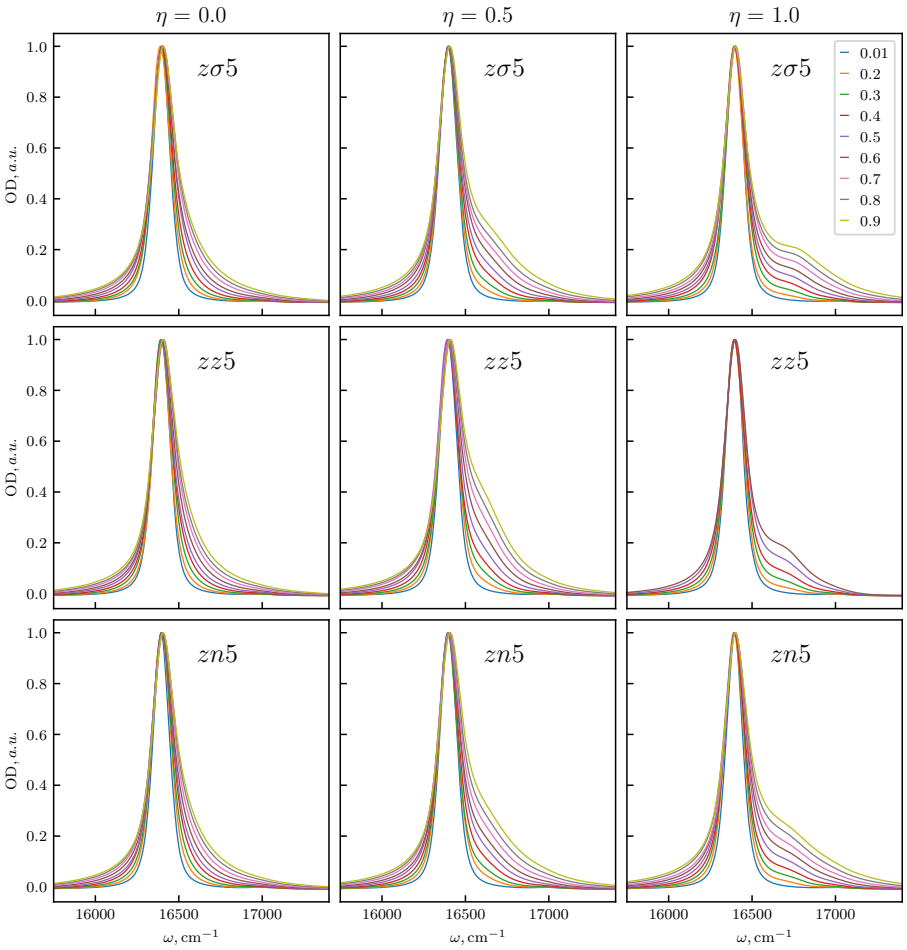

3 pav.: J agregato sugerties spektrai skirtingiems faktorizacijos modeliams su EEA nariiais, esant skirtingiems žadinimo lauko intensyvumams. Vertikalioje ašyje pateiktas optinis tankis, horizontalioje - dažnis, o legendoje - žadinimo intensyvumas.

Žadinimo zondavimo spektras, atvaizduoja trečios ir didesnės eilės netiesiškumus. Parodo nukrypimus nuo sugerties spektro dėl žadinimo impulso poveikio prieš zondavimo impulso. Šiame darbe visi žadinimo zondavimo spektrai suskaičiuoti su 1ps vėlinimo trukme. Taip pat parinkome, taip kad žadinimo impulsas yra 2500 intensyvesnis už zondavimo impulsą. Netiesinis spektras pašalina tiesinę spektro komponentę iš signalo. Nors skirtumai tarp sugerties spektrų buvo nykstami, skirtumai tarp žadinimo zondavimo spektrų (ypač ESA juosta) yra ženklūs (Pav. 4). Pagal teoriją spektras yra sudarytas iš 3 komponenčių: išblyškimo, sužadintos būsenos spinduliavimas ir sužadintos būsenos sugerties (ESA). Kadangi J agregatuose šviesūs eksitonai yra žemiausios energijos eksitonai, sugeriančios ir spinduliuojančios būsenos yra tos pačios. Todėl išblyškimas ir sužadintos būsenos spinduliavimo indėliai persidengia su sudaro neigiamą juostą ties 16400 cm^{-1}. O ESA yra spektro regione nuo 16500 cm^{-1} iki 17000 cm^{-1}ir priklauso nuo modelio.

Su visais modeliai stebima neigiama juosta, kuri yra nejautri skaičiavimo modelio pasirinkimui. Išblyškimui tai yra akivaizdu, nes ši juosta turėtų apytiksliai atitikti sugertie spektrą su neigiamu intensyvumu. O sužadintos būsenos spinduliavimas, yra netiesinė komponentė. Bet yra susieta su viengubai sužadintų eksitonų charakteristikomis ir nepriklauso nuo modelio pasirinkimo.

Reikšmingi skirtumai tarp modelių atsiranda sužadintos būsenos sugertyje (ESA), kurią sukelia trečios eilės nariai (z ir su juo susiję nariai), kai EEA nėra įtraukta. lyginant bozoninį ($\eta = 0$) ir paulioninį modelį ($\eta = 1$) matyti skirtinga ESA piko padėtis. Paulioniniame modelyje ESA pikas yra labiau pasislinkęs lyginant su bozononiu modeliu. O tarpinis atvejis ($\eta = 0.5$) duoda tarpinius ESA piko poslinkius. Lyginant OD ir Ex metodus, matyti, kad OD modelio atveju ESA juostą tendencingai yra labiau pasislinkusi į aukštesnių energijų sritį. Taip pat matome, , kad supaprastinti -R relaksacijos modeliai rodo platesnes ESA juostas lyginant su pilnesniu relaksacijos aprašymo.

Kai EEA yra įjungta (2-oji eilutė, Pav. 4), žadinimo zondavimo spektrai spektrai gęsta didėjant vėlinimo laikui, o linijų formos kinta. Išblyškimo signalas įgauna kairįjį ir dešinįjį „petį“ (paveiksle pažymėta rodyklėmis), kaip buvo stebėta jau dimerui[9], ir pats išblyškimas tampa siauresnis. Tuo tarpu ESA juosta gęsta sparčiau nei išblyškimo juosta.

ESA (sužadintos būsenos sugerties) padėtis priklauso nuo pasirinkto modelio. Ex modelis – išsamiausias, apimantis dalelių koreliacijas ir relaksaciją. Jis labiausiai atitinka koherentines sistemas, kuriose relaksacija yra silpna. Kadangi buvo atliktos tam tikros faktorizacijos, tai gali paveikti ESA piko padėtį

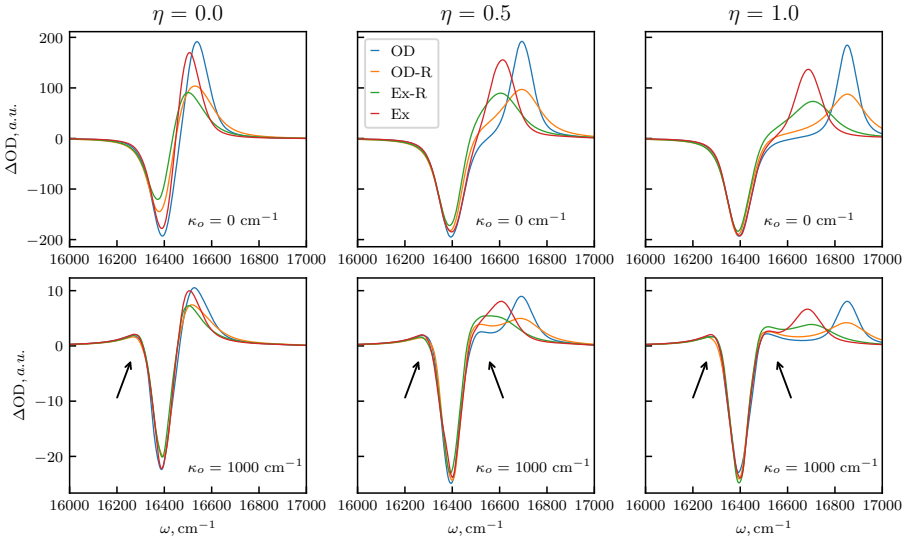

4 pav.: Žadinimo zondavimo spektrai 7 molekulių agregatui, esant stipraus žadinimo sąlygoms ir vėlinimo laikui 1 ps: pirmoji eilutė – anihiliacijos parametras $\kappa_0 = 0$, t. y. EEA neįtraukta. Antroji eilutė – $\kappa_0 = 1000$ cm^{-1}, t. y. EEA stipriai aktyvi. Skaičiavimai pagal Ex metodą paulionams atlikti įtraukiant tik 5 žemiausias eksitonines būsenas, ko visiškai užtenka atkurti signalui. Vertikalioje ašyje pateiktas optinis tankis, horizontalioje - dažnis, o legendoje - modeliai.

esant dideliam intensyvumui, kai turėtų formuotis trigubi sužadinimai, kuriuos atmetėme lygtyse dėl paprastesnės spektrų analizes. EEA slopiną eksitonų lygį iki vieno eksitono, todėl aukštai sužadintos eksitoninės rezonansinės būsenos tampa mažiau reikšmingos. Tokiu atveju daugiaeksitoninių kintamųjų faktorizacija tampa labai svarbi. Ex-R modelis papildomai dar numato greitą daugiaeksitonės konfigūracijos relaksaciją, kas lemia papildomą ESA išplatėjimą. OD modeliai taikomi sistemoms, kuriose vyksta greita relaksacija – visos savybės aprašomos viengubai sužadintų eksitonų juostoje per nekoherentinius eksitonų peršokimus (difuziją). Tokiu atveju ESA juostis atspindi vieno eksitono rezonansus. Tačiau tokiose sistemose, net ir pašalinus daug koherencijos tipo narių signalo informacija išsaugoma. Todėl vietoj pilnų Ex modelio skaičiavimų, kurių sudėtingumas yra N^6, skaičiavimai gali būti reikšmingai sumažinti iki N^4.

Redukuotas eksitonų modelis

Lygčių skaičiaus didėja bent kaip N^4 OD modelyje, o Ex modelyje – N^6, kur N yra molekulių skaičius. Tai tampa neišsprendžiama didelėms sistemoms su tūkstančiais molekulių[64,65]. Ankstesniame poskyryje nagrinėtas 7 chromoforų agregatas yra palyginti nedidelė sistema, leidžianti atlikti pilną Ex modelio skaičiavimą. Tačiau daug didesnėms sistemoms tokie skaičiavimai tampa negalimi ir palyginti modelių negalime.

Tam tikriems molekuliniams agregatams visa didelė sistema gali būti aprašyta tik keletu eksitoninių būsenų[66]. Pavyzdžiui J agregatai, kuriuose tik kelios žemiausios energijos eksitoninės būsenos turi nenulinį šuolio dipolinį momentą. Todėl NEE galime apriboti tik keletu šviesių eksitonų ir su jais susietus kintamuosius. Aukštos energijos eksitonai J agregatuose dažnai niekada neturi reikšmingos užpildos, todėl su jais susietus kintamuosius galime pašalinti. Tačiau tai įmanoma tik eksitoninėje bazėje, nes eksitonai yra kolektyviniai virpesiai ir tarpusavyje sąveikauja tik per sistemos netiesiškumus bei relaksaciją/peršokimus. Šiuos procesus būtina įvertinti, kai atmetinėjame aukštesnės energijos eksitonus. Todėl anksčiau pateikti skaičiavimai gali būti pernelyg apibendrinti, nes reikšmingų kintamųjų yra dar mažiau.

Pirmiausia, paimame mūsų 7 chromoforų sistemą ir parodome, kaip greitai spektras konverguoja didinant įtraukiamų eksitonų skaičių. Mes eksitonus įtraukiame iš eilės nuo žemiausios energijos link aukštesnės. Matome, kad naudojant tik 1 eksitoną, kuris yra ryškiausias, spektruose jau matomos išblyškimo ir ESA savybės, tačiau ESA padėtis pasislenka nuo pilnos 7 eksitonų sistemos

(Pav. 4). Išblyškimo ir spinduliavimo nariai visai nesikeičia. O ESA intensyvumas yra šiek tiek didesnis. Didžiausi nukrypimai pastebimi Ex modelyje. Didinant eksitonų skaičių galima matyti, kad spektrai konverguoja labai greitai. Spektrai susikonvergava jau įtraukus tik t 3 eksitonais. Tai reiškia, kad tą patį rezultatą galima gauti su ženkliai mažesniais skaičiavimo kaštais.

Norint suprasti, koks yra pritaikomumas didesnėms molekulinėms sistemoms, toliau atlikome skaičiavimus sistemoms sudarytoms iš 15 ir 50 chromoforų Visi teoriniai modeliai konverguoja panašiai, todėl skaičiuojame tik OD-R modelį. Šis modelis didesnėms sistemoms generuoja žadinimo zondavimo spektrus, kurie labai artimi pilnesniems modeliams, tuo tarpu skaičiavimo kaštai yra daug mažesni. Lyginant su 7 molekulių atveju, pastebimas labiau išreikštas intensyvumo amplitudės skirtumas tarp skirtingų modelių esant skirtingoms η reikšmėms. Ir taip pat kaip ir su mažesnėmis sistemomis spektrai, nuo eksitonų skaičiaus, konverguoja labai greitai.

50 mazgų sistemoje spektrai taip pat konverguoja, tačiau šiuo atveju nebegalime apskaičiuoti visos 50 eksitonų sistemos. Todėl negalime dalinės sistemos skaičiavimo rezultatų palyginti su pilnos sistemos. Įdomu tai, kad didėjant molekulių skaičiui ESA padėtis tampa nepriklausoma nuo η reikšmės. Taip greičiausiai yra dėl entropinio efekto, kai kombinaciniai sužadinimai tampa daug dažnesni nei virštonio tipo sužadinimai.

NEE taikymas didelės eilės 2D spektrų skaičiavimui

Šiame darbe pritaikėme NEE formalizmą 3-ios ir 5-os eilės 2DES signalų skaičiavimui. Šioje analizėje apribojame dimero ir trimero sistemomis. Siekiant išskirti stipriai netiesines 2D signalų komponenters, taikėme fazės moduliavimo metodą[34].

$\vec{K_1} - \vec{K_2} + \vec{K_3}$ 2DES spektro dinamika paulioniniui chromoforiniam dimerui

Simetriška J tipo paulioninio dimero sistema turi dvi viengubas eksitonines būsenas. Šių būsenų energijas skiria $2J_{12}$ tarpas, kuris yra susijęs su rezonansine tarpchromoforine sąveika. Be aplinkos, žemesnės energijos eksitoninė būsena yra optiškai aktyvus (šviesus), o aukštesnės energijos eksitoninė būsena yra optiškai neaktyvi (tamsi). Be šių dviejų būsenų dar turime kombinacinę dviejų sužadinimų būsena, kurios energija yra lygi visų chromoforų sužadinimo energijų sumai. Tokiam dimerui, tiesinės sugerties spektre būtų viena

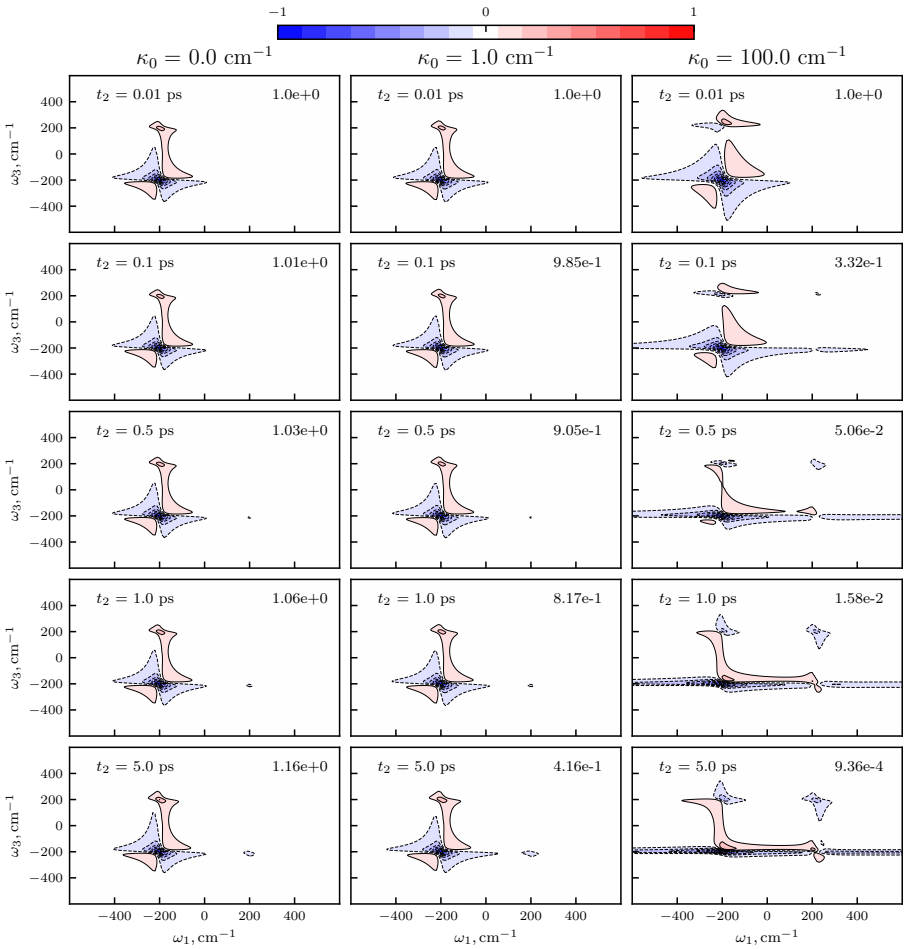

5 pav.: $\vec{K}_1 - \vec{K}_2 + \vec{K}_3$ 2DES J tipo dimero spektras ($J_{12} = -200$ cm^{-1}) , paulionams, esant skirtingoms, vėlinimo trukmėms t_2 ir EEA parametro vertėms. Kiekviena grafikas viršutiniame kairiame kampe turi vėlinimo trukmę; viršutiniame dešiniame - amplitudė, pirmos eilutės atžvilgiu, kur ji yra lygi 1. Pačiame grafiko viršuje yra bendra spalvų juosta, kurios amplitudė atitinka kiekvieno grafiko amplitudę.

juosta, atitinkanti šviesųjį, mažiausios energijos, eksitoną.

Trečios eilės netiesiniai spektrai papildomai apima sužadintos būsenos sugertį (ESA), kur pasireiškia dvigubų eksitonų būsenos. Nepersifazuojantis ($\vec{K}_1 - \vec{K}_2 + \vec{K}_3$) 2DES spektras paulioniškam dimerui yra pateiktas (Pav. 5). Šiame paveiksle yra pateikti 2DES spektrai su trimis skirtingomis anihiliacijos vertėmis: $\kappa_0 = 0$ cm^{-1} - be anihiliacijos, 1 cm^{-1} - maža EEA parametro vertė, ir 100 cm^{-1} - didelė EEA parametro vertė. Reikia turėti omenyje, kad anihiliacijos parametro vertė nėra tiesiogiai susijusi su anihiliacijos laiku, nes procesas yra neeksponentinis, todėl anihiliacijos trukmės negalima priskirti. Kiekvienu atveju buvo suskaičiuoti 2DES su keliomis vėlinimo trukmėmis.

Matomos gerai žinomos trečios eilės savybės dimerui, yra pateiktos kairiame stulpelyje, esant mažai vėlinimo trukmei (Pav. 5). Mažos energijos diagonali smailė ($\omega_1 = \omega_3 = -200$ cm^{-1}) atitinka mažos energijos eksitoną dimere; nediagonalios smailės parodo sistemos koherentiškumus sistemoje. Nediegonali smailė ($\omega_1 = -200$ cm^{-1}, $\omega_3 = 200$ cm^{-1}), yra priešingo ženklo nei diagonali smailė ir atvaizduoja sužadintos būsenos sugertį. Kita nediagonali smailė ($\omega_1 = 200$ cm^{-1}, $\omega_3 = -200$ cm^{-1}) nematoma, nes yra susijusi su tamsiu aukštesnės energijos eksitonu.

Šiuo atveju spektrai mažai keičiasi nuo t_2 vėlinimo laiko. Reikšmingos relaksacijos nematyti, nes diagonali smailė susieta su mažiausios energijos eksitonu. Bet didinant t_2 vėlinimo laiką tampa matoma papildoma nedidelė nediagonali smailė ($\omega_1 = 200$ cm^{-1}, $\omega_3 = -200$ cm^{-1}). Šios intensyvumas auga dėl šiluminės dinamikos. Nors aukštesnės energijos eksitonas yra tamsus, didelis žadinimo impulso intensyvumas išveda sistemą iš trikdžių teorijos režimo, todėl dalis užpildos pereina į tamsią būseną; vėliau šios būsenos lėtai relaksuoja į šviesią būseną, todėl spektrų intensyvumas šiek tiek padidėja net ir be EEA narių.

Kai EEA įjungta, mažo anihiliacijos parametro atveju), smailės gęsta didėjant vėlinimo trukmei, o jų formos yra labiau išplitusios. Padidinus anihiliacijos parametrą, visos kryžminės smailės tampa ryškesnės lyginant su diagonalinėmis smailėmis trumpuose vėlinimo laikuose ($t_2 = 0.5$, 1 ps vėlinimo trukmė), o ilgesniems laikams slopinimas tampa daug stipresnis. Įdomus stebima sąvybė , kad šiuose vėlinimo laikuose atsiranda diagonalinė smailė ties $\omega_1, \omega_3 = +200$ cm^{-1} , kuri buvo optiškai tamsi be anihiliacijos. Labai trumpuose vėlinimo laikuose ($t_2 = 0.01, 0.1$ ps) spektras yra žymiai labiau išplitęs. Ilgesniems vėlinimo laikams apatinė diagonalinė smailė išsiplečia pagal ω_1, o išsiplėtimas pagal ω_3 sumažėja iki to paties lygio, kaip ir be anihiliacijos. Tai

susiję su tuo, kad laikui bėgant sistema grįžta į žemesnius sužadinimo lygius (dėl EEA), kur smailės yra siauresnės.

Be to, esant dideliam EEA parametrui, šalia sužadintos būsenos sugerties (ESA) smailėje atsiranda papildoma smailė. Ši smailė yra priešingo ženklo (mėlyna) ir šiek tiek paslinkta ESA). Ši nauja smailė yra susijusi su papildomu kvantinio kelio indėliu. Kur yra trys sąveikos su K_2 impulsu. Kai nėra EEA, šis kelias indėlio neduoda.

$2\vec{K}_1 - 2\vec{K}_2 + \vec{K}_3$ 2DES spektrų dinamikos paulioniškam chromoforiniam dimerui

Toliau nagrinėjame penktos eilės signalą ties $2\vec{K}_1 - 2\vec{K}_2 + \vec{K}_3$. Kadangi anihiliacija yra penktos eilės procesas optinio lauko atžvilgiu, ji turėtų turėti labiau išreikštą poveikį signalui ties $2\vec{K}_1 - 2\vec{K}_2 + \vec{K}_3$, kai lyginame su signalu ties $\vec{K}_1 - \vec{K}_2 + \vec{K}_3$[67,68,24].

Tačiau eksitoninis dimeras yra labai netiesinė sistema net ir be EEA. Penktos eilės signalas atsiranda ir esant $\kappa = 0$ dėl Pauli draudimo principo. Šio atvejo spektrai, kai EEA išjungtas yra parodyti 6 paveikslo pirmame stulpelyje.

Lyginant $2\vec{K}_1 - 2\vec{K}_2 + \vec{K}_3$ ir $\vec{K}_1 - \vec{K}_2 + \vec{K}_3$ signalus chromoforiniam dimerui, pastebime paulioniškumo efektus: paulionai draudžia dvigubą sužadinimą viename chromofore, todėl signalo smailės atsiranda ties ($\omega_1 = 0$ cm^{-1}, $\omega_3 = \pm 200$ cm^{-1}), kas rodo dvigubo eksitono buvimą, sukurto per $2K_1$ sužadinimą. Laikinė evoliucija yra lėta. Yra matomas bendras smailių intensyvumo gesimas. Šis gesimas yra dėl supaprastinto Markovinio relaksacijos modelio. Supaprastintas relaksacijos modelis per daug stipriai gesina daugiaeksitonines koherencijas, šiuo atveju z kintamąjį.

Kai EEA įjungta (antras 6 paveikslo stulpelis), atsiranda keli svarbūs pokyčiai. Pasirodo papildomos smailės ties $\omega_1 = -400$ cm^{-1} , $\omega_3 = \pm 200$ cm^{-1}. Šios struktūros ties $\omega_1 = -400$ cm^{-1}gali būti siejamos su mažesnės energijos dvigubo eksitono sužadinimu. Nepaisant, kad nei viengubo eksitono būsena, nei dvigubo eksitono būsena ties -400 cm^{-1} neegzistuoja. Lyginant su smailėmis ties $\omega_1 = 0$, šių naujų smailių intensyvumas didėja didinant vėlinimo trukmę, . Tai yra susiję su EEA procesu, sistemos žadinimo metu. EEA yra lokalus chromoforinis procesas, kuris tikėtina pašalina eksitonų nustatytas simetrijas net žadinimo impulsų veikimo metu. Dėl to, veikiant $2\vec{K}_1$(dvi sąveikos su lauku), eksitonai yra sukuriami du kartus, todėl gaunamas dvigubas eksitoninis koherentiškumas. Šis reiškinys yra grynas NEE formalizmo bruožas.

Esant dideliam EEA (trečias 6 paveikslo stulpelis), visos smailės signale

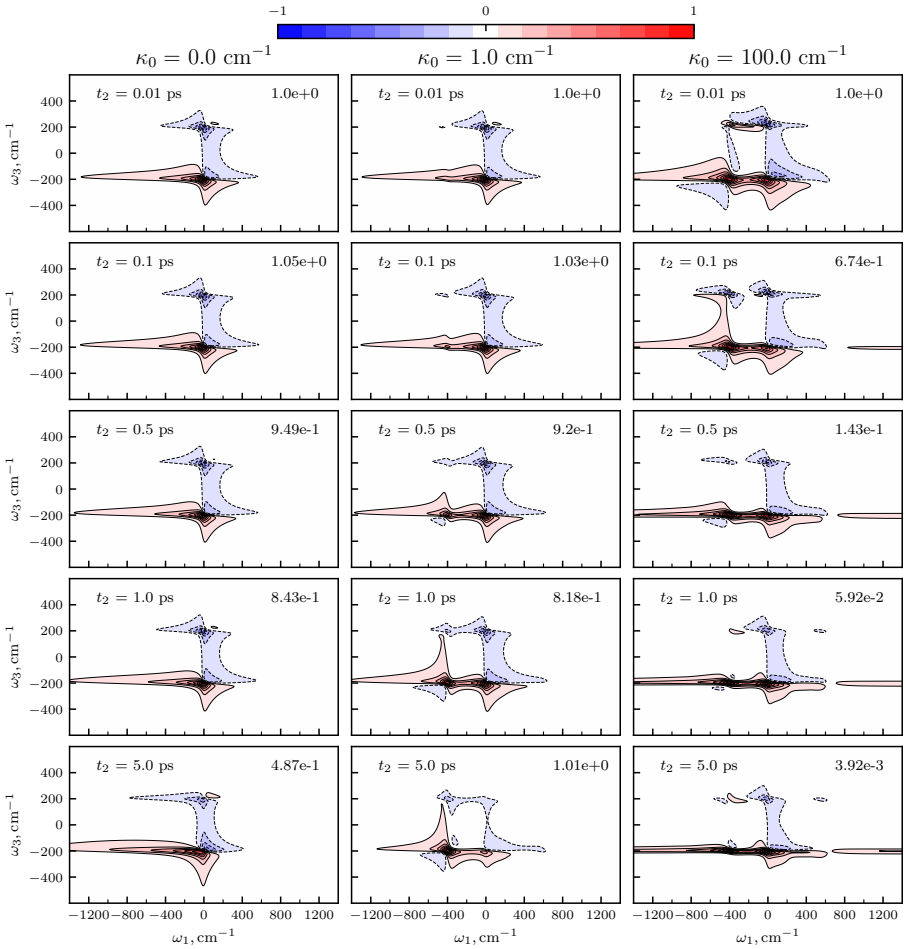

6 pav.: $2\vec{K}_1 - 2\vec{K}_2 + \vec{K}_3$ 2DES spektrai j tipo dimerui ($J_{12} = -200\ \mathrm{cm}^{-1}$) paulionams, esant skirtingoms vėlinimo trukmėms ir įvairioms EEA parametro vertėmis. Žymėjimai paaiškinti Pav. 5.

silpsta, tačiau nevienodai kintant vėlinimo trukmiai. Struktūros ties $\omega_1 = -400$ cm^{-1}yra intensyvesnės, bet greitai suyra; kiti bruožai apskritai yra platesni, tačiau ilgesniais vėlinimo laikais šie susilpnėja ir susiaurėja ašyje ω_3. Ilgiems vėlinimo laikams linijų formos, lyginant su atveju be EEA yra ryškiai iškraipytos.

Taip pat esant dideliam EEA, atsiranda smailė ties $\omega_1 = +400$ cm^{-1}. Šios smailės kilmė yra ta pati kaip ir smailės ties $\omega_1 = -400$ cm^{-1}. Tačiau smailė ties $\omega_1 = +400$ cm^{-1} yra papildomai susijusi su „tamsiojo“ eksitono „atsivėrimu“. Kadangi EEA yra lokalus chromoforinis procesas, jis ardo eksitoninės sistemos simetriją ir pakeičia eksitonų savybes, atverdamas tamsiąsias pernašas.

$\vec{K_1} - \vec{K_2} + \vec{K_3}$ 2DES spektrų dinamikos trimerui

Paulioninis chromoforinis dimeras yra mažiausia sistema, kurioje atsispindi agregato savybės. Tačiau paulioninis dimeras turi tik vieną dvigubai sužadinta būseną. Didesnėse sistemose dvigubai sužadintos būsenos sudaro būsenų juostą. Todėl toliau tikriname, ar minėtos savybės pastebimos chromoforiniame trimere. Paulionis trimeras teoriškai turi tris dvigubai sužadintas būsenas. Reikia atkreipti dėmesį, mūsų sistemoje dvigubai sužadintų būsenų struktūra yra tokia pati kaip viengubai sužadintų būsenų: viena būsena yra ties -400 cm^{-1}, ir dvi išsigimosios būsenos $+200$ cm^{-1}. Tik žemiausios energijos eksitonas yra optiškai aktyvus. 2DES spektre, kai $\kappa_0 = 0$ matome vieną diagonalinę smailę ir sužadintos būsenos sugertį ties $\omega_3 = 0$ cm^{-1} , rodančią chromoforų koherenciją. Didelio t_2 vėlinimo metu, kaip ir dimerui, atsiranda kryžminė smailė ties $\omega_1 = 0$ cm^{-1}. Įjungus EEA, pradeda reikštis smailių gesimas. Padidinus anihiliacijos parametrą, gesimas vyksta sparčiau (ypač diagonalinios smailės), o kryžminės smailės išryškėjelabiau. Taip pat kaip ir buvo dimero atveju, savybės, kurios be EEA buvo uždraustos, vėl yra sustiprinamos EEA, kuri ardo eksitoninis simetrijas.

$2\vec{K_1} - 2\vec{K_2} + \vec{K_3}$ 2DES spektrų dinamika trimerui

$2\vec{K_1} - 2\vec{K_2} + \vec{K_3}$ 2DES spektras trimerui iš esmės atkartoja ypatybes, kurias stebėjome dimerui. Esant nulinės anihiliacijos atvejui, signalas yra išsidėstes ties $\omega_1 = -400$ cm^{-1}, kas atitinka žemiausios energijos eksitono sukūrimą. Smailė ties $\omega_3 = -400$ cm^{-1} atitinka mažiausios energijos eksitoną, o ties $\omega_3 = 0$ cm^{-1} – koherentiškumą tarp viengubų ir dvigubų eksitonų.

Didžiąją dalį spektro lemia vienas ryškus eksitonas, nes bendros savybės primena dimerą. Įjungus anihiliaciją, smailės gęsta greičiau, ir atsiranda papildomų spektrinių smailių ties $\omega_1 = -800$ cm^{-1}. Tai atkartoją tendencija, kuri buvo matyta dimero atveju, kur tuo atveju buvo ties $\omega_1 = -400$ cm^{-1}. Šie požymiai atsiranda tose padėtyse, kur vyksta dvigubas šviesaus eksitono sužadinimas. Anihiliacija, kai ir kitais atvejais, sukelia eksitonų simetrijos pažeidimą sužadinimo metu ir eksitonai pakartotinai sužadinami. Esant didelėms anihiliacijos parametrų vertėms, linijų formos ties ω_3 tampa išplaukusios. Esant trumpai vėlinimo trukmei smailės yra išplėstos simetriškai, tuo tarpu ilgėjant vėlinimo trukmei pikų intensyvumai persiskirsto dėl netolygaus anihiliacijos poveikio visame eksitonų juostos diapazone.

2DES spektrai bozonams

Toliau pateikiame tuos pačius spektrus, kurie buvo skaičiuoti ir paulionų atvejui, bozonams. Dimerui, $\vec{K}_1 - \vec{K}_2 + \vec{K}_3$ bozoniniame spektre pagrindinis skirtumas nuo paulionų atvejo yra tas, kad kryžminės smailės, kurios susijusios su eksitonų koreliacijomis, bozonų atveju nėra matomos. Sužadintos būsenos sugerties (ESA) stiprus signalas pasireiškia ties ($\omega_1 = -200$ cm$^{-1}, \omega_3 = 0$ cm^{-1}) ir yra pasislinkęs maždaug per pusę anharmoniškumo parametro vertės nuo pagrindinės smailės ($\omega_1 = -200$ cm$^{-1}, \omega_3 = -200$ cm^{-1}) ; jis susideda iš chromoforo virštoninio sužadinimo ir kombinacinio juostos sužadinimo. Šie požymiai yra simetriškai atsikartojami ir ties ties $\omega_1 = 0$. Esant kai nėra EEA, matome nežymų signalo slopinimą. Tai yra priešingas elgesys lyginant su paulionų atveju, kur buvo stebėtas nedidelis augimas. Taip yra, nes bozonų atveju, NEE lygtyse nėra nuo užpildos priklausančio poveikio šuolio dipoliniams momentams. Tuo tarpu paulionams šuolio dipolių momentų nariai efektyviai yra padauginti iš $(1 - 2\eta\hat{\sigma}_{uu})$. Esant didelėms EEA parametro reikšmėms, spektrai tampa žymiai platesni ir pasižymi spartesniu signalo gesimu laike. Trimero atveju $\vec{K}_1 - \vec{K}_2 + \vec{K}_3$ spektruose matomos tos pačios tendencijos kaip ir dimero atveju.

Išvados

1. Parodėme kaip galima efektyviai faktorizuoti NEE ir sutrumpinti tikrinių funkcijų erdvėje. Todėl galime efektyviai suskaičiuoti didelių molekulinių chromoforų agregatų stipriai netiesinius spektrus. Labiausiai jautri netiesinėms savybėms yra sužadintos būsenos sugerties (ESA) smailė,

kurią reikia tirti siekiant nustatyti sistemos savybes esant stipriam sužadinimui.

Kaip jau minėta, faktorizacija yra reikalinga dėl ribotų skaičiavimo resursų siekiant uždaryti lygčių hierarchiją. Hierarchija yra begalinė, todėl negali būti tiesiogiai sprendžiama. Idealios faktorizavimo schemos nėra - skirtingos schemos pabrėžia skirtingus reiškinius. Pavyzdžiui, vienas iš paprastesnių modelių, tiesioginės faktorizacijos modelis gali būti taikomas jei tik sugerties linijos slinkimas nuo žadinimo intensyvumo stebimas. Tuo tarpu z kintamoji įtraukimas gali būti svarbus jei matoma ESA juosta.

Skirtingos faktorizacijos schemos leidžia atitinkamus lygčių supaprastinimus, kas leidžia efektyvesnius ir greitesnius skaičiavimus. Paprasčiausi lygčių rinkiniai leidžia labai greitus skaičiavimus. Tačiau tam tikrų schemų sprendiniai gali būti nestabilūs, pavyzdžiui $zz5$ modelis nekonverguoja esant dideliam žadinimo intensyvumui. Šių nestabilumų priežastis yra susieta su komutatoriaus simetrijos pažeidimu, kai faktorizuojami aukštesnės eilės nariai. Pavyzdžiui $\langle \hat{b}^\dagger \hat{b}^\dagger \hat{b}\hat{b} \rangle \to \langle \hat{b}^\dagger \hat{b} \rangle \langle \hat{b}^\dagger \hat{b} \rangle$ abu $\hat{b}\hat{b}$ ir $\hat{b}^\dagger \hat{b}^\dagger$ išdalinami ir dvigubo sužadinimo savybės, kurios buvo apibrėžtos komutaciniu sąryšiu, yra atmetamos. O pavyzdžiui $\langle \hat{b}^\dagger \hat{b}^\dagger \hat{b}\hat{b} \rangle \to \langle \hat{b}^\dagger \hat{b}^\dagger \hat{b} \rangle \langle \hat{b} \rangle$ yra dalinai pažeidžiama ir išbalansuojami įvairūs nariai, ir tokių lygčių sprendinys tikėtina diverguotų.

NEE buvo panaudotos eksitoninėje bazėje, toks aprašymas labai efektyvus J tipo agregatams. Tokios sistemos yra patogios eksitoniam modeliui, nes tik mažiausios energijos eksitonas yra optiškai šviesus. Tačiau aprašyme naudojant tik vieną eksitoną turime neteisingą ESA smailę. Įtraukus kelis papildomus eksitonus ESA smailė sukonverguoja. Tai reiškia dvigubų eksitonų rezonansai nėra būsenos suformuotos tik iš vieno eksitono būsenų sandaugos. Tačiau įtraukus tik kelius žadinimo energijomis artimus eksitonus pakanka atstatyti dvigubų eksitonų rezonansus. Tai reiškia tik eksitonai, kurių energijos artimos sąveikauja.

Kitas aspektas, kuris prisideda, kodėl neužtenka vieno eksitono, yra eksitonų šiluminė aktyvacija. Šiluminėje pusiausvyroje $k_B T$ ruožas eksitonų juostoje turės užpildas. Todėl svarbą turi kiek eksitonų patenka į šį ruožą. Tai yra apibrėžta eksitoninėje bazėje ir netinka naudoti chromoforų bazėje.

2. Mes parodėme NEE kartu su nauju komutaciniu sąryšiu apibendrintomis

dalelėmis. Mes išbandėme $\eta = 0.5$ atvejį, kuris yra tarpe tarp paulionų ir bozonų. Suskaičiuotų sprendinių savybės yra tarpe tarp paulionų ir bozonų savybių. Suskaičiuotuose sugerties ir žadinimo zondavimo spektruose matome, ESA juostos poslinkis yra viduryje tarp paulioninio ir bozoninio atvejų, kai tarpusavyje lyginame spektrus.

3. EEA įtraukimas suvienodina skirtingus modelius. Koherentinės ir tiesioginės faktorizacijos schemos labiausiai išsiskiria nuo kitų modelių. Nors spektrai supanašėja įtraukus EEA, bet zz modelio nestabilumas išlieka esant dideliam žadinimo intensyvumui. Bet tai pasireiškia didesniems intensyvumams lyginant su variantu be anihiliacijos.

   Parodėme, kaip molekulinės sistemos sugerties spektras gali būti praturtintas papildomis savybėmis esant dideliam žadinimo intensyvumui. Tam reikia spręsti NEE taikant neartutinius metodus. Lygtys turi būti uždarytos ir tam yra keletas būdų. Įdomiausias variantas, yra stipriai netiesinių narių faktorizavimas NEE lygtyse. Skirtingos faktorizavimo schemos gali išryškinti skirtingus procesus, tai gali būti panaudota specifiniuose NEE pritaikymuose. Analizė palengvėja įtraukus EEA narius, nes EEA slopina stipriai sužadintų būsenų formavimąsi. Dėl šios priežasties EEA sumažina skirtumus tarp modelių. Todėl NEE su EEA galima efektyviai taikyti, ir skaičiavimai priklauso nuo paprastų lygčių.

4. 2DES kryžminės smailės stipriai priklauso nuo EEA parametro: net smailės, kurios turėtų būti tamsios ir neturėtų turėti šuolio dipolio momento tampa matomos. $2\vec{K}_1 - 2\vec{K}_2 + \vec{K}_3$ signale matomos smailės siejamos su draudžiamais šuoliais ir dvigubais rezonansais. Šios smailės yra susietos su nukrypimais nuo trikdžių teorijos režimo. Šiuo atveju sužadinimas nebūtinai atitinka šuolį tarp konkrečių sistemos būsenų. Žadinimo proceso metu gali būti inicijuojami tam tikri rezonansai, kurie seka molekulines simetrijos atrankos taisykles, o ne eksitonų. Taip tamsiuose eksitonuose sudaro užpilda. Tada įvyksta relaksacija į šviesias būsenas ir stebimos nuo laiko priklausančios spektrinės ypatybės neįprastose vietose.

   Trikdžių teorijos rėmuose, medžiagos hamiltoniano tikrinės būsenos (eksitonai mūsų modelyje), kai optinis laukas yra išjungtas, yra stacionarios būsenos; laukas tik sukuria šuolius tarp šių būsenų. Tačiau kai išorinis laukas yra pastovus tada pilnas trumpalaikis hamiltonianas turi papildomą stacionarią sistemos-lauko sąveiką. Net jeigu medžiagos hamilto-

nians yra diagonalus (pavyzdžiui eksitonų atvaizdavime), trumpalaikis sistemos-lauko hamiltonianas nebūtų diagonalus ir jo naujos stacionarios būtų polaritonai[69]. Atitinkamai šios atrankos taisyklės yra kitokios lyginant su eksitonais.

Mūsų atveju optinis laukas yra impulsinis, ir žadinimo metu, kai laukas įjungtas, sistema laikinai pereina į polaritoninį režimą ir net tamsūs eksitonai (tamsūs, kai laukas išjungtas) atsidaro žadinimui. Šis simetrijos pažeidimas yra susietas su užpildos poveikiu šuolio dipoliniam momentui lygtyse 7-10, kur efektyviai esant didelėms užpildoms turime $\mu_n(t) \to (1 - 2\eta\sigma_{nn})\mu_n(t)$.

5. NEE kartu su fazės moduliavimo metodu įgalina apibendrintai suskaičiuoti poliarizaciją, kuri yra bazinis dydis apibūdinantis įvairaus tipo spektrus. Pateiktos stipriai netiesinės NEE lygtys kartu su fazės moduliavimo metodu gali būti taikomos tirti didelę spektroskopinių metodų įvairovę. Fazės moduliavimas leidžia paprastai atskirti fazių derinimo kryptis. Skaitinis NEE sprendinys išreikštai atsižvelgia ir į žadinimo impulso savybes; įtraukia ir atsižvelgia į impulsų persidengimo efektus. Pavyzdžiui, dėl laike nesurikiuotų sąveikų, kurios atsiranda dėl baigtinės impulsų trukmės, net kai impulsų centrai yra surikiuoti. Šis metodas buvo efektyviai panaudotas 3-5 eilių spektrų skaičiavimuose. Pavyzdžiui signalui $m_1K_1 + m_2K_2 + m_3K_3$ reikėtų suskaičiuoti $(2\,|m_1| + 1) \cdot (2\,|m_2| + 1) \cdot (2\,|m_3| + 1)$ pastumtos fazės ėminių. Tada taikoma 5D Furje transformacija (2 dimensijos atitinka t_1 ir t_3, o likusios yra kiekvienam bangų maišymosi bangos skaičiaus vektoriui).

BIBLIOGRAPHY

1. R. E. Blankenship, *Molecular Mechanisms of Photosynthesis*, 2nd ed. (Wiley Blackwell, Oxford, UK, Chichester, UK, Hoboken, USA, 2014) p. 296.
2. H. van Amerongen, L. Valkunas, and R. van Grondelle, *Photosynthetic Excitons* (World Scientific, Singapore, New Jersey, London, Hong Kong, 2006) p. 590.
3. F. Würthner, T. E. Kaiser, and C. R. Saha-Möller, Angewandte Chemie International Edition **50**, 3376 (2011).
4. N. J. Hestand and F. C. Spano, Chemical Reviews **118**, 7069 (2018).
5. T. Kobayashi, ed., *J-aggregates* (World Scientific, Singapore, 2012).
6. Y. Du, X. Liu, and S. Zhu, Frontiers in Chemistry **9**, 718709 (2021).
7. J. L. Bricks, Y. L. Slominskii, I. D. Panas, and A. P. Demchenko, Methods and Applications in Fluorescence **6**, 012001 (2017).
8. L. Chen, R. Zheng, Q. Shi, and Y. Yan, The Journal of Chemical Physics **132**, 024505 (2010).
9. V. Bubilaitis, J. Hauer, and D. Abramavicius, Chemical Physics **527**, 110458 (2019).
10. A. Gelzinis, R. Augulis, V. Butkus, B. Robert, and L. Valkunas, Biochimica et Biophysica Acta (BBA) - Bioenergetics **1860**, 271 (2019).
11. P. Hamm and M. Zanni, *Concepts and Methods of 2D Infrared Spectroscopy* (Cambridge University Press, Cambridge, 2011).
12. S. Mukamel, *Principles of nonlinear optical spectroscopy* (New York : Oxford University Press, 1995).
13. P. Tian, D. Keusters, Y. Suzaki, and W. S. Warren, Science **300**, 1553 (2003).
14. E. Fresch, F. V. A. Camargo, Q. Shen, C. C. Bellora, T. Pullerits, G. S. Engel, G. Cerullo, and E. Collini, Nature Reviews Methods Primers **3**, 84 (2023).

15. D. Abramavicius, B. Palmieri, D. V. Voronine, F. Šanda, and S. Mukamel, Chem. Rev. **109**, 2350 (2009).

16. M. Fushitani, Annual Reports Section "C" (Physical Chemistry) **104**, 272 (2008).

17. V. Sundström, T. Gillbro, R. A. Gadonas, and A. Piskarskas, The Journal of Chemical Physics **89**, 2754 (1988).

18. V. Barzda, V. Gulbinas, R. Kananavicius, V. Cervinskas, H. van Amerongen, R. van Grondelle, and L. Valkunas, Biophysical Journal **80**, 2409 (2001).

19. C. J. Bardeen, Annual Review of Physical Chemistry **65**, 127 (2014).

20. V. May, The Journal of Chemical Physics **140**, 054103 (2014).

21. T. Yonehara, K. Goushi, T. Sawabe, I. Takasu, and C. Adachi, Japanese Journal of Applied Physics **54**, 071601 (2015).

22. J. Süß, J. Wehner, J. Dostál, T. Brixner, and V. Engel, The Journal of Chemical Physics **150**, 104304 (2019).

23. B. Kriete, J. Lüttig, T. Kunsel, P. Malý, T. L. C. Jansen, J. Knoester, T. Brixner, and M. S. Pshenichnikov, Nature Communications **10**, 4615 (2019).

24. J. Dostál, F. Fennel, F. Koch, S. Herbst, F. Würthner, and T. Brixner, Nature Communications **9**, 2466 (2018).

25. J. Chmeliov, J. Narkeliunas, M. W. Graham, G. R. Fleming, and L. Valkunas, Nanoscale **8**, 1618 (2016).

26. F. Fennel and S. Lochbrunner, Physical Review B **92**, 140301 (2015).

27. B. Brüggemann and T. Pullerits, New Journal of Physics **13**, 025024 (2011).

28. W. Metzner, M. Salmhofer, C. Honerkamp, V. Meden, and K. Schönhammer, Reviews of Modern Physics **84**, 299 (2012).

29. F. A. Evangelista, The Journal of Chemical Physics **141**, 054109 (2014).

30. D. Abramavicius, EPL (Europhysics Letters) **101**, 57007 (2013).

31. V. Bubilaitis and D. Abramavicius, The Journal of Chemical Physics **161**, 104106 (2024).

32. V. Bubilaitis and D. Abramavicius, Chemical Physics **588**, 112445 (2025).

33. V. Bubilaitis and D. Abramavičius, Lithuanian Journal of Physics **65**, 1 (2025).

34. H.-S. Tan, The Journal of Chemical Physics **129**, 124501 (2008).

35. V. Agranovich and B. Toshich, Sov. Phys. JETP **26**, 104 (1968).

36. V. M. Agranovich, *Excitations in Organic Solids*, edited by G. Czajkowski, International Series of Monographs on Physics Ser. No. v.142 (Oxford University Press, Incorporated, Oxford, 2009).

37. E. Merzbacher, *Quantum mechanics*, 3rd ed. (Wiley, New York, 1998) includes index. - Previous ed.: 1970.

38. R. Shankar, *Principles of quantum mechanics*, second edition, corrected at 19th printing ed. (Springer, New York, NY, 2014).

39. V. Chernyak and S. Mukamel, Journal of the Optical Society of America B **13**, 1302 (1996).

40. V. Chernyak, W. M. Zhang, and S. Mukamel, The Journal of Chemical Physics **109**, 9587 (1998).

41. M. Schröter, S. Ivanov, J. Schulze, S. Polyutov, Y. Yan, T. Pullerits, and O. Kühn, Phys. Rep. **567**, 1 (2015).

42. A. G. Redfield, IBM J. Res. and Dev. **1**, 19 (1957).

43. L. Valkunas, D. Abramavicius, and T. Mančal, *Molecular Excitation Dynamics and Relaxation.* (Wiley-VCH Verlag GmbH & Co. KGaA, Weinheim, Germany, 2013).

44. H.-P. Breuer and F. Petruccione, *The Theory of Open Quantum Systems* (Oxford University PressOxford, 2007).

45. T. Renger and R. A. Marcus, The Journal of Chemical Physics **116**, 9997 (2002).

46. M. Reppert, A. Kell, T. Pruitt, and R. Jankowiak, The Journal of Chemical Physics **142**, 094111 (2015).

47. D. Abramavicius, Y.-Z. Ma, M. W. Graham, L. Valkunas, and G. R. Fleming, Physical Review B **79**, 195445 (2009).

48. W. R. Jeffries, C. M. Aikens, and K. L. Knappenberger, The Journal of Physical Chemistry C **127**, 19035 (2023).

49. E. Collini, The Journal of Physical Chemistry C **125**, 13096 (2021).

50. X. Gao and E. Geva, Journal of Chemical Theory and Computation **16**, 6491 (2020).

51. J. Segarra-Martí, V. K. Jaiswal, A. J. Pepino, A. Giussani, A. Nenov, S. Mukamel, M. Garavelli, and I. Rivalta, Faraday Discussions **207**, 233 (2018).

52. J. Dostál, J. Pšenčík, and D. Zigmantas, Nature Chemistry **8**, 705 (2016).

53. P. Malý, J. Lüttig, P. A. Rose, A. Turkin, C. Lambert, J. J. Krich, and T. Brixner, Nature **616**, 280 (2023).

54. J. Lüttig, S. Mueller, P. Malý, J. J. Krich, and T. Brixner, The Journal of Physical Chemistry Letters **14**, 7556 (2023).

55. M. Cho, *Two-dimensional optical spectroscopy* (Taylor & Francis, Boca Raton, 2009).

56. W. Wagner, C. Li, J. Semmlow, and W. S. Warren, Optics Express **13**, 3697 (2005).

57. D. Keusters, H.-S. Tan, and Warren, The Journal of Physical Chemistry A **103**, 10369 (1999).

58. C. Shannon, Proceedings of the IRE **37**, 10 (1949).

59. S. Mukamel and D. Abramavicius, Chemical Reviews **104**, 2073 (2004).

60. P. Malý and T. Mančal, The Journal of Physical Chemistry Letters **9**, 5654 (2018).

61. M. Bruschi, F. Gallina, and B. Fresch, Physical Chemistry Chemical Physics **24**, 27645 (2022).

62. X. Fan, A. Wei, T. Klamroth, Y. Zhang, K. Gao, and L. Wang, Physical Review B **107**, 134301 (2023).

63. F. Milota, V. I. Prokhorenko, T. Mancal, H. von Berlepsch, O. Bixner, H. F. Kauffmann, and J. Hauer, The Journal of Physical Chemistry A **117**, 6007 (2013).

64. Y. Wan, A. Stradomska, J. Knoester, and L. Huang, Journal of the American Chemical Society **139**, 7287 (2017).

65. A. S. Bondarenko, T. L. C. Jansen, and J. Knoester, The Journal of Chemical Physics **152**, 194302 (2020).

66. J. Sperling, A. Nemeth, J. Hauer, D. Abramavicius, S. Mukamel, H. F. Kauffmann, and F. Milota, The Journal of Physical Chemistry A **114**, 8179 (2010).

67. C. Heshmatpour, P. Malevich, F. Plasser, M. Menger, C. Lambert, F. Šanda, and J. Hauer, The Journal of Physical Chemistry Letters **11**, 7776 (2020).

68. C. Heshmatpour, J. Hauer, and F. Šanda, Chemical Physics **528**, 110433 (2020).

69. T. Khazanov, S. Gunasekaran, A. George, R. Lomlu, S. Mukherjee, and A. J. Musser, Chemical Physics Reviews **4**, 041305 (2023).

70. P. Malý, J. Lüttig, S. Mueller, M. H. Schreck, C. Lambert, and T. Brixner, Physical Chemistry Chemical Physics **22**, 21222 (2020).

71. K. Zakutauskaitė, M. Mačernis, H. H. Nguyen, J. P. Ogilvie, and D. Abramavičius, The Journal of Chemical Physics **158**, 015103 (2023).

CURRICULUM VITAE

First name Vytautas
Last name Bubilaitis
Email vytautas.bubilaitis@ff.vu.lt

Education:

2013 - 2017 Bachelor's Degree In Physics,
Physics Study Program,
Vilnius University, Faculty Of Physics

2017 - 2019 Master's Degree In Physics,
Theoretical Physics And Astrophysics Study Program,
Vilnius University, Faculty Of Physics

NOTES

NOTES

NOTES

Vilniaus universiteto leidykla
Saulėtekio al. 9, III rūmai, LT-10222 Vilnius
El. p. info@leidykla.vu.lt, www.leidykla.vu.lt
bookshop.vu.lt, journals.vu.lt
Tiražas 15 egz.